
MAGNETIC
TRAPS

Gas-Dynamic Multiple-Mirror Trap GDMT

D. I. Skovorodin^{a,b,*}, I. S. Chernoshtanov^{a,b,**}, V. Kh. Amirov^a, V. T. Astrelin^{a,b}, P. A. Bagryanskii^a,
A. D. Beklemishev^{a,b}, A. V. Burdakov^{a,c}, A. I. Gorbovskii^a, I. A. Kotel'nikov^a, E. M. Magomedov^d,
S. V. Polosatkin^{a,b,c}, V. V. Postupaev^{a,b}, V. V. Prikhod'ko^{a,b}, V. Ya. Savkin^a, E. I. Soldatkina^{a,b},
A. L. Solomakhin^a, A. V. Sorokin^a, A. V. Sudnikov^{a,b}, M. S. Khristo^{a,b}, S. V. Shiyankov^a,
D. V. Yakovlev^a, and V. I. Shcherbakov^d

^a Budker Institute of Nuclear Physics, Siberian Branch, Russian Academy of Sciences, Novosibirsk, 630090 Russia

^b Novosibirsk State University, Novosibirsk, 630090 Russia

^c Novosibirsk State Technical University, Novosibirsk, 630073 Russia

^d SuperOx, Moscow, 117246 Russia

*e-mail: D.I.Skovorodin@inp.nsk.su

**e-mail: I.S.Chernoshtanov@inp.nsk.su

Received March 24, 2023; revised May 30, 2023; accepted June 24, 2023

Abstract—This work is devoted to the project of a new-generation open trap, gas-dynamic multiple-mirror trap (GDMT), proposed at the Budker Institute of Nuclear Physics, Siberian Branch, Russian Academy of Sciences. The aim of the project is to substantiate the possibility of using open traps as thermonuclear systems: a source of neutrons and, in the future, a thermonuclear reactor. The main objectives of the project are to develop technologies for long-term plasma maintenance in an open trap, optimize neutron source parameters based on the gas-dynamic trap, and demonstrate methods for improving plasma confinement. The magnetic vacuum system of the facility consists of a central trap, multiple-mirror sections that improve the longitudinal plasma confinement, and expanders designed to accommodate plasma flux absorbers. The facility is to be built in several stages. The starting configuration is broadly similar to the GDT facility and includes a central trap with strong magnetic mirrors and expanders. It solves two main problems: optimization of the parameters of the neutron source based on the gas-dynamic trap and study of the physics of the transition to the configuration of a diamagnetic trap with a high relative pressure $\beta \approx 1$, which significantly increases the efficiency of the system. This work describes the technical design of the starting configuration of the facility and outlines the physical principles on which the GDMT project is based.

Keywords: open magnetic trap, magnetic confinement, controlled thermonuclear fusion

DOI: 10.1134/S1063780X23600986

1. INTRODUCTION

Open traps [1–4] were an important field of early research in the physics of magnetic confinement of high-temperature plasma. The inspiring increase in plasma parameters demonstrated by several generations of successive tokamaks has made tokamaks a mainstream in the fusion research. The physics and technology of open traps continued to develop as an alternative direction of research. The continuation of works on open traps was motivated by the potential physical and engineering advantages of linear magnetic systems for plasma confinement, which needed to be proved in a real experiment. Fundamentally, open magnetic traps are steady-state and allow a high relative plasma pressure to be reached in the confinement region $\beta = 8\pi p_{\perp} / B_v^2 \approx 1$ (where p_{\perp} is the transverse plasma pressure, B_v is the vacuum magnetic field created by coils) and, in the case of axisymmetric con-

figurations, under certain conditions, they may have transverse diffusion coefficients ten times lower than those of toroidal systems [5]. We will briefly mention the possibility of the most efficient use of modern magnetic technologies, since the magnetic field on the plasma axis is only slightly less than the field on the conductors; significantly less stressful working conditions for surfaces in contact with plasma; modularity of facilities, which makes them maintainable even for the reactor scale. To date, the field of open traps has come to an important logical stage in its development. The main physical problems identified in the early stages of studies of linear magnetic systems (MHD stability, anomalous losses due to the development of microinstabilities) have been successfully solved.

In this work, we discuss the next-generation open magnetic trap project, which should demonstrate the possibility of the production and quasi-steady-state confinement of the plasma with sub-reactor param-

ters. This project is a certain compromise, in which the duration of the existence of the plasma was limited to a few seconds, which made it possible to significantly simplify the design of plasma absorbers and limiters, the magnetic system and the plasma heating system. If this scientific program succeeds, this compromise can be removed by gradually modernizing the individual modules and systems of the facility.

Gas-dynamic multiple-mirror trap (GDMT) is a new-generation open trap for confining hot plasma, the concept of which is being developed at the Budker Institute of Nuclear Physics, Siberian Branch, Russian Academy of Sciences [6, 7]. The aim of the project is to substantiate the possibility of creating a thermonuclear system based on an open magnetic trap: a source of neutrons and, in the future, a thermonuclear reactor. In addition to the physical principles tested on previous-generation facilities, the GDMT project should allow the study of new plasma confinement methods and demonstrate a significant increase in the efficiency of open traps [8]. As methods for suppressing losses from traps, we consider diamagnetic confinement of the plasma with a relative pressure $\beta \approx 1$ [9, 10], and also the use of multiple-mirror [11, 12] and helical sections [13, 14].

A neutron source based on a gas-dynamic trap [15–18] can apparently be considered as the open-type thermonuclear system closest to the practical implementation. The main purpose of such a source is to test the materials of a future thermonuclear reactor in a fast neutron flux. The plasma in the neutron source is confined in an axisymmetric solenoid whose magnetic field is enhanced at the ends. The main method of heating the plasma in a trap is the oblique injection of powerful beams of neutral particles (also called atomic beams), which are ionized in the plasma and captured in the trap as high-energy ions. As a result, two ion components are formed in the plasma: warm ions of the target plasma and an anisotropic population of fast ions. Fast ions ensure the occurrence of thermonuclear reactions in the plasma. Picking the density of fast ions near the turning points makes it possible to control the neutron emission profile along the facility creating compact zones with a high neutron flux. The energy efficiency of the neutron generation is determined by the particle confinement time and energy in the trap. In the basic version, to limit neutron losses, the technology of the gas-dynamic confinement of the target plasma is used, which is based on the use of regions with a strong magnetic field—magnetic mirrors—at the ends of the trap and expanders behind them. The calculations show that this technology makes it possible to obtain $\sim 10^{18}$ neutrons per second in the D–T fusion reaction at a plasma heating power of ~ 50 MW [18]. The improvement of the longitudinal confinement of plasma expands the range of its practical application. Problems such as afterburning of minor actinides, production of valuable isotopes or creation of a hybrid fis-

sion reactor with a thermonuclear driver are considered [19, 20].

To test the physical foundations of a neutron source based on a gas-dynamic trap, the GDT facility was designed and operated at the Budker Institute of Nuclear Physics, Siberian Branch, Russian Academy of Sciences [21]. It demonstrated the stable plasma confinement with a population of fast ions with the average particle energy of about 10 keV, while the plasma pressure reaches half the magnetic field pressure [22]. In such systems with the two-component plasma, the deceleration time of the anisotropic population of fast ions is determined by their collisions with electrons. Therefore, to increase the lifetime of fast ions and, thus, to increase the efficiency of the open trap as a thermonuclear system, the key task is to increase the electron temperature. The GDT was the first of open systems where the plasma electron temperature of ~ 1 keV was obtained under quasi-steady-state conditions [23–25], which was previously achieved only in short pulses in the multiple-mirror trap GOL-3 (Russian acronym of Corrugated Open Trap) [26]. In recent years, the ALIANCE [18, 27] and WHAM Neutron Source [28] projects have been proposed worldwide, which involve the construction of a series of plasma facilities, the ultimate goal of which is to create a source of thermonuclear neutrons. The GDMT project allows solving similar problems and also developing physics and technologies for improving longitudinal confinement of the plasma in open traps.

Currently, longitudinal losses are considered to be the main channel for plasma and particle energy losses from the GDT trap, and the reduction of which is the main focus of the GDMT project. At the same time, plasma turbulence caused by the development of various kinds of instabilities, the loss of fast ions as a result of charge exchange, and recycling in the near-wall region are also important factors in the degradation of plasma energy confinement. These problems are effectively solved in the GDT facility but can become significant when the design of the facility and plasma parameters are changed. For example, intense drift turbulence and significant turbulent plasma transport across the magnetic field were observed in ambipolar traps (GAMMA-10, TMX-U) with suppressed longitudinal losses. In the basic GDMT mode similar to the GDT one, the problem of drift turbulence is not expected to be so acute, but the new confinement modes definitely need the experimental verification in terms of suppressing turbulent transport.

In the future, the suppression of plasma losses makes it possible to consider open traps as a power reactor for thermonuclear fusion. In addition to relative simplicity, an open trap has several attractive advantages: excellent confinement of fast ions in an axially symmetric magnetic field and the possibility of achieving a high relative plasma pressure β .

An axisymmetric trap with the high-pressure plasma has many features in common with the field reversed configuration (FRC) [29] and, along with it, has the fundamental possibility of using alternative tritium-free fuels that are inaccessible to toroidal systems. To achieve this goal, it is necessary to make a big step, in terms of plasma parameters and in terms of its confinement time. One of these steps can be the transition to the diamagnetic confinement regime [9]. The displacement of the magnetic field by the high-pressure plasma leads to an increase in the mirror ratio and a decrease in gas-dynamic losses through the mirror. The idea of the diamagnetic confinement method is to achieve an extremely high relative pressure $\beta \approx 1$, at which the magnetic field is almost completely ousted from the plasma. The plasma lifetime in this regime should be determined by transverse diffusion of the plasma from the confinement zone [10] and by collisionless losses caused by the violation of the adiabatic motion of particles [30]. The study of the possibility of the formation of such a plasma state in a trap, its stability, equilibrium features and lifetime scalings is a part of the physical program of the GDMT facility.

As an additional method for the suppression of longitudinal losses, which is compatible with gas-dynamic and diamagnetic confinement modes, the GDMT project provides for the use of special multiple-mirror (or more complex helical [13, 14]) sections. These sections are to be used instead of single magnetic mirrors to limit the plasma flow from the trap along the magnetic field. The magnetic field in the multiple-mirror sections forms a sequence of mirror traps. If the mean free path of the particles is comparable to the distance between the mirrors, the plasma flow becomes diffusive [11]. At thermonuclear temperatures, pair collisions can provide the required scattering rate only at a high density $n = 10^{16} - 10^{18} \text{ cm}^{-3}$; therefore, for a long time, a multiple-mirror reactor was considered fundamentally as a pulsed device. However, it was shown in experiments with the GOL-3 multiple-mirror trap that collective ion scattering can provide optimal conditions for plasma confinement at a moderate density [31, 32]. At a trap length of 12 m, the energy lifetime of a plasma with an ion temperature of 1–3 keV and a density of about 10^{15} cm^{-3} reached 1 ms, which is almost two orders of magnitude higher than the classical estimates. A multiple-mirror system with a length of about 10–20 m can apparently increase the energy efficiency of a neutron source based on a gas-dynamic trap by an order of magnitude, making it possible to achieve a thermonuclear power gain of $Q \sim 0.5$. Therefore, the study of the operation of multiple-mirror sections in the steady-state mode is an important part of the research program at the GDMT facility.

The GDMT facility has a modular structure, so the physical tasks of the project can be solved at different stages of its construction. In the initial configuration,

the magneto-vacuum system of the facility includes a central section with strong magnetic mirrors and expanders behind the mirrors designed to accommodate plasma absorbers. The plasma is to be heated by oblique injection of powerful beams of neutral particles and additional input of the microwave power. The main physical task of the starting configuration is to simulate the physical processes in a neutron source based on the gas-dynamic trap. The magnetic system of the initial configuration of the GDMT facility is designed in such a way as to provide flexibility in conducting experiments. An important task is a significant increase in the duration of the existence of the hot plasma in comparison with experiments on the GDT facility. In addition to demonstrating the steady-state parameters of the plasma, the facility should make it possible to proceed to the study of technologies for long-term maintenance of the discharge. The efficiency of traps in the basic gas-dynamic operating mode is determined by the magnitude of the magnetic field in the mirror (under condition of the suppression of transverse losses), therefore, in order to achieve the best plasma parameters for a discharge duration on the order of a second, it is advisable to use superconductors to create mirror coils. To simplify the design of the facility, it is currently proposed to use copper coils to create a central solenoid in combination with superconducting mirrors.

Section 2 of the work describes the design of the initial configuration of the GDMT facility, its magnetic system and the plasma heating system. Section 3 is devoted to the issues of plasma confinement, heating, and stability in the initial facility configuration. The results of the numerical simulation for the selected design and parameters of the GDMT facility are presented. Section 4 discusses additional methods to improve hot plasma confinement in a trap.

2. DESCRIPTION OF THE STARTING CONFIGURATION OF THE GDMT FACILITY

The scientific program of the GDMT project integrates the ideas and technologies that have emerged during the development of several fields of research on open traps. Part of the tasks can be performed on a limited facility configuration, which we further refer to as the GDMT starting configuration. The allocation of the starting configuration reduces the time from the decision to start the project to obtaining the first significant scientific results. The initial configuration of the GDMT facility basically repeats the configuration of the GDT facility currently operating at the Budker Institute of Nuclear Physics, Siberian Branch, Russian Academy of Sciences [33]. The plasma in the facility is created and held in an axisymmetric magnetic solenoid with end sections that serve to suppress its losses along the magnetic field lines. In the initial facility configuration such sections are compact solenoids with high (magnetic induction higher than 10 T)

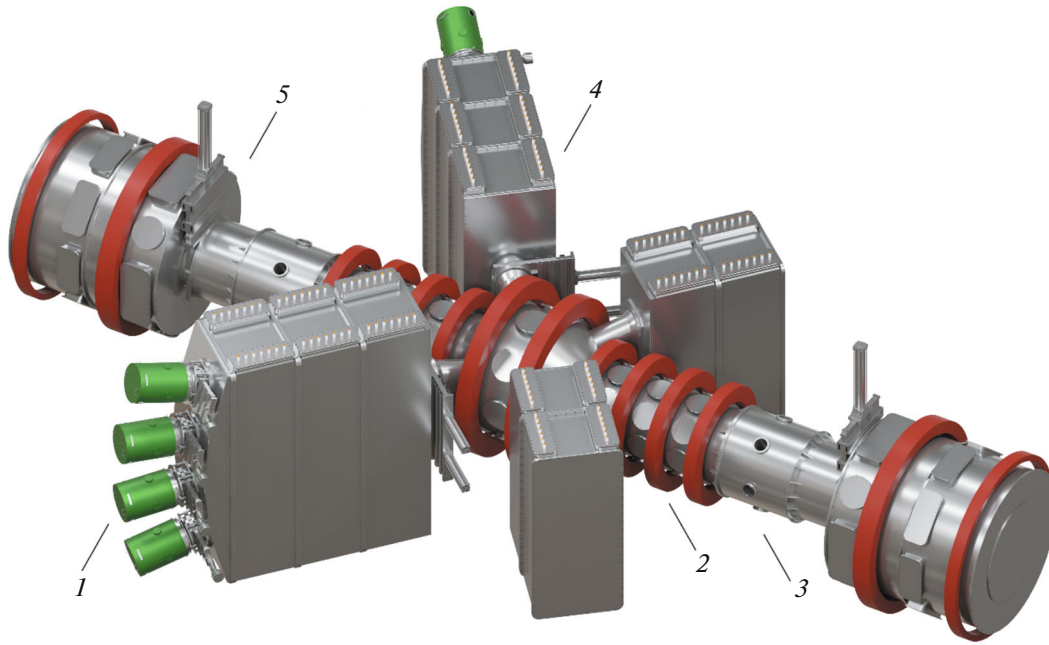


Fig. 1. General view of the starting configuration GDMT facility: (1) atomic beam injector, (2) solenoid and vacuum chamber of the central section, (3) cryostat of the magnetic mirror module, (4) neutral injection chamber, and (5) chamber and coils of the expander section.

magnetic field—magnetic mirrors. The GDMT experimental program involves studies in a trap with single magnetic mirrors and in a full facility configuration with more complex end sections, which are to be used to study promising schemes for suppressing longitudinal losses: multiple-mirror [34] and helical [35] plasma confinement.

An important feature of the facility is the achievement of a quasi-steady-state regime, in which the losses of energy and plasma particles are compensated by systems for heating and replenishing with substance. The duration of operation of most systems in the initial GDMT configuration is chosen to be two seconds, and the duration of operation of the neutral injection system (beams of hydrogen atoms) at the initial stage of work is 0.3 s. The chosen time of the experiment exceeds the characteristic time for the establishment of equilibrium energy fluxes between the plasma components, which is on the order of magnitude of 50 ms (Subsection 3.2). Limiting the pulse duration to two seconds greatly simplifies the design of electrodes for plasma heating and stabilization systems due to the possibility of operating in transient thermal conditions, allows the use of storage power sources for the solenoid and heating systems, and also simplifies the vacuum system because of the possibility of using pumping methods that require regeneration. At the same time, the experimental complex allows an increase in the duration of the discharge up to a completely steady-state mode when the pulse elements of the magnetic solenoid are replaced by superconduct-

ing ones and the corresponding modernization of plasma heating systems.

The maintenance of a high-temperature plasma discharge with a duration of 0.3–2 s occurs due to the injection of beams of fast neutrals with a total power of up to 24 MW and an energy of hydrogen atoms of 30 keV, as well as the injection of microwave radiation with a power of up to 6 MW into the plasma (Subsection 2.2). In this case, the following plasma parameters averaged over the cross section are expected: the electron temperature is about 1 keV, the temperature of warm ions is 1–2 keV, the densities of warm and fast ions are about $5 \times 10^{13} \text{ cm}^{-3}$ (Subsection 3.2). The neutral injection system includes eight neutral beam injectors divided into two groups located on both sides of the facility (Fig. 1). A group of four injectors is connected to a common vacuum chamber of the rectangular cross section (neutral injection chamber), in which the elements of the beam path are located: a neutralization gas target, a deflecting magnet, a calorimeter, and titanium sorption pumps. The dimensions of the neutral injection chamber are determined, to a large extent, by the requirements for the pumping rate of hydrogen, which accompanies the beams of fast neutrals. The average beam injection angle is 50.9° with respect to the facility axis.

During the discharge, a steady-state flow of particles is established along the magnetic field lines, which transfers most of the power spent on plasma heating. The magnetic field is produced by a system of copper and superconducting coils (Subsection 2.1), which

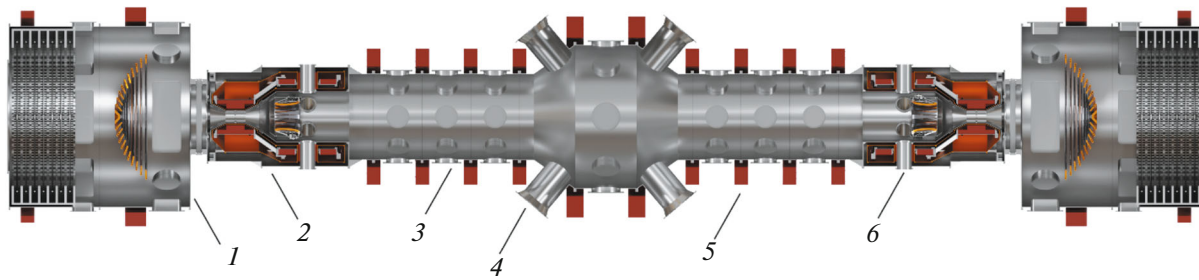


Fig. 2. Sectional view of the vacuum chamber and magnetic system of the starting configuration of the facility GDMT facility: (1) vacuum chamber of the expander section, (2) magnetic mirror module, (3) vacuum chamber of the central section, (4) atomic beam input ports, (5) central section of the solenoid, and (6) microwave input ports.

have a circular shape. The centers of the coils are located on an axis coinciding with the axis of the vacuum chamber. Mirror coils, which produce a magnetic field up to 20 T, are used to repeatedly reduce the steady-state longitudinal flow of particles, which ensures the required confinement time of the warm plasma component. After leaving the magnetic mirror, the plasma flow expands in a decreasing magnetic field and is absorbed at the plasma absorber in the end vacuum chamber (Fig. 2). In the radial direction, the discharge is limited by limiters-electrodes (Subsection 2.3) located in the central vacuum chamber. By applying a potential to the limiter, the plasma rotation profile in crossed fields is controlled, which implements the plasma “vortex confinement” scheme (Subsection 3.4) with suppressed transverse magneto-hydrodynamic (MHD) losses [36]. For additional control of the potential distribution in the plasma, a potential is applied to the sections of the plasma absorber in the end chamber, which is a system of insulated electrodes that completely intercepts the plasma flow [37].

2.1. Magnetic System and Vacuum Chamber

In the starting configuration, the magnetic solenoid of the GDMT facility consists of copper coils in the central section (Fig. 2), superconducting coils located in the magnetic mirror cryostat (magnetic mirror module) and copper coils in the expansion section.

The coils of the central section produce an extended confinement region with a uniform Fig. 3 (curve 1) or smoothly changing Fig. 3 (curve 2) magnetic field along the axis of the facility. In the first case, the magnetic system ensures the maximum deviation of the field from the average value over the homogeneity region $R < 300$ mm, $z_{\min} < z < z_{\max}$ no more than 1.5%, where z_{\min} and z_{\max} are longitudinal boundaries of a homogeneous region. The confinement region ends with magnetic mirrors. For a monotonic increase in the magnetic field from the confinement region to the magnetic mirror and for matching

the magnetic flux, transition coils are included in the solenoid, which are a part of the magnetic mirror cryostat. The maximum length of the fast ion confinement region is achieved in the mode with the uniform field and can be up to 6 m. An important design feature of the GDMT solenoid is the possibility of changing the confinement region length by increasing the number of solenoid sections and by changing the magnetic field profile. In view of this, one of the main requirements for the magnetic system of the central section is the possibility of restructuring the magnetic field distribution, which is ensured by an independent power supply of all solenoid coils. The possibility of rearranging the profile makes it possible to carry out various experiments with a spatial distribution of the density of fast ions that varies over a wide range.

The maximum magnetic field in the central section is 1.5 T. The power supply system of the solenoid makes it possible to implement two types of time dependences of the magnetic field shown in Fig. 4. In the “plateau” mode (Fig. 4, top), the distribution of currents is preliminarily produced in the coils which provides a magnetic field with a given spatial profile, after which a transition to the current stabilization

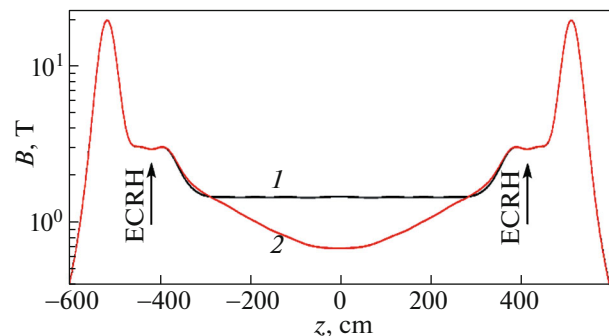


Fig. 3. Magnetic field distribution along the axis of the facility: (1) uniform distribution with the magnetic induction value $B = 1.5$ T for experiments with high relative plasma pressure and (2) gradually increasing field distribution.

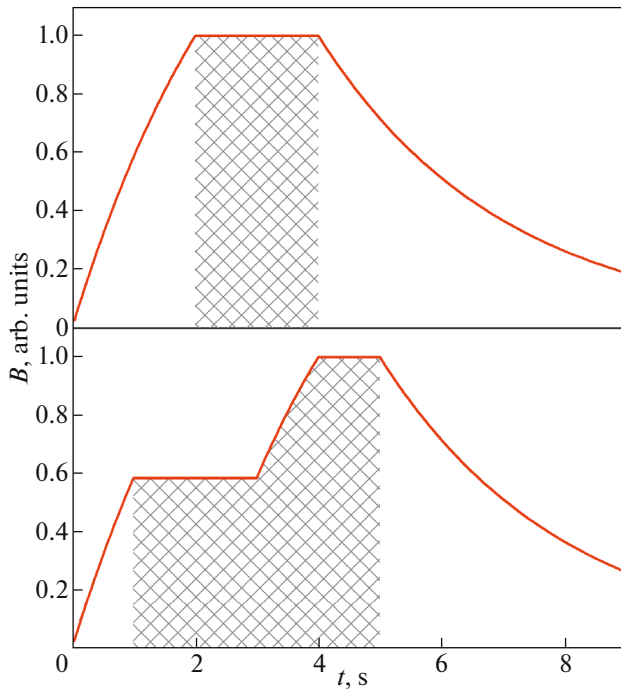


Fig. 4. Time dependences of the magnetic field in the central section of the solenoid: the standard “plateau” mode (top), the special “stepped” field rise mode (bottom). Hatching shows the time periods during which the plasma experiment is carried out.

mode takes place, in which an experiment lasting up to 2 s is carried out. The second mode (Fig. 4, bottom) includes two “plateau” stages and is intended for experiments on diamagnetic plasma confinement (Subsection 4.1). It is assumed that the transition to the diamagnetic mode is carried out in a relatively weak magnetic field, after which the magnetic field can be increased. At all stages of this experiment, it is required to maintain the uniformity of the magnetic field, which is achieved through the implementation of the programmed time dependence of the currents in the coils, as well as the use of a feedback system.

In addition to ensuring the required uniformity of the magnetic field, the cross sections of the windings and the inner diameter of the coils are determined by the need to place a vacuum chamber inside the solenoid and the location of ports for diagnostics and

plasma heating systems. Table 1 shows the parameters of the discussed version of the windings of the central section. The coils are made of a hollow square copper conductor, and their design is similar to that recently used in the windings of the toroidal field of the T-15MD tokamak [38]. The general parameters of the central section of the magnetic system are given in Table 2.

The power supply system for the solenoid coils is based on supercapacitor energy storage devices. Each coil is connected to an individual storage device with an IGBT key operating in the PWM modulation mode and implementing a programmed time dependence of the current pulse.

The coils of the expander section (Fig. 2) operate in a constant mode and are designed to correct the magnetic field in the expansion zone of the plasma flow after leaving the magnetic mirror. Using coils, one can change the curvature of the field lines to improve the MHD stability of the plasma, as well as vary the size of the plasma flow incident on the end electrode system. An additional function of the coils is the screening of the magnetic mirror field, which is necessary for the operation of titanium arc evaporators (see below).

As is shown in Subsection 3.1, the efficiency of plasma confinement in linear systems depends significantly on the magnitude of the magnetic field in the mirror, so the mirror coil should create the maximum technically achievable magnetic field. Recent progress in the field of high-temperature superconductors (HTSC) [39–42] makes it possible to expect a magnetic field of up to 20 T in coils based on an HTSC tape within this project. The development of such solenoids for CTF applications and gaining experience in their operation are an important part of the research program at the GDMT facility. Taking into account the risks associated with the creation of mirror coils with a field of 20 T on the axis and a relatively large inner aperture of the solenoid, a backup option is provided: development and manufacture of a mirror coil based on a low-temperature superconductor (LTSC) with a magnetic field of 12 T on the axis. In both HTSC and LTSC versions, the magnetic mirror solenoid (Fig. 5, MS) has a significant inductance, which imposes restrictions on the variation rate of the magnetic flux near the winding. In view of this, the coils closest to the magnetic mirror should operate in a con-

Table 1. Parameters of the coils of the central section and power supplies based on supercapacitors

Coil	$Z_{\text{center}}, \text{ mm}$	$\Delta Z \times \Delta R, \text{ mm}$	$R_{\text{inner}}, \text{ mm}$	N	$I_{\text{max}}, \text{ kA}$	$R, \text{ m}\Omega$	$C, \text{ F}$	$U, \text{ V}$
C1	430	250×300	1100	120	12.5	32.6	100	1000
C2	1200	200×250	700	80	10.5	14.2	80	750
C3	1875	200×250	700	80	10.5	14.2	80	750
C4	2550	200×250	700	80	13.75	14.2	110	750
C5	3225	200×250	700	80	13.75	14.2	110	750

Table 2. Parameters of the central section of the magnetic system and storage power supplies

Magnetic field energy, MJ	27.5
Energy in storage, MJ	314
Copper mass, t	24
Conductor temperature, °C	<60
Repetition period, min	10
Active power, MW	27

tinuous mode and, in the case of transition coils, they should also be superconducting. Transition coils (Fig. 5, C6, C7) provide a monotonic increase in the magnetic field from the central section to the magnetic mirror, partially shield it from pickups that occur during the pulse of the central section, and also create a 3 T constant field region for ECR-heating of the plasma. The requirements for the magnetic field in the region of the transition coils make it possible to consider for their manufacture a cable based on the NbTi niobium–titanium alloy, which allows current adjustment by up to 20% during the increase in the magnetic field in the central section.

The initial conductor for winding the magnetic mirror solenoid is a tape with a second-generation high-temperature superconductor (REBCO) 12 mm wide, developed and manufactured by SuperOx Ltd. [41]. Like other high-field solenoids based on HTSCs [40, 42], the magnetic mirror solenoid is manufactured using the pie winding technology, which ensures its maximum strength. To further increase the mechanical strength, a reinforced conductor is used,

which is obtained by soldering Hastelloy C276 tapes on both sides of the original HTSC tape. At present, the most promising is the winding of pies with inter-turn polymer insulation, as well as partial insulation of the end surface in contact with copper thermal bridges located inside double pies. The winding of the mirror unit has a T-shaped cross section, which can be obtained by assembling double pies with a variable inner diameter and by dividing the winding into two independent solenoids. All double pies are connected to each other in series using junctions on the outer turns.

The development of an HTSC magnetic mirror solenoid requires a separate study to reduce the risks associated with high requirements for the solenoid and the specifics of operation under the conditions of the GDMT. In particular, the key issues are the method of cooling the solenoid, its resistance to superconductivity breakdowns and the requirements for the corresponding protection systems, as well as significant EMF on the winding due to flux linkage with the pulse coils of the GDMT solenoid. In view of this, within the draft design, a variant of a magnetic mirror solenoid made of LTSC based on an alloy of niobium and tin (Nb_3Sn) is also being developed. The proposed design of such a solenoid is based on a multicore cable made of LTSC cores [43]. The magnetic field at the center of the solenoid is 12 T, and the magnetic flux is equal to that of the HTSC solenoid. A T-shaped winding with current gradation is considered, which is an inner and outer solenoid wound in layers on a single reel with two different types of cable and connected in series. The parameters of the LTSP solenoid are given in Table 3.

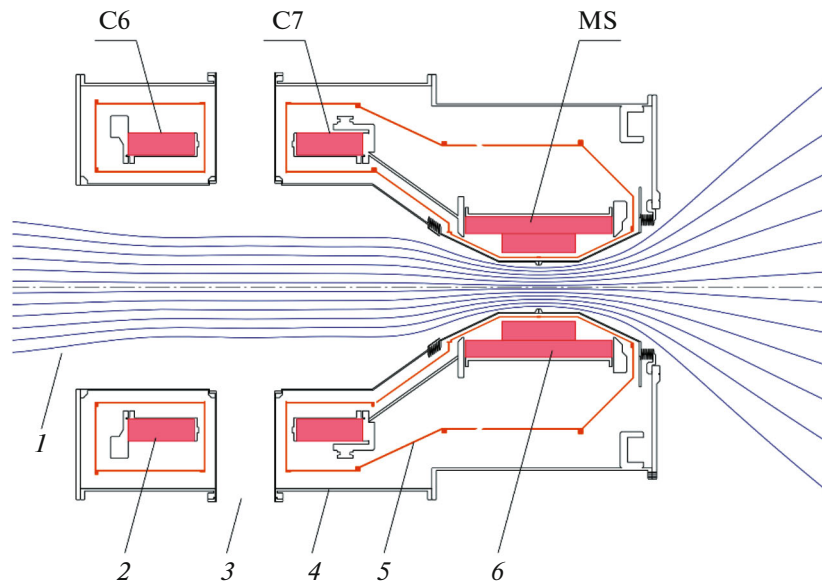
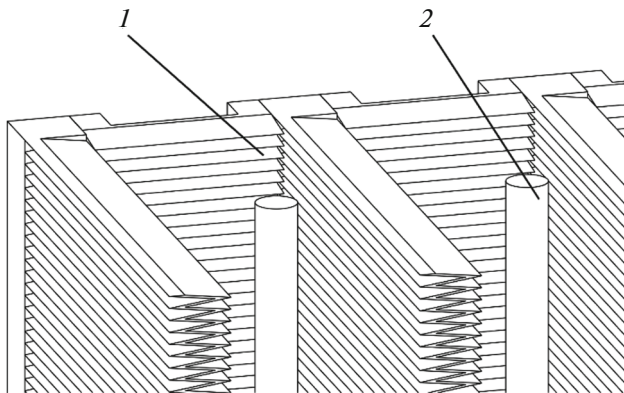
**Fig. 5.** Cryostat and magnetic mirror module coils: (1) magnetic field line, (2) transition coil, (3) microwave beam input port, (4) vacuum chamber of the cryostat, (5) cryostat heat shield, and (6) solenoid of the HTSC-based magnetic mirror.

Table 3. Parameters of GDMT magnetic mirror solenoid. $*I_c$ is the critical current calculated along the loading straight line of the solenoid at a temperature of 4.2 K taking into account the anisotropic properties of the superconductor

	HTSC; T-type	HTSC; 2-section	LTSC
Coil length, mm	504	504	493
Inner diameter of a coil, mm	240	240	283
Number of turns (inner/outer section)	12132	5000/7200	2427
Working current (I), A	716	515/887.4	2385
Current supplies (I/I_c)*	0.8	0.55/0.62	0.8
Working temperature, K	<4.5	<15	<4.5
Inductance, H	26.1	4.26/12	1.24
Stored energy, MJ	6.7	7.3	3.5
Magnetic field in the center, T	20	20	12
Max. magnetic field on a conductor, T	21.6	21.5	12.8

The vacuum chamber of the central section has a main diameter of 1200 mm, which increases to 2000 mm in the neutral beam injection zone. The chamber is assembled from cylindrical and conical sections, the seal between which is made of elastomers. The inner wall of the cryostat, which is attached to the chamber of the central section, acts as the first wall for the plasma discharge, and also provides space for limiters-electrodes, plasma replenishing systems and various diagnostic equipments. In the gap between the superconducting transition coils, there are ports designed to introduce microwave beams into the plasma perpendicular to the axis. The vacuum chamber of the expander section has a diameter of 2500 mm and is connected to the magnetic mirror cryostat through a vacuum gate with a diameter of 900 mm. In addition to various diagnostics, a sectioned plasma absorber (Subsection 2.3) and a titanium sorption pump are located in the vacuum chamber. Main pumping out of the central chamber occurs through the neutral injection pipes (Subsection 2.2), in which sorption pumps are also mounted.

**Fig. 6.** Titanium sorption pump: (1) aluminum pumping panel and (2) titanium rod.

The vacuum system of the facility consists of standard high-vacuum pumps that provide pumping up to working vacuum before the onset of the experiment, and a high-performance pumping system that allows maintaining an acceptable concentration of neutral hydrogen in the trap during the experiment. The high-performance hydrogen vacuum pumping systems of the GDMT facility are built on the basis of sorption pumps with a sputtered titanium getter. Figure 6 shows such a pump installed in a neutral injection chamber (Section 2.2); pumps of a similar design are located in the beam receiver chamber and chamber of the expander section. In contrast to the prototype of this pump at the ASDEX-U facility [44], which is based on the thermal evaporation of titanium, GDMT plans to use arc evaporators to renew the titanium film, which are widely used in experimental facilities at the Budker Institute of Nuclear Physics, Siberian Branch, Russian Academy of Sciences [45, 46] and other plasma facilities [47]. To periodically apply a new titanium layer on the pumping panels 1, an arc discharge occurs between the titanium rod 2 and the surrounding surfaces, which leads to uniform sputtering of the rod body due to the retrograde motion of the cathode spots. Aluminum pumping panels Fig. 6 (1) have a corrugated S-shaped surface with additionally increased roughness due to sandblasting.

Table 4 shows the values of hydrogen fluxes to various parts of the vacuum chamber during the pulse of the facility operation under the conditions of trapping 75% of the power of neutral beams in the plasma and ionization of 100% of the gas from the gas puffing system.

2.2. Systems of Plasma Heating

The main means of plasma heating and the formation of a population of fast ions in the GDMT facility is the neutral injection system. The Budker Institute of Nuclear Physics, Siberian Branch, Russian Academy

Table 4. Leakage rate of atomic hydrogen at a pulse

	Flow, s^{-1}	Flow, equiv. A
Injection chamber	8.3×10^{21}	1330
Receiver chamber	7.7×10^{20}	123
Expander chamber	1.7×10^{22}	2680
Central chamber	1.1×10^{21}	180

of Sciences has extensive experience in the development and operation of fast neutral injectors for plasma heating [29, 33, 47]. An important feature of the GDMT experiment, as well as thermonuclear applications of open-type traps [18], is no need for the high energy of accelerated atoms, which opens up the possibility of using injectors based on positive ion sources. Within this project, it is planned to develop an atomic hydrogen injector with a particle energy of 30 keV, an ion beam power of 4.8 MW and a pulse duration of at least 0.3 s. The design of the injector is a development of the previously developed design of the injector with ballistic focusing of an atomic beam [48], in which it is planned to implement several changes: transition to a slit ion-optical system (IOS) with increased grid thickness and increased accelerating voltage; use of long-pulse arc generators with active cooling; use of a neutralization chamber of increased length with active shielding of the magnetic field and a copper liner cooled to 77 K. Figure 7 shows a sectional view of the GDMT injector. The injector parameters are given in Table 5.

The neutral beam injection system of the GDMT facility (Fig. 8) consists of two identical modules, each of which includes a beam path chamber and a beam receiver vacuum chamber located opposite each other. Each module contains four neutral injectors located in the same plane and spaced at an angle of 10° with

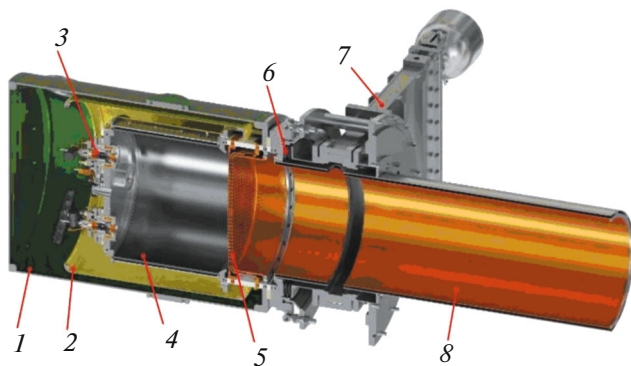


Fig. 7. Sectional view of the GDMT injector: (1) outer case/magnetic shield, (2) high-voltage shield, (3) plasma arc generator, (4) discharge chamber, (5) ion optical system, (6) bellows, (7) vacuum gate valve, and (8) neutralizer.

Table 5. GDMT neutral injector parameters. In addition to protons, molecular ions H_2^+ , H_3^+ , and H_2O^+ are accelerated in the ion-optical system (IOS), which lead to the appearance after neutralization of hydrogen atoms with energies $E/2$, $E/3$, and $E/18$, where E is the energy of the main component of the neutral beam

IOS electrode diameter, mm	340
Number of IOS electrodes	3
IOS type	Slit
Mesh curvature radius, mm	6000
Working gas	Hydrogen
Accelerating voltage, kV	30
Ion current, A	160
Ion beam power, MW	4.8
Plasma source type	Arc
Pulse duration, s	0.3
Energy composition of the beam by current ($E:E/2:E/3:E/18$)*, %	85 : 10 : 4 : 1
Angular divergence along slits, mrad	12
Angular divergence across slits, mrad	20

respect to each other. To provide the energy deposition profile in the plasma most compact in the radial direction, the IOS slits are directed along the injection plane. In addition to deflecting magnets and ion receivers, rotary calorimeters are located in the main chamber Fig. 8 (6) designed to measure the power of neutral beams when adjusting the injectors and its control in the course of experiments. The injection chamber is connected to the main vacuum chamber of the facility using a special elongated vacuum gate Fig. 8 (9) and trapezoidal nozzle Fig. 8 (7) attached to the conical part of the vacuum chamber of the facility. Calculations of the trajectories of atomic beams show that the power losses in the inlet nozzles are negligible, however, they reach $\approx 2\%$ in the outlet nozzles due to the increased angular divergence along one of the coordinates.

The axes of neutral beams of one injection module are located in a vertical plane making an angle with the facility axis of 50.9° and intersecting it at the point $z = 0$. The design provides for a change in the impact parameter of atomic beam injection (displacement of the beam aiming point from the facility axis in the radial direction), which can lie in the range from 0 to 150 mm, corresponding to the rotation of the injector in the vertical plane in the range of angles of 1.5° . In most operating modes of the GDMT, a partial absorption of the power of atomic beams by the plasma is assumed, which is characterized by a “capture” coefficient that takes values up to 95% in the operating mode. The capture coefficient can change over time during the operating pulse of the facility. The atomic beam receiver, located in the corresponding chamber,

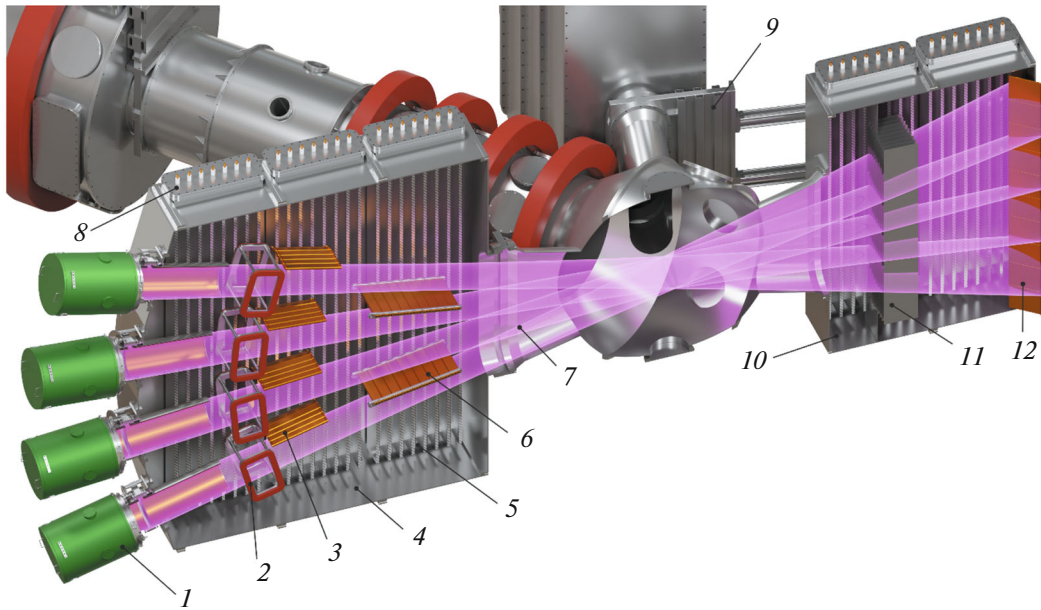


Fig. 8. Sectional view of the neutral injection system of GDMT: (1) ion source, (2) deflecting magnet, (3) receiver of deflected ions, (4) vacuum chamber of the neutral injection module, (5) titanium sorption pump, (6) rotary calorimeter, (7) neutral injection pipe, (8) array of titanium arc evaporators, (9) vacuum gate of a neutral injection module, (10) vacuum chamber of atomic beam receiver, (11) gas delay unit, and (12) atomic beam receiver.

is designed to dissipate the “passed” power of atomic beams and minimize the flow of hydrogen entering the main chamber from the receiver.

One of the key elements of the vacuum chamber of the injection system is a titanium sorption pump, which occupies the side surfaces of the chamber. The residual gas pressure in the injection chamber during the pulse is determined by the leakage of hydrogen from the neutralizer and from the deflected ion receiver. To ensure acceptable power losses of the atomic beam (<3%) during the propagation from the neutralizer to the outlet nozzle, the pumping rate in the injection chamber should be higher than 5000 m³/s. Pumps of identical design are also located in the beam receiver chamber. In this chamber, the principle of differential pumping is implemented by using a baffle and a louvered “gas delay,” which mini-

mally interacts with fast atoms of the beam but effectively traps the gas from the beam receiver.

The particle beam at the neutralizer outlet contains charged components accompanying the atomic beam (Table 6). Ions are deflected by a magnet, Fig. 8 (2), through the windings of which a current is passed, which is corrected taking into account the scattered magnetic field from the solenoid of the facility. In GDMT injection modules, it is proposed to use a magnet design without a ferromagnetic yoke. This solution reduces the gas density at the outlet of the neutralizer but requires an increase in the current in the magnet windings compared to the design used traditionally.

Other methods of additional plasma heating are expected to be used in the GDMT facility in addition to the injection of beams of fast atoms. First of all, it is planned to implement resonant cyclotron microwave heating of electrons. Experiments at the GDMT facility showed that plasma heating on the electron cyclotron resonance (ECR) frequency, even with a relatively low power (20% of the neutral injection power), leads to a significant increase in the plasma electron temperature and expansion of the experimental capabilities of the facility [23, 24]. In this regard, the GDMT facility in the basic configuration is equipped with an electron-cyclotron microwave plasma heating system with a power of 2 to 6 MW and a pulse duration of up to 2 s.

The ECR heating scheme with oblique injection of the extraordinary microwave mode and its absorption at the first harmonic of the cyclotron resonance (X1)

Table 6. Power of atomic and ion beams of particles (kW) at the outlet of the neutralizer

Total power	4800
Neutrals 30 keV	2940
Neutrals 15 keV	400
Neutrals 10 keV	200
Ions 30 keV	1160
Ions 15 keV	70
Ions 10 keV	30

was used at the GDT facility. Oblique injection of radiation in a strong magnetic field through a cryostat noticeably complicates the design of the facility. In addition, effective absorption is obtained in a narrow range of parameters because of the strong refraction of radiation in the plasma, which greatly limits the possibility of using this method of additional heating. In this regard, in the GDMT, it is proposed to use the ECR heating method based on the absorption of an extraordinary wave at the second harmonic of the cyclotron resonance (X2), which is well developed on tokamaks. If the plasma density is noticeably lower than the density corresponding to the cutoff, this method is less sensitive to the plasma density distribution because of weak refraction. However, the efficiency of radiation absorption strongly depends on the uniformity of the magnetic field in the region of cyclotron resonance. To increase the uniformity of the magnetic field, two identical superconducting transition coils are used in the GDMT (Fig. 5), between which there are ports for the injection of microwave radiation perpendicular to the facility axis. It is also possible to use the ECR heating method in the GDMT based on the absorption of an ordinary wave at the first harmonic of the cyclotron resonance (O1). This method is similar to X2 in terms of the required parameters of the plasma and magnetic field, but has somewhat lower absorption efficiency and requires the use of microwave radiation with a frequency less than in two times. This reduces the maximum plasma density for ECR heating due to the radiation cutoff ($B_{\text{ECR}} = 3 \text{ T}$) at the plasma density of $17.5 \times 10^{14} \text{ cm}^{-3}$ for X2 to $0.9 \times 10^{14} \text{ cm}^{-3}$ for O1. The use of ECR heating at the second harmonic also makes it possible to use gyrotrons with a frequency of 170 GHz worked out for ITER. For these reasons, heating at the second harmonic of the extraordinary wave was chosen for ECR heating at the GDMT.

The ECR heating system is based on a scheme of input of a microwave beam into the plasma perpendicular to the facility axis between the transition coils (Fig. 5). Radiation with a frequency of 170 GHz is injected with a polarization corresponding to an extraordinary wave in plasma and is absorbed under resonance conditions at the second harmonic of the electron cyclotron frequency in a magnetic field of $\sim 3 \text{ T}$. Adjusting the magnetic field between the transfer coils makes it possible to control the radial profile of the energy release in the plasma by changing the position of the resonant surfaces as shown in Fig. 9a. The plasma boundary in this figure corresponds to the limiter aperture radius $R = 16 \text{ cm}$, which determines the plasma diameter in the region of the transition coils. In Fig. 9a, the magnetic field B_0 at the point where the microwave beam crosses the facility axis corresponds to the second harmonic of cyclotron resonance for electrons at a frequency of 170 GHz. A series of constant field surfaces plotted in the range of

$(0.99-1.01)B_0$ shows a strong dependence of the shape of the “cold” resonant surface on the current in the coils, therefore, for a reliable implementation of the heating scheme, it is required to maintain the field in the ECR zone with an accuracy of $\pm 0.05\%$ during the pulse of the facility.

Due to the high radiation frequency, refraction has little effect on beam trajectories in the range of operating plasma densities up to 10^{14} cm^{-3} . The radiation absorption parameters in this configuration mainly depend on the magnetic field. At the field value at the intersection point of $B = B_0$, the resonant surfaces have the shape shown in Fig. 9b and lead to heating of the central plasma regions characterized by incomplete radiation absorption, which is about 50% for the above calculation. When the magnetic field increases ($B = 1.001B_0$, Fig. 9c), in turn, the peripheral annular region of the plasma is heated, and complete radiation absorption is also expected. Microwave beam trajectories in plasma shown in Fig. 9b, c are obtained by geometric-optical calculation of propagation and absorption of microwave radiation for a flat radial profile of the plasma density of $3 \times 10^{13} \text{ cm}^{-3}$ and the boundary corresponding to the limiter radius $R = 16 \text{ cm}$. The electron temperature of the plasma on the axis is 300 eV and drops linearly to zero at the plasma boundary. At a further increase in the magnetic field, the absorption region moves along the radius following the resonant surface, and absorption ($>50\%$) is maintained as long as the local electron temperature exceeds $\sim 30 \text{ eV}$ at the plasma density of $3 \times 10^{13} \text{ cm}^{-3}$.

2.3. System of Electrodes

For controlled dissipation of longitudinal and transverse energy flows, two types of electrodes in direct contact with the plasma are used in the GDMT. The first type is radial limiters located near magnetic mirrors (Fig. 10). The limiters are outside the confinement zone of fast ions and are located in the region with a fixed magnetic field of 3 T (between the point of the microwave beam input and the mirror). The adjustment of the plasma diameter in the central section is implemented by cooling and absorption of the plasma on the outermost magnetic surface, which is projected onto the limiter. In this case, the adjustment of the plasma radius is carried out by changing the passage aperture, which is set from the movable sectors of the limiter. An alternative approach that provides the possibility of the discrete adjustment of the diameter of the limiting magnetic surface is the manufacture of a set of ring electrodes with different apertures and their replacement in accordance with the requirements of the experimental program. To control the plasma rotation profile, the limiter needs to be supplied with a potential of $\sim T_e/e$ [36], which corresponds to a scale value of 1 kV in accordance with the calculated plasma parameters in the GDMT (Subsection 3.2).

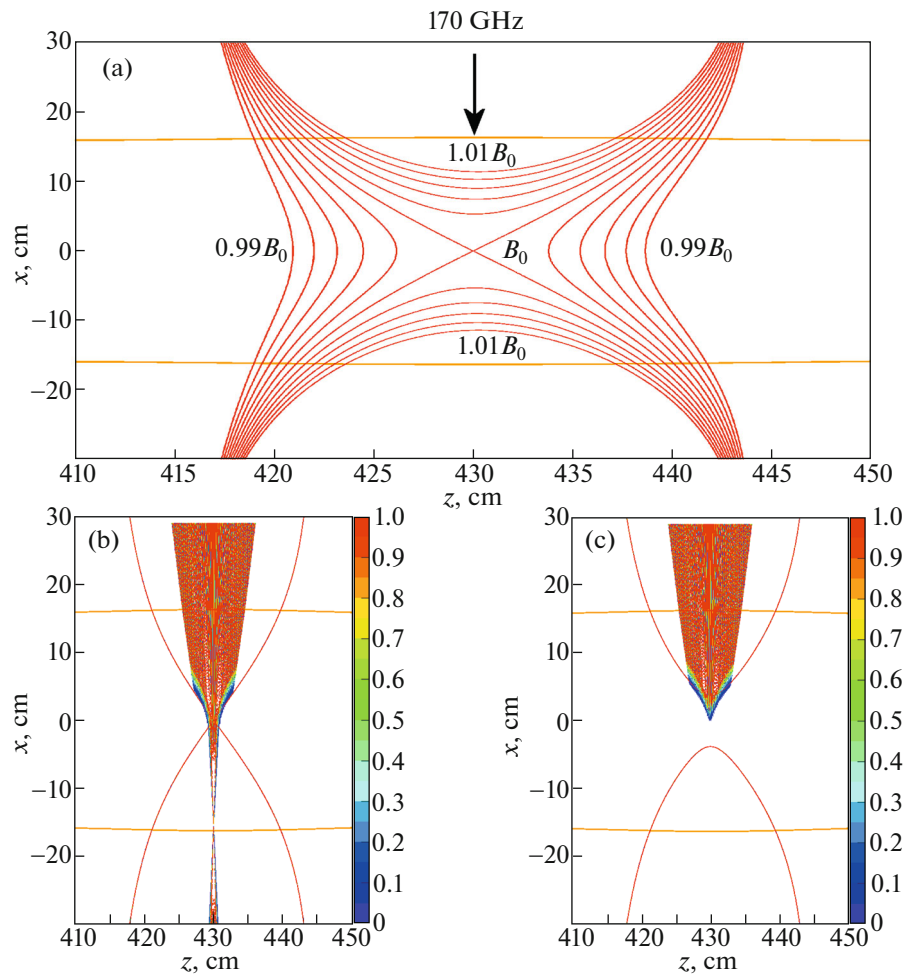


Fig. 9. Scheme of electron-cyclotron plasma heating. (a) The position of the resonant surfaces at different magnetic field values in the region of the transition coils. The orange lines show the plasma boundaries. (b) Beam trajectories in the “central ECR heating” mode. (c) Beam trajectories in the “peripheral ECR heating” mode. The color of the beams corresponds to the ratio of the current beam power to the initial one.

The thermal limiter operating conditions vary depending on the plasma confinement regime in the GDMT and the transverse transport coefficients. In regimes characterized by the suppressed MHD plasma activity, heating of the limiter surface is uniform in azimuth. In the case of the development of a large-scale MHD instability, a complete loss of plasma can occur with the release of the stored energy, which is about 200 kJ, in the azimuth-localized region in about 10 μ s. The surface of the limiter interacting with the plasma is made of molybdenum, which is deposited on a heat-conducting copper alloy base with internal cooling channels.

The plasma absorber (Fig. 10) is designed to absorb the power of the plasma flow leaving the central section through the magnetic mirror. During the discharge, the absorber surface is bombarded by a flow of ions with an energy of the main component of up to 5 keV, as well as a small fraction of ions with an energy

of up to 30 keV (which arises in the case of the development of instabilities of the anisotropic component in the central section). For more effective suppression of the electron flow [49] emitted by the surface of the absorber, as well as to reduce the surface power density, it is proposed to consider a design (Fig. 11), in which the angle between the field line and the surface is about 45° for all field lines in the expanding plasma flow. A feature of this scheme is also the presence of slits between the electrodes, which ensure the pumping out of the gas formed as a result of the neutralization of the ion flow. Plasma absorber rings are electrodes isolated from each other, to which a potential of up to 2 kV with respect to a grounded vacuum chamber can be applied, which may be necessary for the additional discharge stabilization under ECR heating conditions [37].

The size of the plasma “imprint” on the absorber surface is determined by the magnetic flux inside the

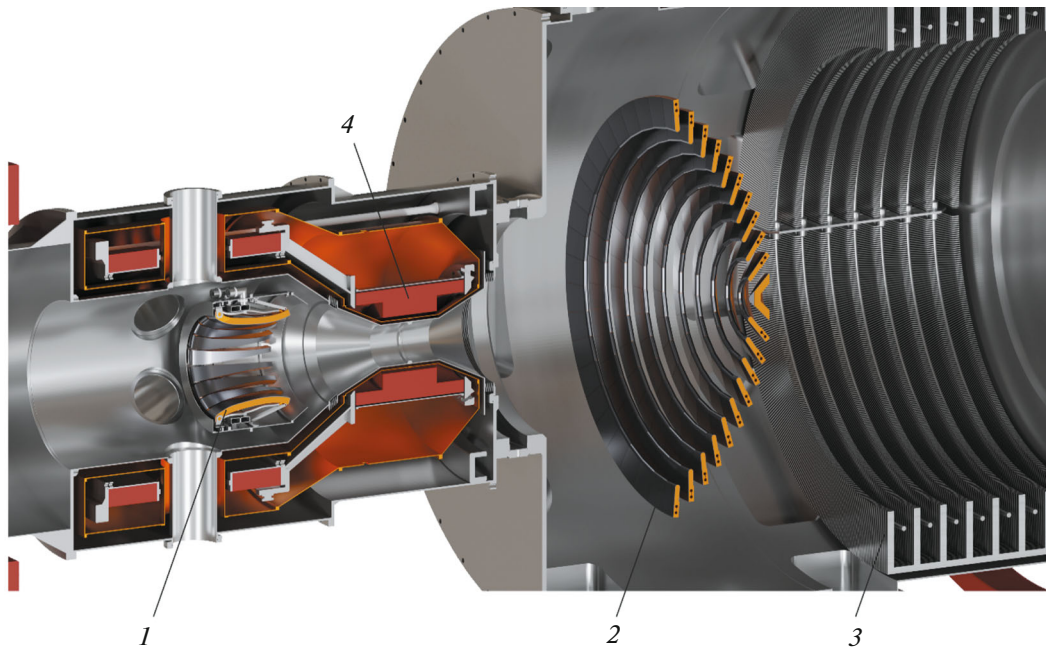


Fig. 10. Sectional view of a magnetic mirror module, expander section and system of GDMT electrodes: (1) limiter, (2) plasma absorber, (3) sorption pump, and (4) solenoid of the magnetic mirror.

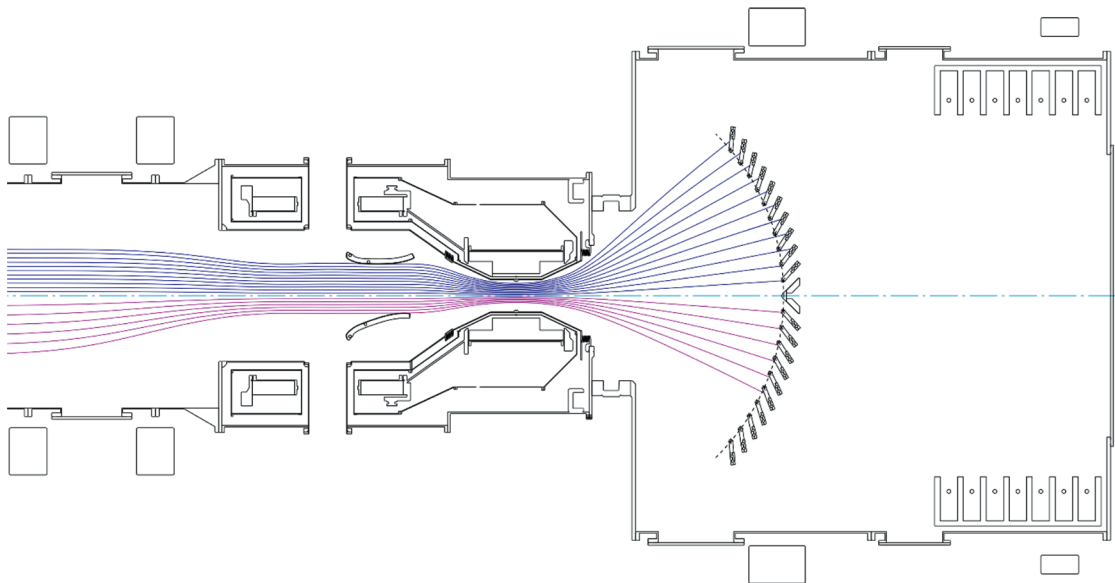


Fig. 11. Electrodes of the GDMT facility in a cross section. Field lines for a uniform magnetic field profile in the central section are shown with values $B = 1.5$ T (top) and $B = 0.3$ T (bottom).

boundary magnetic surface with plasma, which is controlled by changing the diameter of the limiter aperture. In this case, the maximum magnetic flux is limited by the vacuum chamber of the magnetic mirror solenoid. The most stressful thermal modes of the operation of the plasma absorber are modes with low

magnetic flux (small limiter aperture), in which the power density on the surface of the absorber can reach 10 MW/m^2 during a pulse duration up to 2 s. The same as in the case of the limiter, the plasma absorber electrodes are coated with molybdenum and operate in a transient thermal regime.

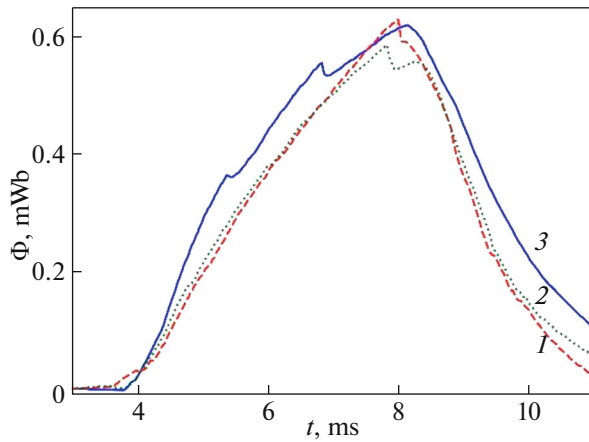


Fig. 12. Comparison of the dynamics of plasma diamagnetism using various methods for creating an initial plasma target: (1) ECR breakdown, (2) electron beam, and (3) gas discharge source.

2.4. Filling of a Trap with Starting Plasma

The plasma heating methods planned at the GDMT facility (atomic injection and ECR heating) require the creation of a sufficiently dense plasma “target” capable of absorbing a significant fraction of the injected power in order to achieve the target plasma parameters during its subsequent heating and replenishing with neutral gas. The starting plasma is characterized by the linear density of the ionized component in the range from 10^{14} to 10^{16} cm^{-2} , corresponding to the fraction of the trapped power of atomic beams of at least 10% at the initial stage of the discharge, which suffices for maintenance and increase in the stored plasma energy during the pulse. In this case, it is obvious that the diameter of the starting plasma should significantly exceed the diameter of the atomic beams at the point of their intersection. Taking this into account, and also based on the experience of working on the GDT facility [33], it can be estimated that this diameter in the GDMT facility should be 30–60 cm.

The design of the GDMT facility suggests the possibility of using several methods for producing the starting plasma. The most common technique in open-type traps is the axial injection of a plasma jet from a gas-discharge source through one of the magnetic mirrors. Experiments on the GDT facility demonstrated the high reliability of this method, which makes it possible to create a starting plasma with a linear density of higher than 10^{15} cm^{-2} when plasma is injected through the mirror from a point with the magnetic field expansion coefficient $K \sim 150$ close to $K \sim 200$ for the GDMT facility. The second possible method for creating the starting plasma is the injection of a narrow (~ 1 cm) electron beam with an energy of 20–50 keV. In recent experiments at the GDT facility [50], it was shown that injection of a

beam with a power of 200 kW or higher and an energy of 20 keV makes it possible to ionize the gas in the trap and create a starting plasma with a linear density of higher than 10^{14} cm^{-2} allowing the implementation of discharge modes similar to those with a gas-discharge source (Fig. 12). The mechanism of ionization and energy transfer of beam electrons to the plasma is based on the excitation of Langmuir turbulence in the zone of the maximum beam current density [51].

An alternative to the methods described above is gas ionization using microwave electromagnetic radiation in the ECR plasma heating system. This or a similar method was previously implemented on open-type facilities [52, 53] and relatively recently on the GDT facility [54]. The method is based on the generation of a population of “overheated” electrons with an energy of higher than 10 keV during ECR heating, which ionize the gas. The plasma target obtained in this manner also allows the initial capture of atomic beams with the subsequent exit into the stage of a quasi-steady-state plasma discharge (Fig. 12). The basic implementation of this method under GDMT conditions involves the use of a separate gyrotron for ECR plasma heating at the first harmonic of cyclotron resonance in the region between the cryostat and the central section of the solenoid at a frequency of up to 80 GHz. It is also planned to study the possibility of the breakdown using the main microwave heating system at a frequency of 170 GHz under conditions of electron cyclotron resonance at the second harmonic, the potential performance of which is indicated by some experimental data on tokamaks [55].

3. PHYSICAL PROCESSES IN THE GAS-DYNAMIC TRAP MODE

3.1. Longitudinal Plasma Confinement

The classical open trap is the Budker–Post mirror cell [1, 2], in which the plasma is confined in the longitudinal direction between the mirrors. The plasma is sufficiently rarefied and almost collisionless, so that the reciprocal collision frequency is much higher than the time of flight of the particle through the trap. Separate particles are confined due to the conservation of the adiabatic invariant—the magnetic moment $\mu = mv_{\perp}^2/2B$. When a particle moves into the high-field region, its energy passes from the longitudinal to the transverse degrees of freedom. Particles are reflected from magnetic mirrors with a sufficiently large pitch angle θ between the velocity vector and the direction of the magnetic field (since the pitch angle depends on the local magnetic field, here, we consider this quantity in the middle plane of traps, where usually the magnetic field is minimum). We traditionally refer to such a population as trapped particles, in contrast to transient particles, which immediately leave the confinement region along the magnetic field. A

“loss cone” is formed in the velocity space, the boundary of which is determined by the formula

$$\sin^2 \theta_{LC} = 1/R = B_{\min}/B_{\max}, \quad (1)$$

where θ_{LC} is the pitch angle at the boundary of the loss cone in the central plane of the trap, and R is the ratio of the magnetic field in the mirror B_{\max} and in the center of the trap B_{\min} (mirror ratio). The trapped particles can undergo a large number of oscillations in the trap [56]. In the real plasma, there are a number of processes, such as pair collisions and scattering of particles by waves, leading to an exchange between populations of trapped and drift particles. Because of the loss cone, the distribution function of particles in the Budker–Post mirror cell is anisotropic. Further, we call processes, in which the anisotropy of the distribution function is significant, kinetic ones. The opposite limiting case, with the ion distribution in the velocity space close to the isotropic one, is called gas-dynamic.

Scattering of particles due to pair collisions leads to diffusion in the velocity space into the loss cone. At a low collision frequency, it remains almost empty, and the ion lifetime τ_{kin} is determined by the following relation:

$$\tau_{\text{kin}} = \tau_{ii} \ln R, \quad (2)$$

where τ_{ii} is the time between ion-ion collisions. The power thermonuclear amplification factor Q in the simplest mirror trap can reach values on the order of 1 [57]. In fact, the time for the dense plasma to escape from such a trap is less than τ_{kin} due to scattering of ions by waves caused by plasma instabilities, the most dangerous of which is the drift-cone cyclotron instability (see Section 3.5). It develops because of the depletion of the distribution function in the loss cone at low transverse particle energy values.

The solution to the problem of plasma microinstabilities is the transition to the confinement of the collisional plasma in the gas-dynamic regime [58]. If the facility length satisfies the condition $L \geq \lambda_{ii} (\ln R)/R$, where L is the distance between the trap mirrors, and λ_{ii} is the mean free path of ions, then the ion distribution function in the entire velocity space is close to the Maxwellian one. In this case, the ion lifetime is determined by the gas-dynamic plasma outflow through the magnetic mirror

$$\tau_{\text{gdt}} = RL/v_{Ti}, \quad (3)$$

where v_{Ti} is the thermal velocity of ions. Equation (3) gives an estimate of the limiting plasma loss rate and does not depend on the collision frequency. The lifetime increases linearly with the mirror ratio, so it is advisable to make it sufficiently large, $R \gg 1$. The linear dependence of the plasma lifetime on the facility length makes it theoretically possible to create a reactor based on the gas-dynamic trap [58], but its length is large ($L > 5$ km), and the reactor power, accordingly, is excessively high.

The creation of a fusion reactor requires the use of additional methods of plasma confinement in a trap to be discussed in Section 4. However, a simple gas dynamic trap is attractive as a basis for creating a fusion neutron source. To this end, a trap scheme with the two-component plasma was proposed, which combines the advantages of kinetic and gas-dynamic confinement regimes [15]. The trap is an axisymmetric solenoid with strong mirrors filled with the sufficiently dense target plasma, which is confined in the gas-dynamic regime. By means of oblique injection of atomic beams, an anisotropic population of fast ions is produced in the plasma. Fast ions oscillate between turning points, being confined in the kinetic mode, and ensure the course of thermonuclear reactions in the plasma. In addition to beam trapping, “warm” plasma with a temperature of about 1 keV stabilizes the drift-cone instability and also determines the MHD stability of the plasma, providing contact with the region behind the mirror [36].

Fast ions decelerate due to Coulomb collisions with the target. At an ion energy above $\sim 15T_e$, deceleration is determined by friction against electrons with a slight change in the direction of the velocity vector, and at a lower energy, they begin to efficiently transfer energy also to the ion component of the target plasma, by means of pitch-angle scattering [59]. An anisotropic distribution of fast ions is formed in the trap. Due to this, the ion density is peaked near the turning points, which makes it possible to control the spatial profile of the yield of thermonuclear neutrons. Collisional deceleration of fast ions leads to heating of the target plasma. At plasma parameters typical for a thermonuclear neutron generator, the target plasma electron temperature should have a scale value of 1 keV for the deceleration time of fast ions to be acceptable. Therefore, further we call this component warm plasma in order to emphasize the difference between its parameters and those of the initial low-temperature starting plasma.

The lifetime of fast ions in a neutron source is determined mainly by electron deceleration

$$\tau_d = \frac{3}{4\sqrt{2\pi}} \frac{m_i}{n_e e^4 \Lambda} \sqrt{T_e^3/m_e}, \quad (4)$$

where τ_d is the deceleration time, n_e , T_e is the density and temperature of plasma electrons, m_e and m_i are electron and ion masses, e is the electron charge, Λ is the Coulomb logarithm. The ion deceleration time increases sharply with an increase in the electron temperature, which is determined by the balance between heating from fast ions and longitudinal energy losses. A feature of open traps is the direct contact of the hot plasma along the magnetic field lines with the surfaces of the plasma absorbers. In this regard, the electron thermal conductivity is often considered as an obstacle to achieving a high plasma temperature in an open trap. The electron heat flux is actually not that high,

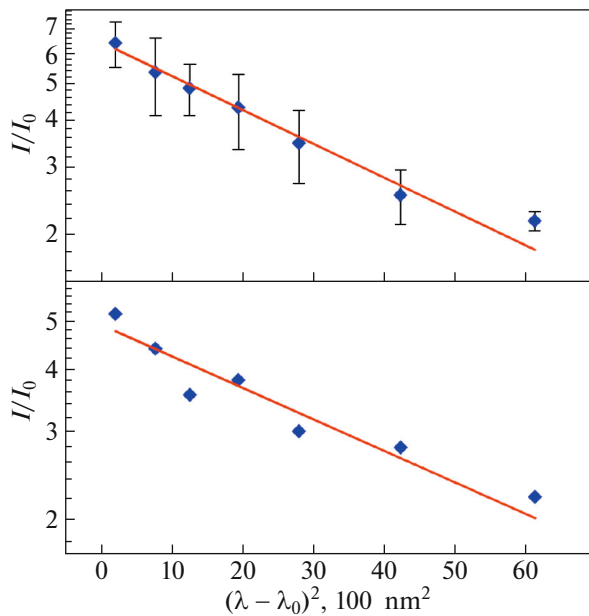


Fig. 13. Thomson scattering spectra measured on a GDT facility and electron temperatures calculated from them. The top graph is the spectrum in a single shot ($T_e = 940 \pm 130$ eV), bottom graph is the spectrum averaged over a series of shots ($T_e = 661 \pm 51$ eV).

since because of the high electron mobility, the ambipolarity condition leads to the fact that the plasma is positively charged. In this case, an electrostatic barrier is formed, which keeps most of the electrons in the trap, and the heat flux to the absorbing plate, carried by the electrons, is strongly suppressed and coincides in order of magnitude with the ionic one. As they move towards the wall, the electrons are decelerated by the electrostatic field, while the ions, on the contrary, are accelerated. Therefore, the vast majority of the energy lost to the wall is taken out by ions accelerated in the ambipolar field, which, in principle, can be used for the energy recovery.

The losses of hot electrons from the plasma and the accompanying losses of energy from the confinement region can greatly increase if there is a counter flow of cold secondary electrons from the surface of the absorbers, which freely penetrates into the hot plasma. The location of the absorbers in an expanding magnetic field behind the mirror makes it possible under certain conditions to almost completely suppress the recirculation of cold electrons even under conditions of strong secondary emission from their surface. As was shown in [60], the plasma in an expander quickly becomes collisionless as it moves away from the mirror, even if it is in the gas-dynamic mode in the central section of the trap. Therefore, secondary electrons can be reflected by the magnetic mirror and absorbed on the wall surface. In this case, they do not affect the ambipolar balance of the plasma in the central trap

and do not cause an increase in the losses of hot electrons. Trapped electrons can oscillate in the volume of the expander between the trap mirror and the electrostatic barrier near the wall [60]. Scattering of transient particles leads to the filling of the “well” in Yushmanov’s effective potential [61]. If the expansion coefficient, which is conveniently called the mirror ratio of the expander $K \geq (m_i/m_e)^{1/2}$, the negative charge of trapped electrons leads to the transfer of most of the potential jump from the wall into the bulk of the expander. This makes it possible to avoid unipolar arcs on plasma absorbers at nuclear fusion temperatures in the central trap. The decrease in the electric field near the wall also effectively restricts the flow of secondary electrons from the wall into the hot plasma volume. In recent years, more accurate theoretical models have been elaborated, including those based on the rigorous solution of the kinetic equation for electrons in an expander [62–65].

A striking example of the suppression of electron heat conduction behind the mirror of an open trap is the demonstration of the possibility of heating electrons to a temperature acceptable for a thermonuclear neutron source. For this purpose, a series of experiments with additional ECR heating with a power of 700 kW was carried out at the GDT facility [23, 24]. In this case, the electron temperature measured in a series of pulses was 661 ± 51 eV at the density on the order of $6 \times 10^{12} \text{ cm}^{-3}$, moreover, in separate pulses of this series, the electron temperature of about 1 keV was measured (Fig. 13).

3.2. Simulation of Plasma Parameters in a Starting GDMT Configuration by the DOL Code

Oblique injection of high-power atomic beams into the warm target plasma is assumed as the main method of heating in the GDMT facility. Injection leads to the formation of a population of fast “sloshing” (performing longitudinal oscillations between turning points) ions with a substantially non-Maxwellian distribution function and an average energy much higher than the temperature of electrons and target ions. Fast ions are confined in the adiabatic regime due to the conservation of the magnetic moment.

This section presents the results of the discharge simulation in the GDMT in the two-component plasma mode using the DOL code. This code was originally developed to optimize the parameters of a thermonuclear neutron source based on a gas-dynamic trap [66, 67]. The DOL (Russian acronym of Long Open Traps) code is intended for simulating axisymmetric linear traps in which powerful neutral injection is used as the main heating method [68]. Such traps are, e.g., the GDT and GOL-NB facilities [34] and the first stage of the GDMT project. The code allows simulating the accumulation of hot ions and their distribution function, as well as the time evo-

lution of the temperature and density of electrons and warm ions by numerically solving the kinetic equation for hot ions and equations describing the mass and energy balance in the target plasma. The simulation results are important for the analysis of the plasma stability and the choice of stable operating modes (in this section, stability is not considered, Subsections 3.4 and 3.5 are devoted to the analysis of MHD and kinetic instabilities), as well as for optimizing such GDMT parameters as the magnitude and profiles of the vacuum magnetic field, and the gas blowing rate.

In the DOL code, the plasma is assumed to be axisymmetric and to have a sharp boundary (the radial profiles for of all parameters are assumed to be rectangular). Radial losses are considered to be insignificant and are not taken into account, the dependence of the plasma radius on the longitudinal coordinate is found from the condition of the conservation of the magnetic flux inside the plasma column. In addition, the possibility of the excitation of kinetic instabilities is neglected and longitudinal transport is considered to be classical. The ion distribution function is divided into two parts: fast and thermal (target) ions. The methods for describing these components vary greatly.

To find the distribution function of fast ions, the non-steady-state kinetic equation is solved numerically. The following assumptions are made for this component:

1. collisions are considered to be quite rare, so the kinetic equation can be averaged over the period of bounce oscillations (we mean longitudinal oscillations of ions between turning points);

2. the phase distributions of the Larmor rotation and longitudinal motion are assumed to be uniform, which makes it possible to exclude this pair of variables from consideration;

3. the magnetic moment of the particles is considered to be conserved, which implies the smallness of the Larmor radius compared to the gradient dimensions of the magnetic field;

4. the difference in the ambipolar electrostatic potential is considered to be small compared to the energies of fast ions, which makes it possible to significantly simplify the parametrization of the phase space.

Taking into account these assumptions, the distribution function of fast ions, which depends on six coordinates, is reduced to the function $F(\epsilon, Y)$, where ϵ is the energy, and the variable $Y = \sin^2\theta$ is proportional to the ratio of the magnetic moment to the energy and describes the dependence on the pitch angle θ of the particles at the field minimum. The kinetic equation for ions of the α type is written as

$$\frac{dF_\alpha}{dt} = \sum_{\beta} C_{\alpha,\beta} + S_\alpha - L_\alpha,$$

where $C_{\alpha,\beta}$ is the operator of Coulomb scattering of α -type particles on β -type particles, the functions S_α and

L_α describe sources and sinks of particles. The equality of the distribution function to zero on the boundary of the loss cone Eq. (1) is used as a boundary condition. Coulomb collisions are calculated in terms of the Rosenbluth–Trubnikov potentials, which are calculated using the particle distribution function averaged over the pitch angle θ (the operator $C_{\alpha,\beta}$ conserves the energy). Sources of fast ions arise from the capture of atomic beams; in sinks, in addition to the loss cone, the charge exchange of fast ions on atomic beams is also taken into account.

Electrons and thermal ions of each type are described by a pair of parameters—the total energy W_α and the number of particles N_α (α is the type of particles). It is assumed that confinement of these particles is close to the equilibrium one, and the spatial distributions obey the Boltzmann law:

$$n_\alpha(z) = n_{0,\alpha} \times \exp(-e_\alpha\varphi(z)/T_\alpha),$$

where $n_{0,\alpha}$ is such a constant that the total number of particles in the trap is equal to N_α , T_α is temperature, and φ is the electrostatic potential determined from the quasi-neutrality equation. It should be noted that this formula gives an inaccurate estimate when approaching mirrors and is inapplicable to regions behind mirrors. However, the use of this formula is justified in the main volume of the central cell. The particle balance and energy equations

$$\begin{aligned} \frac{dN_\alpha}{dt} &= J_{\text{src},\alpha} + J_{\text{inj},\alpha} - \frac{N_\alpha}{\tau_{\parallel\alpha}}, \\ \frac{dW_\alpha}{dt} &= P_{\text{src},\alpha} + P_{\text{inj},\alpha} - \frac{E_{\parallel\alpha}N_\alpha}{\tau_{\parallel\alpha}} + \sum_{\beta} P_{\alpha,\beta}, \end{aligned}$$

take into account the sources of matter and energy associated with gas puffing and additional heating ($J_{\text{src},\alpha}$ and $P_{\text{src},\alpha}$), charge-exchange losses of matter and energy in beams ($J_{\text{inj},\alpha}$ and $P_{\text{inj},\alpha}$) longitudinal losses with the characteristic time $\tau_{\parallel\alpha}$ and average energy taken out of traps per particle, $E_{\parallel\alpha}$, and also energy exchange powers $P_{\alpha,\beta}$, due to Coulomb collisions with warm and fast plasma components. The main problem in this approach is the determination of the longitudinal loss rate. The analytical solutions are known for two limiting cases, the “kinetic” one, corresponding to the “classical” mirror cell in the limit of rare collisions [1] (see Eq. (2), formulas for estimating $\tau_{\parallel\alpha}$ and $E_{\parallel\alpha}$ are taken from [57, 68, 69], and “gas-dynamic” one, arising in the limit of frequent collisions [58] (see Eq. (3)). In the intermediate mode, when $L \sim \lambda_{ii}$ ($\ln R)/R$, we use the approximation:

$$\tau_{\parallel\alpha} = \tau_{\text{kin},\alpha} + \tau_{\text{gdt},\alpha}, \quad E_{\parallel\alpha} = \frac{\tau_{\text{kin},\alpha}}{\tau_{\parallel\alpha}} E_{\text{kin},\alpha} + \frac{\tau_{\text{gdt},\alpha}}{\tau_{\parallel\alpha}} E_{\text{gdt},\alpha},$$

where subscripts “kin” and “gdt” correspond to kinetic and gas-dynamic limits.

When calculating the magnetic field, the model assumes paraxiality: the curvature of the field lines is considered negligible, and the magnetic field perturbation is found from the balance of radial pressures

$$\frac{B^2}{8\pi} + p_{\perp} = \frac{B_v^2}{8\pi}.$$

Note that this expression is inapplicable near magnetic mirrors. However, this can be neglected, since the plasma pressure near the mirrors is low compared to the magnetic field pressure.

Based on this model, a 1D numerical code has been developed. Typical calculation time using the DOL code is from several hours to a day.

The configuration of the GDMT plant was simulated using the DOL code. The magnetic field profile was determined by the geometry and arrangement of the coils of the central solenoid C1–C5, transition and mirror coils. The currents in the coils of the central section can vary arbitrarily over a wide range, and the maximum achievable field in the center (see Subsection 2.1) is 1.5 T. The mirror sections have a fixed current, and the magnetic field on the system axis reaches a maximum value of about 20 T in them. The transition coils were chosen so that a region with a magnetic field of about 3 T was formed between the transition coils on each side of the facility. In the future, these regions can be used for ECR heating of the plasma. In the calculations, the currents in the coils were selected to obtain a region with a uniform magnetic field in the central region: the field in the central cross section had a given B_0 value, and the square of the field deviation from B_0 integrated over a 3.6 m long section at the center of the traps was minimized. The characteristic profiles of the magnetic field obtained as a result of this procedure are shown in Fig. 3, Subsection 2.1. The parameters of the atomic beams injected into the center of the facility were assumed to be as follows: the particle energy of 30 keV, the total power of 24 MW, the ratio of ion currents entering the accelerating system: 70% of the main component H^+ , 20% of H_2^+ molecular ions and 10% of H_3^+ molecular ions, the angle between the axis of the injector and the facility axis of 50.9° , the angular spread of the beam of 1.5° , the radius of the beams in the plasma region at a level of 0.37 is 8 cm. The plasma radius in the central cross section a (where it is the largest one) can vary from 10 to 30 cm; the lower limit is determined by the transverse size of the atomic beams, and the upper one is determined by the radius of the vacuum chamber. In addition, the plasma radius was limited by the maximum magnetic flux, $\Phi_{\max} = 1 \text{ T} \times \pi (30 \text{ cm})^2$, which passes the mirror without touching the facility walls.

To search for optimal operating modes, a series of calculations was carried out, the results of which are shown in Table 7. Calculations were performed for the

transition mode between gas-dynamic and kinetic ones: $\tau_{\text{kin}}/\tau_{\text{gdt}} \approx 3$. An important parameter is the ratio of the plasma radius to the Larmor radius of fast ions ρ_{inj} , for which the energy and pitch angle coincide with similar values for particles of atomic beams. The ratio a/ρ_{inj} affects the fraction of the energy contained in fast ions which is transferred to the cold peripheral plasma surrounding the main hot part of the plasma column in a real facility. We recall that the DOL code assumes that the plasma parameters are uniform along the radius. It should be noted that this quantity is $a/\rho_{\text{inj}} \approx 2.6$ for the GDT facility. In order to achieve agreement between the GDT experimental data and the DOL code simulation results, it is required to increase the energy losses of fast ions in calculations by a factor of two to three compared to the loss rate given by Coulomb collisions in the main part of the plasma column. Qualitatively, this can be estimated under the assumption that all fast ions reaching the plasma boundary are lost. Then the fraction of fast ions not lost during the first Larmor revolution lies in the range from $1 - \rho_{\text{inj}}/a$ for a thin beam to $(1 - \rho_{\text{inj}}/a)^2$ for a wide beam. This range is from 0.38 to 0.62 for the GDT facility (this agrees with the increase in the losses of fast ions in 2–3 times). The quantity a/ρ_{inj} was not less than 4 in the simulation of the GDMT facility. The DOL code apparently overestimates plasma parameters at the lower limit $a/\rho_{\text{inj}} = 4$. When this parameter increases to $a/\rho_{\text{inj}} = 7$, it can be expected that the losses in the peripheral plasma do not exceed a quarter of the trapped power. For comparison, Table 8 presents calculations of the same modes as in Table 7, but with the reduced trapped power; the highest reduction factor $(1 - \rho_{\text{inj}}/a)^2$ is taken.

A typical time dependence of plasma parameters is shown in Fig. 14. The density of fast ions and electrons increases, when fast atoms are injected. The energy is transferred from fast ions to electrons and target ions, which leads to an increase in their temperature. An increase in the density and temperature of the target plasma leads to an increase in the energy loss rate through mirrors up to a value equal to the input power. Since the time of the energy exchange through Coulomb collisions exceeds the time of the gas-dynamic outflow of the target plasma, the temperatures of ions and electrons in the steady-state state are not equal. The characteristic time of the transition to the steady-state state is on the order of the deceleration time of ions on electrons and is on the order of several tens of milliseconds at typical parameters.

The characteristic dependence of the density of fast and target ions on the longitudinal coordinate is shown in Fig. 15. Density peaks are formed at the turning point of fast ions. Due to the increase in the electron density at the turning points, the ambipolar potential peaks are also formed, which leads to a decrease in the density of target ions.

Table 7. Calculated plasma parameters

Relative plasma thickness a/ρ_{inj}	4				7			
	15		25		15		25	
Plasma radius a , cm	0.52		0.31		0.91		0.55	
Magnetic field in the center B_0 , T	0.52		0.31		0.91		0.55	
Injection power P_{inj} , MW	12	24	12	24	12	24	12	24
Ratio of the confinement times of warm ions τ_{kin}/τ_{gdt}	3.07	2.95	3.12	2.95	2.99	3.01	3.14	3.02
Effective confinement time of warm ions $\tau_{ }$, ms	3.0	3.2	5.7	7.3	1.8	1.7	3.0	2.8
Substance injection rate J_{src} , equiv. kA	1.15	2	1.25	2	1.35	2.6	1.6	3
Electron temperature T_e , keV	0.76	0.94	0.77	0.98	0.58	0.72	0.58	0.71
Temperature of warm ions T_i , keV	1.52	2.07	1.55	2.16	1.01	1.42	1.04	1.39
Relative pressure $\beta = 8\pi p/B_v^2$	0.39	0.64	0.60	0.84	0.11	0.20	0.18	0.32
Beam fraction trapped by plasma, %	73	91	80	94	61	81	70	88
Density of warm ions in the central plane, 10^{13} cm^{-3}	3.1	6.5	2.8	4.0	2.9	5.2	2.2	3.8
Density of fast ions in the central plane, 10^{13} cm^{-3}	3.0	4.6	1.6	2.2	2.6	4.6	1.6	2.7
Maximum density of fast ions, 10^{13} cm^{-3}	4.3	6.1	2.4	3.1	3.9	6.8	2.4	3.8

Table 8. Calculated plasma parameters taking into account the decrease in the power trapped from the heating beams in $(1-\rho_{inj}/a)^2$ times caused by energy losses of fast ions in the peripheral plasma

Relative plasma thickness a/ρ_{inj}	4				7			
	15		25		15		25	
Plasma radius a , cm	0.52		0.31		0.91		0.55	
Magnetic field in the center B_0 , T	0.52		0.31		0.91		0.55	
Injection power P_{inj} , MW	12	24	12	24	12	24	12	24
Ratio of the confinement times of warm ions τ_{kin}/τ_{gdt}	2.99	2.99	3.12	3.01	3.07	3.01	3.01	3.01
Effective confinement time of warm ions $\tau_{ }$, ms	3.0	3.0	5.4	6.8	1.9	1.7	3.1	2.8
Substance injection rate J_{src} , equiv. kA	0.66	1.3	0.75	1.39	1.35	2.0	1.2	2.3
Electron temperature T_e , keV	0.61	0.78	0.62	0.79	0.53	0.66	0.52	0.64
Temperature of warm ions T_i , keV	1.1	1.58	1.14	1.61	0.87	1.23	0.86	1.21
Relative pressure $\beta = 8\pi p/B_v^2$	0.22	0.42	0.37	0.64	0.08	0.15	0.13	0.25
Beam fraction trapped by plasma, %	53	77	62	83	50	73	59	81
Density of warm ions in the central plane, 10^{13} cm^{-3}	2.5	4.5	1.8	3.0	2.2	4.1	1.7	3.0
Density of fast ions in the central plane, 10^{13} cm^{-3}	1.8	3.2	1.1	1.8	2.0	3.6	1.2	2.2
Maximum density of fast ions, 10^{13} cm^{-3}	2.6	4.6	1.6	2.5	3.0	5.4	1.9	3.2

The simulation using the DOL code shows that discharges with the following characteristic parameters are achievable in the central cell of the first GDMT stage: the temperature of electrons and target

ions is about 1 keV, the density of warm ions is several units per 10^{13} cm^{-3} , the average energy of fast ions is about ten kiloelectronvolts, the densities of fast and target ions are comparable, the pressure of fast ions is

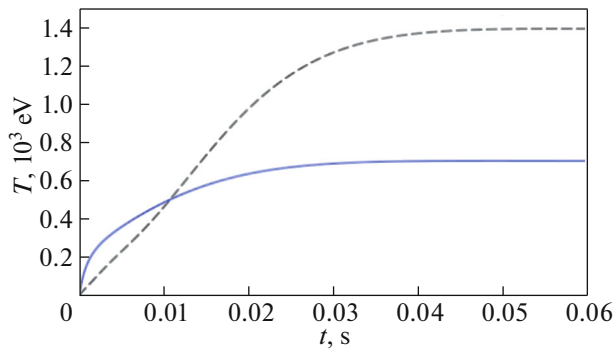


Fig. 14. Time dependence of the electron temperature (solid line) and temperature of warm ions (dotted line). The calculation corresponds to the last column of Table 7.

on the order of the pressure of a vacuum magnetic field. The target plasma temperature and the ion lifetime increase with a decrease in the blowing rate, while the confinement of target ions changes from gas dynamic to kinetic one. However, depletion of the loss cone during the transition to the kinetic confinement can provoke the drift-cone instability (see Subsection 3.5) and/or worsen the electrical coupling of the plasma with the end electrodes (see Subsection 3.4), which limits the achievable parameters. Apparently, in the optimal operating modes of the GDMT, the confinement of target ions is transitional between kinetic and gas-dynamic ones.

Due to the axial symmetry and quasi-one-dimensionality in the simulation using the DOL code, it is impossible to get answers to a number of important issues (these issues are discussed in the following sections):

- In regimes with weak gas blowing (the kinetic regime of the confinement of warm ions), the electrical coupling with the end plates can be greatly weakened because of the decrease in the longitudinal losses of the background plasma. Together with high β , this can worsen the MHD stability of the plasma. MHD plasma instabilities in the GDMT are discussed in Subsection 3.4.
- The distribution function of fast ions differs significantly from the Maxwellian one, which, in combination with high β , can provoke the excitation of kinetic instabilities and anomalous transport. Methods for suppressing anomalous transport are discussed in Subsection 3.5.
- In regimes with a small plasma radius and kinetic confinement of warm ions, β approaches unity, which actually corresponds to the transition to the diamagnetic confinement regime. Due to the use of a model profile for radial dependences, the DOL code describes the plasma with β close to unity incorrectly. The possibility of the transition to diamagnetic con-

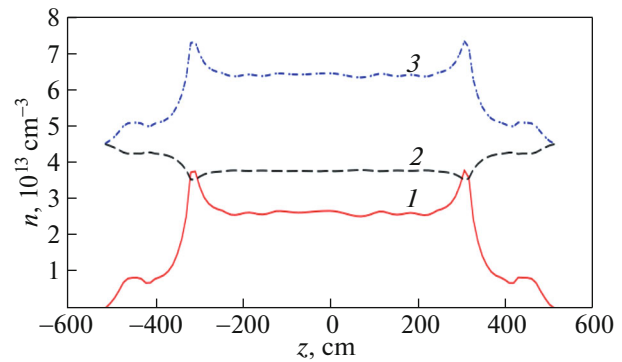


Fig. 15. Dependence of the concentration of fast ions (curve 1), target ions (curve 2) and electrons (curve 3) on the longitudinal coordinate. The calculation corresponds to the last column of Table 7.

finement of the plasma in the first stage of the GDMT is analyzed in Subsection 4.1.

Note that the above plasma parameters were obtained for the configuration without additional confinement improvers such as multiple-mirror and helical sections, as well as without additional ECR heating. The use of additional methods for suppressing longitudinal losses, as well as switching to the diamagnetic confinement regime, lead to a significant change in the parameters of the target plasma and hot ions. The expected plasma parameters when using additional loss suppression methods are discussed in Subsections 4.1 and 4.2.

3.3. Recycling and Gas Conditions in the Facility

3.3.1. Requirements for vacuum conditions in the central solenoid and expanders. A feature of linear magnetic traps for plasma confinement is a large circulating gas flow in the system, associated with a constant plasma flow from the confinement region at a rate of $\sim 10^{22} \text{ s}^{-1}$ and the corresponding flow of matter from the gas inlet system, which makes it possible to maintain a steady-state plasma density in the confinement region. In terms of vacuum requirements, this means that the plasma efficiently transports material from the central traps to the expander section, and is the powerful pumping means.

The main means of pumping hydrogen into the central trap are pumps with sprayed titanium getter mounted in the chambers of the neutral injection system and connected to the confinement chamber through nozzles with a total gas conductivity of higher than $500 \text{ m}^3/\text{s}$ for hydrogen (see Subsection 2.2). In addition to getter pumps with a total pumping rate to $18000 \text{ m}^3/\text{s}$, the facility is equipped with a set of turbo-molecular pumps providing pumping heavier gases and impurities, as well as keeping vacuum in the experiment standby mode.

In the standby mode, the residual gas flow into the vacuum chamber is determined by degassing from the walls. It is well known that the main fraction of the residual gas is water in an unheated vacuum system. A feature of the GDMT vacuum system are titanium arc sputtering pumps, which can efficiently pump out water vapor due to their reduction to titanium oxide and hydrogen, which is also absorbed by the getter pumps. Therefore, pumping of water from the central traps during the operation of titanium arc sputtering systems in the injection chambers also occurs through the neutral injection nozzles at a rate of several tens of m^3/s . This feature significantly speeds up the preparation of the facility chamber for experiments compared to using only turbomolecular pumps, which have limited performance due to long branch pipes with the low gas conductivity.

The impurity ions have a limited effect on plasma confinement in the GDMT because of the high heating power and relatively low energy lifetime of about 5 ms. The specific radiation power in the plasma does not exceed $10^{-25}n_en_{\text{imp}}[\text{W}/\text{cm}^3]$ in the temperature range up to 10 keV for most chemical elements [70]. It is possible to estimate the limiting content of impurities in the plasma on the basis of this specific radiation power value. For a typical GDMT scenario (column 3 of Table 7) ($n_e = 4.4 \times 10^{13} \text{ cm}^{-3}$, $a = 25 \text{ cm}$, $V = 1.6 \text{ m}^3$) the impurity concentration of $2 \times 10^{11} \text{ cm}^{-3}$ corresponds to a radiation power of 1.4 MW, which is 15% of the power of the neutral injection system trapped into the plasma. This estimate seems to be strongly overestimated for light impurities (such as oxygen and carbon), since at a plasma temperature above 100 eV, the specific radiation power of these impurities decreases in several times with respect to the maximum value corresponding to a plasma temperature of 15 eV. It should also be noted that, in contrast to tokamaks, the mechanisms leading to the accumulation of impurities in the hot plasma region are not known in the gas-dynamic trap.

An important issue is the influence of the gas absorbed on the walls on the plasma behavior in the GDMT facility. The characteristic number of water molecules absorbed on the surface is 10^{15} cm^{-2} [71]. These molecules can be desorbed during the discharge due to the irradiation of the wall with a flow of neutrals or ultraviolet radiation. The total number of molecules on the surface ($\sim 3.5 \times 10^{20}$) is much less than the amount of substance introduced into the plasma for replenishment (10^{22} s^{-1}), so that the effects of desorption from the walls can be expected to affect only the initial stage of the discharge for several tens of milliseconds. Despite this, the possibility of preparing the surface of the chamber is provided for by carrying out cleaning cycles with a constant low-power discharge introduced in the form of radio-frequency or microwave waves.

The input of the neutral gas into the plasma in the central section can significantly reduce the lifetime of fast ions due to charge exchange losses. Under a typical scenario of the facility operation (fast ion density of 10^{13} cm^{-3} , plasma density of $5 \times 10^{13} \text{ cm}^{-3}$, electron temperature of 0.8 keV, and plasma radius of 25 cm), the energy lifetime of fast ions is about 7 ms. The input of a hydrogen atom into the plasma leads to its charge exchange with a fast ion and the exit of the resulting fast neutral out of the plasma. We assume that thermal hydrogen molecules get on the plasma boundary, where they are ionized and partially dissociated with the formation of suprathermal (Franck–Condon) neutrals. For estimates, we assume that the flux of epithermal neutrals into the plasma is 10% of the total flux of molecules to the surface. Assuming the characteristic thickness of the layer on which ions interact with neutrals to be equal to the free path of Franck–Condon neutrals with respect to ionization (4 cm), we find that the characteristic charge-exchange lifetime of a fast ion becomes equal to its deceleration time in the plasma at the flux of epithermal neutrals through the plasma boundary of $8 \times 10^{15} \text{ cm}^{-2} \text{ s}^{-1}$ corresponding to the pressure in the vacuum chamber of $3 \times 10^{-3} \text{ Pa}$. We also note that the small path length of the thermal molecule with respect to ionization (less than 5 mm at a temperature above 10 eV and a concentration of $2 \times 10^{13} \text{ cm}^{-3}$) prevents gas pumping from the central section by the plasma flowing into the expander, since the gas coming to the surface of the plasma column is ionized with a high probability in the plasma located in the “shade” of the limiter, recombines at the limiter, and returns back to the vacuum chamber of the central section. The real situation has to be studied experimentally and, if necessary, additional measures to reduce the concentration of neutrals should be used.

3.3.2. Interaction of a plasma flow with a surface.

An ambipolar potential drop of about $5T_e$, which accelerates the ions leaving the central solenoid, should occur between the central region and the plasma absorbers in a GDMT facility. Thus, it is expected that the plasma absorbers is bombarded with ions having an energy of about 5 keV.

It is assumed that the surface of the plasma absorbers is made of molybdenum, which is considered to be most resistant to the formation of unipolar arcs. The path length of protons with an energy of 5 keV in molybdenum is about 20 nm. There is a significant scatter in the data on the diffusion rate of hydrogen in molybdenum [72], however, for estimates, the diffusion coefficient can be taken as $D[\text{m}^2/\text{s}] = 1.7 \times 10^6 \exp(-0.84/kT)$, where the temperature T is expressed in kelvin [73], which gives a characteristic diffusion depth during the time of the experiment (of 2 s) on the order of $1 \mu\text{m}$ at a surface temperature of 300°C . At a magnetic field expansion coefficient of 200, the relative concentration of hydrogen in the

metal in 2 s of irradiation reaches $n_{\text{H}}/H_{\text{Mo}} = 0.2$ in the absence of desorption.

Hydrogen implanted in the plasma absorber may be accumulated in the thickness of the material in the form of a solid solution or hydride or be desorbed from the surface of the plasma absorber into the plasma. The diffusion and desorption rates depend significantly on the presence of impurities in the material and on the surface, the amount of accumulated hydrogen and the surface temperature, so it is currently impossible to accurately predict the backflow of hydrogen atoms from the surface. In view of this, absorption and diffusion of hydrogen into the surface, which temporarily reduce the load on pumping systems during the pulse [74], and the release of additional hydrogen from the material due to the high energy of ions incident on a hydrogen-saturated surface [75] can be expected in experiments.

3.3.3. Processes with neutral hydrogen in the plasma in the expander. The most important processes involving molecular hydrogen in the expander plasma are electron impact ionization, charge exchange and elastic collisions.

The ionization rate of molecular hydrogen ($\text{H}_2 + e \rightarrow \text{H}_2^+ + 2e$) is about $5 \times 10^{-8} \text{ cm}^3/\text{s}$ at plasma temperatures in the range of 50–200 eV expected in an expander [76]. It should be noted that the H_2^+ molecules formed as a result of ionization dissociate with a sufficiently high probability in collisions with electrons $\text{H}_2^+ + e \rightarrow \text{H} + \text{H}^+ + e$ with the formation of a fast neutral. This reaction rate is about $10^{-7} \text{ cm}^3/\text{s}$. The cross section of resonant charge exchange on molecular hydrogen ($\text{H}_2 + \text{H}^+ \rightarrow \text{H}_2^+ + \text{H}$) at the ion energy of 5 keV is $1.2 \times 10^{-15} \text{ cm}^2$ that gives the reaction rate of $1.2 \times 10^{-7} \text{ cm}^3/\text{s}$.

In the expected operation scenario, the plasma density in the mirror is about $5 \times 10^{13} \text{ cm}^{-3}$. The outflowing plasma expands along the magnetic field lines and is accelerated by the ambipolar potential, so for estimates, it can be assumed that the plasma density at the plasma absorber (at the expansion ratio of 200) is on order of 10^{11} cm^{-3} .

The mean free path of a thermal hydrogen molecule with respect to ionization is about 20 cm at the plasma density of 10^{11} cm^{-3} . Thus, the behavior of neutral hydrogen depends essentially on the energy of molecules desorbed from the surface: the mean free path at thermal desorption is much smaller than the plasma diameter, while these dimensions become comparable at ion-stimulated desorption. In this case, there is a certain probability of an uncontrolled increase in the plasma density on the surface of the plasma absorber because of a positive feedback over density (molecular hydrogen desorbed from the surface is ionized, accelerated in the Langmuir layer on the surface, bombards and heats the surface, which

leads to an increase in desorption and an increase in the plasma density in the expander).

The plasma temperature in the GDMT is determined by the balance between energy inflow (when the energy is transferred from trapped fast ions and the microwave energy is absorbed during ECR heating) and its outflow. It can be assumed that the energy lost from the facility is released in the plasma absorbers due to the deceleration of the ions accelerated by the ambipolar electric potential that get into them, as well as thermal electrons. The presence of a neutral gas expander in the tank leads to an increase in energy losses from the plasma due to the formation of an electron-ion pair in the plasma due to ionization of a hydrogen molecule by the electron impact.

The energy transferred to the plasma absorber by such a pair is equal to the temperature of the plasma electrons in the central section by the order of magnitude. Taking the surface area of the plasma as $S = 1 \text{ m}^2$ and neutral gas density in the expander as $n_{\text{H}_2} = 10^{13} \text{ cm}^{-3}$, we obtain the equivalent flux of atoms getting into the plasma

$$F = 0.25V_{\text{TH}_2}2n_{\text{H}_2}S \approx 1000 \text{ equiv. A,}$$

where V_{TH_2} is the thermal velocity of hydrogen molecules.

The number of electron-ion pairs formed in the expander and the additional energy losses associated with them are comparable to the flow of ions flowing from the central section of the facility and the energy carried out by this flow at the specified gas density in the expander, so that the gas density in the expander should not exceed 10^{13} cm^{-3} for the effective plasma confinement.

It should be pointed out that the ionization path length of thermal molecules is less than the plasma radius in almost the entire expander, so that screening of the paraxial region from the neutral gas flow could be expected. In this case, however, there are mechanisms for the penetration of neutrals onto the axis of the plasma column (the formation of Franck–Condon atoms during the dissociation of hydrogen molecules, heating of the molecular gas during collisions with ions, etc.). To estimate the penetration depth of hydrogen into the plasma and the associated energy losses from the plasma, the numerical simulation of the behavior of the neutral gas into the expander is required.

3.3.4. Methods for replenishing plasma with substance. Plasma confinement regimes that are of interest for creating a neutron source are assumed to be studied in the initial configuration of the GDMT facility. In these regimes, the plasma is two-component, i.e., it includes the fraction of fast ions formed as a result of atomic injection and the target plasma with an ion temperature of about 1–2 keV. The confinement time of warm plasma is much less than the confinement time of fast ions and the time of experiment.

It is determined by gas-dynamic losses and is several milliseconds. The system of replenishing the plasma with substance serves to compensate for these losses and maintain a constant plasma density.

The most developed and simplest plasma replenishment method is the supply of gas (hydrogen) to the plasma boundary. The characteristic ionization time of hydrogen atoms penetrating into the plasma is several times longer than the characteristic time of their charge exchange on fast ions for the planned plasma parameters in the central section of the facility. As a result, gas puffing into the central region leads to high charge exchange losses. Based on this, the gas should be introduced into the plasma in the region between the turning point of fast ions and the mirror, while it is necessary to prevent the penetration of gas into the region of fast ion confinement.

The main difficulty in creating such a replenishment system is that the path length of a thermal hydrogen molecule in the plasma with respect to the electron impact ionization process $H_2 + e \rightarrow H_2^+ + 2e$ is less than 1 mm at the planned plasma parameters ($n_e = 5 \times 10^{13} \text{ cm}^{-3}$, $T_e = 800 \text{ eV}$), i.e., thermal molecules cannot penetrate into the central regions of the plasma. Franck–Condon atoms formed during the dissociation of H_2 and H_2^+ molecules can penetrate into the plasma somewhat deeper. At an atomic energy of 2 eV, their path length is determined by the resonant charge exchange ($H_2 + H^+ \rightarrow H_2^+ + H$) and is about 5 mm. The neutrals formed in this process with energies on the scale of the ionic temperature of the plasma have a free path on the scale of 10 cm and can freely penetrate into the plasma and exit it onto the chamber wall. An obvious disadvantage of this replenishment method is a significant energy flux (comparable to the plasma heating power) carried by neutrals to the wall of the vacuum chamber in the local region of gas puffing.

It should be noted that cold nonthermalized ions in the region near the mirror significantly affect the distribution of the electric potential along the facility axis and, accordingly, the confinement time of the thermal plasma component. In addition, an important issue is the power of radiation losses associated with the introduction of neutral particles into the plasma. For atomic hydrogen at a plasma temperature above 10 eV, the radiation energy per ionized atom is 10 eV and is almost temperature independent. Based on this, a simple estimate of the power consumption for ionization gives a value of $\sim 100 \text{ kW}$, which, however, can increase significantly when atoms interact with the lower temperature plasma due to an increase in the specific energy of line radiation.

Alternative technologies for replenishing plasma with substance should also be pointed out. Pellet injection is one of the main methods of plasma replenishment in tokamaks, which are in operation and

under construction. Pellet injection systems for tokamaks are well developed, however, the use of this method on open traps requires the solution of a number of fundamental issues. First, due to the short plasma confinement time, the pellet injection frequency should be at least 1 kHz, while the currently developed technologies allow the creation of modules with an injection frequency of up to 50 Hz [77]. In addition, one should take into account the features of the application of this method in GDMT related to its possible impact on confinement of fast ions, the MHD plasma stability, and the replenishment uniformity over the cross section.

Another frequently discussed replenishment method is the injection of dense plasma bunches across the magnetic field. The possibility of injecting a plasma bunch of 10^{19} particles into a GLOBUS-M tokamak with a magnetic field of 0.4 T to a depth of up to 40 cm was shown in [78]. At the same time, however, the current level of the development of this technology does not allow it to be considered as the main method of replenishment with substance but the development and testing of a prototype of such an injector is envisaged as part of the GDMT experimental program.

3.4. MHD Stability of Plasma

Plasma confinement time estimates in the GDMT are based on the assumption that the plasma is in a steady-state and axisymmetric equilibrium state. This can be considered if the plasma configuration is stable. If there is no MHD stability, flute or ballooning modes develop. They lead to plasma convection and, at the sufficiently large amplitude, to a dramatic decrease in the confinement time. Ensuring the MHD stability of the plasma in axisymmetric open traps is a complex problem, which is the subject of numerous works and constructive proposals summarized in a review [79]. Without taking special measures, the plasma in axisymmetric traps is MHD-unstable. Ensuring stability requires the creation of such zones in the trap, where the favorable shape of the magnetic field lines is combined with an increased plasma pressure. If the region of the expander behind the mirror is used as a stabilizer, then one the stability is compensated by a significant increase in longitudinal losses, and if this is a specially introduced non-paraxial cell, then the compensation is the need to reduce the ultimate plasma pressure (and thermonuclear efficiency) in the entire trap and the complication of the magnetic system.

Experiments at the GDT facility showed that the losses in case of refusing the MHD stabilization by expanders are less than the energy cost of maintaining sufficient pressure in them, when a special method of limiting convection is used. This method of limiting convection was called “vortex confinement” [36, 80] and has been used in the main operation mode of the

GDT facility for more than 10 years. Thus, the struggle to ensure the traditionally understood MHD plasma stability in the GDT was inexpedient. The mirror successfully operates in the regime with plasma oscillations around an axisymmetric unstable equilibrium [81], and no confinement degradation is observed. According to the project, it is planned to use the same vortex containment mode in a GDMT. Its effectiveness at $\beta < 0.6$ can be considered proven.

Flute and ballooning instabilities are distinguished by the limitations of the physical model: “flutes” are electrostatic, and are characterized by a constant perturbation potential along the equilibrium field line, and the description of ballooning modes is more complete, and takes into account the possibility of bending magnetic field lines during convection. If the flute modes are stabilized, then ballooning effects should be taken into account at high β . In reality, this is the same convective instability, and for any β , the “flutes” are slightly modulated along the magnetic field, but this may not have a strong effect on their dynamics. At high pressures $\beta > 0.6$, ballooning effects should become significant even in paraxial traps of the GDMT type. In particular, the effectiveness of end-face stabilization and vortex confinement methods should decrease. There is no experience of the GDT operation in such regimes, so we have to focus on theory [82]. For regimes with high β , in particular for the regime with a “diamagnetic bubble,” a stabilization method by a conducting wall has been developed, which can be combined with vortex confinement at the onset of the discharge.

3.4.1. Vortex confinement at low β . The vortex confinement regime requires maintenance of biasing potentials on the plates of radially sectioned endplates and/or limiters, i.e., the use of these surfaces in contact with the plasma as electrodes. The currents from the electrodes require a power supply system, i.e., the vortex confinement also has an energy cost. However, this cost is not too high: it is much less than the cost of longitudinal losses, and, in addition, part of the energy consumption remains in the plasma the same as from additional resistive heating. The use of electrodes has its own difficulties: it is necessary to maintain good contact with the plasma, while simultaneously suppressing electrode erosion and arc discharges to the chamber elements. To overcome them, the experience of the GDT operation is useful.

The vortex confinement method [36, 80] is based on three physical effects:

1. *Differential plasma rotation suppresses radial convection and sets the characteristic scale of plasma oscillations near axisymmetric equilibrium.* The effect of suppression of turbulent convective transport by the differential rotation is well known in tokamaks [83]. Its essence is that in a differential flow, flutes or convective cells extended along the radius are deformed and break up into smaller ones. In contrast to tokamaks, in

open traps of the GDT and GDMT types, the layer of the differential rotation in the plasma is not formed in a self-consistent way as a result of the nonlinear evolution of turbulence but is produced using boundary conditions (potentials on the electrodes). Its localization (in the flow layer projected onto the electrode junction) and amplitude are set by the experimentalist. It should be noted that the differential rotation does not affect the rigid mode $m = 1$ (where m is the azimuthal wavenumber), which corresponds to the displacement of the plasma as a whole along with the rotation.

2. *Closure of the longitudinal plasma currents to the endplates through the near-electrode potential jump creates an effective channel for dissipation of the fluctuation energy.* In the low-temperature plasma, when the potential jump is small and the potentials of the plasma and electrode are close, this closing of currents can be directly used for MHD stabilization (“line-tying”) [80]. Indeed, the origin of the flute instability is the polarization of the flux tubes when the axial symmetry is broken in a nonuniform magnetic field due to the incomplete closure of the azimuthal diamagnetic plasma current. Closing the excess current through the plasma absorber makes it possible to partially eliminate this polarization. Since the near-electrode potential jump is proportional to the electron temperature, dissipation is not sufficient for the complete MHD stabilization in the GDT and at the design parameters of the GDMT but it significantly inhibits convection. The deceleration of convection strongly affects the large-scale modes, having almost no effect on the short-wave flutes. This difference is due to the fact that the polarization current is inversely proportional to the azimuthal size of the flute. In this case, the same speed of “ascent” of the flute corresponds to the same azimuthal electric field, which means a smaller polarization potential difference and a smaller closing longitudinal current for flutes of a smaller azimuthal size. Thus, the effect of line-tying is proportional to $1/m^2$. In addition, the diamagnetic current, polarization, and the cross-field convection velocity are inversely proportional to the magnetic field in the trap, so that the line-tying works better in a high field.

3. *Stabilization of the MHD instability by the effect of the finite Larmor radius of ions (FLR effect) suppresses short-wave flutes in the presence of a significant population of injected fast ions* [80]. This effect is described by drift correction to the MHD equations. Its meaning is that the azimuthal diamagnetic current of ions has inertia (since its carriers, ions, have mass) and kinetic energy. The current flows along the constant pressure contour, and the kinetic energy is proportional to its length. For a circular contour, it is minimum, and increases rapidly when distorted by flutes. If the shape of the pressure profile is not distorted, the same as in the case of displacement of the plasma as a whole, then the effect is absent. The FLR effect increases with increasing the ion pressure fraction (as during the

beam heating in GDT and GDMT), but does not affect the rigid mode $m = 1$ at all.

Although the vortex confinement method is based on these three well-known effects, it is not limited to them. Indeed, the effects of the differential rotation and FLR do not affect the rigid mode $m = 1$ at all, and depolarization through the ends can only slow down the displacement of the plasma from the axis to the limiter, but not stop it completely. In this regard, the rigid mode $m = 1$ was considered the most dangerous for traps of the GDT type.

The vortex confinement theory [36, 80] predicts the possibility of the nonlinearly dissipative saturation of flute modes under the conditions of the above effects, even if these modes are unstable. The existence of such quasi-steady-state MHD oscillations in the gas-dynamic trap plasma may not lead to a noticeable degradation of confinement, and in the case of a negative applied potential to the central sections of the plasma absorber, cause a positive effect: discharge pinch. Indeed, quasi-steady-state modes $m = 1, 2$ and pinch of the population of fast ions are observed in the vortex confinement regimes in the GDT [81], which can be considered as a qualitative confirmation of the theory.

In the vortex confinement theory, four related conditions arise to ensure implementation of the regime with low convective losses:

1. The layer of the differentially rotating plasma should separate the inner and outer convection zones caused by the saturated mode. Plasma confinement is good enough only in the inner zone. This is implemented at a sufficient depth of the applied potential, and the radius of the differential rotation zone should be large enough.

2. The amplitude of the saturated mode with respect to the applied bias should not lead to the plasma drift beyond the limiter. This is realized at sufficiently large dissipation in the near-electrode layer (with a sufficiently strong current coupling of the electrodes with the plasma, i.e., a sufficient current of longitudinal ion losses).

3. The FLR effect should be sufficient to suppress higher azimuthal modes. If this condition is not met, then the convective losses increase due to the connection of the outer and inner convection zones through multiple x -points of the separatrix.

4. The created differential rotation of the plasma should not itself lead to the excitation of new instabilities, in particular, the Kelvin–Helmholtz instability. To this end, the effective viscosity from the FLR effect and the near-electrode dissipation should be sufficient for its stabilization (and the potential for rotation generation cannot be too large).

These conditions are related, since the width of the differential rotation layer at a given potential determines the velocity, and cannot be less than the mode saturation amplitude with respect to the displacement.

As a result, with realistic parameters, it turns out to be comparable with the plasma radius. This hinders the idea of generating multiple layers of differential rotation to improve confinement. In addition, various types of possible MHD instabilities in gas-dynamic traps (flute, centrifugal, temperature-gradient and Kelvin–Helmholtz ones) at low β are all “flute” ones in the spatial structure and differ only in the dominant type of excitation. Therefore, conditions 1–4 also take into account convection during their development.

Failure to meet conditions 3 and 4 does not lead to a complete loss of vortex confinement but reduces its efficiency (transverse diffusion increases). It is quite difficult to ensure their implementation during the entire discharge. Indeed, the relative magnitude of the FLR effect is determined by the ratio of the drift magnetic velocity to the velocity $E \times B$ of the drift, $|\nabla p_i|/en |\nabla \phi|$, where p_i is the ion pressure, n is the density, ϕ is the plasma potential. In general, the plasma potential is not equal to the potential applied to the electrodes but depends on the effective viscosity of the plasma and the discharge scenario, e.g., angular momentum injection with atomic beams. In experiments on GDT and in simulations, the FLR efficiency for fulfilling conditions 3 and 4 in a quasi-steady-state discharge is sufficient if $U = P_i/en\phi \sim 5$, where P_i is the ion pressure on the axis. Such a ratio can be maintained using feedback or programming of the applied potential, but this has not yet been verified in experiments. Below we obtain vortex confinement scalings based on conditions 1 and 2 for two cases: “with strong FLR effect,” $U > 5$, and with “weak FLR effect.”

For discharges with a weak FLR effect, condition 1 is formulated in theory [35, 80] as

$$\kappa/H < 0.2,$$

where the dimensionless parameters κ and H are responsible for the increment of the flute instability and the near-electrode dissipation rate, respectively. At a parabolic radial pressure profile and paraxial equilibrium, they can be approximately written as:

$$\kappa = 2 \left(\frac{T_e}{e\phi} \right)^2 \left(\frac{a}{\rho_*} \right)^2 \left(\frac{a}{L_\kappa} \right)^2 \left(\frac{P_i}{P_e} + 1 \right),$$

$$H = \frac{1}{R_{\text{eff}}} \left(\frac{T_e}{e\phi} \right) \left(\frac{a}{\rho_*} \right)^3 \frac{a}{L_p},$$

so the first condition looks like

$$R_{\text{eff}} \left(\frac{T_e}{e\phi} \right) \frac{\rho_* L}{L_\kappa^2} \left(\frac{P_i}{P_e} + 1 \right) < 0.1.$$

Here, the plasma parameter values are reduced to the value on the magnetic axis in the central cross section of the trap, a is the radius of the differential rotation layer (on the order of the plasma radius), ϕ is the potential difference across the vortex confinement

electrodes, ρ_* is the Larmor radius calculated from the ion mass and electron temperature, L_p is the effective length of the trap from the plasma mass density, L_κ is the effective length of the trap calculated from the mean curvature of the field with the longitudinal pressure distribution weight, R_{eff} is the effective mirror ratio of the trap.

In the notations of [35, 80], the effective length of the trap in terms of the plasma mass density is

$$L_p = \int \frac{\rho(z) B_0(0)}{\rho(0) B_0(z)} dz,$$

where density ρ is taken on the plasma axis, and $z = 0$ is the center of the device; the effective length of the trap calculated from the mean curvature of the field is:

$$L_\kappa^2 = 1/\langle B(z)\alpha(z)g(z) \rangle,$$

where $g(z) = p(z)/p(0)$ is the pressure weight function, angle brackets mean averaging along the field line, and $\alpha(z)$ characterizes the paraxial magnetic well in accordance with $1/B = 1/B_0(z) + \alpha(z)r^2$. In a vacuum field $\alpha = (2B_0 B_0'' - B_0'^2)/8B_0^3$, and $\alpha > 0$ corresponds to the unfavorable curvature of the field lines. The positive L_κ^2 values correspond to the linear instability of the flute modes, which is typical for an axisymmetric mirror cell without special stabilizers and for GDMT. The system is linearly stable at $L_\kappa^2 < 0$ and should be operable even without the vortex confinement. The parameter L_κ depends not only on the configuration of the magnetic system, which is variable in GDMT, but also on the operating mode of the facility: the height of the pressure peak of sloshing ions and the flow regime in the expanders. The expected L_κ values vary from 1 to 10 m in the range of design parameters of the first phase of the GDMT. In a configuration with multiple-mirror sections, the range is likely to shift towards lower values, which correspond to more unfavorable curvature and stronger linear instability.

Another complicated parameter is R_{eff} . The connection of the plasma with the electrodes of the plasma absorber is characterized by the density of the ion current on them, and the natural parameter for normalizing this current is the current of plasma ions with the thermal velocity. If we refer both to the flux tube, we get

$$R_{\text{eff}} = \tau_{\parallel} v_* / L_p,$$

where $v_* = \sqrt{T_e/M_i}$, τ_{\parallel} is the lifetime of ions in terms of longitudinal losses. In the classical gas-dynamic regime of longitudinal losses with cold ions, $R_{\text{eff}} = R = B_{\text{max}}/B_{\text{min}}$. However, the possibility of moving towards the kinetic regime is considered for the GDMT, which means a decrease in the loss rate compared to the gas-dynamic one. This is equivalent to the increase in R_{eff} compared to the magnetic mir-

ror ratio. Multiple-mirror sections should produce the same effect. The operation with a wide range of field values at the center of traps at a constant field in mirrors and at different density values is provided for in the first phase of the GDMT. This means that a trap has to work in a wide range of R_{eff} values.

In terms of the first vortex confinement condition, the higher the applied potential ϕ , the better. Nevertheless, the GDT experience shows that the optimal (in terms of efficiency and experimental feasibility) vortex confinement potential is of the order of the electron temperature. A lower one is ineffective, and a higher one does not improve anything, in particular due to the reduction of the FLR effect and the generation of Kelvin–Helmholtz instability but increases the likelihood of arcing. For further estimates, we assume that $e\phi/T_e \sim 1$. In addition, the ratio of ion and electron pressures in a trap with injection can be roughly estimated $P_i/P_e \sim 5$ that corresponds to the best GDT regimes.

Taking into account the above, the scaling of the first vortex confinement condition for GDMT with a weak FLR effect in the regime of gas-dynamic losses from a plasma with a fixed field in a magnetic mirror and with sloshing ions can be represented as $T_e^{1/2} B^{-2} < C$, i.e., as the condition limiting the electron temperature versus the magnetic field at the center of the trap $T_e^{\text{max}} \propto B^4$.

The second condition, the constraint on the saturation amplitude of the mode or the width of the vortex layer, is written as $\Delta/a = 2\xi_d = 2.34(f/H)^{1/3} < 1$ in the notation of [35, 80], while $f = -2\kappa P_0' m^2 \xi_d / 3H$, where m is the number of the dominating mode, and $P_0' \approx -0.8$ is the characteristic of the radial pressure profile. From here we get $\xi_d^3 = -3.2\kappa P_0' m^2 \xi_d / 3H^2$. If the FLR effect is insignificant, then the mode corresponding to approximately circular convective cells in the vortex layer dominates: $m \sim \pi/\xi_d$ (in the opposite limit $m = 1$). Now the condition $2\xi_d < 1$ can be rewritten as

$$2.5R_{\text{eff}} \left(\frac{\rho_*}{a} \right)^2 \frac{L_p}{L_\kappa} \sqrt{\left(\frac{P_i}{P_e} + 1 \right)} < 1/2\pi.$$

Thus, the second condition, the same as the first condition, gives a constraint on the electron temperature with a slightly weaker scaling, $T_e^{\text{max}} \propto B^3$, and, what is important, determines the minimum plasma radius a .

At the strong FLR effect ($P_i/en\phi > 5$) the first condition of the vortex confinement should be replaced by a softer one

$$\kappa/H < 2H^{1/3},$$

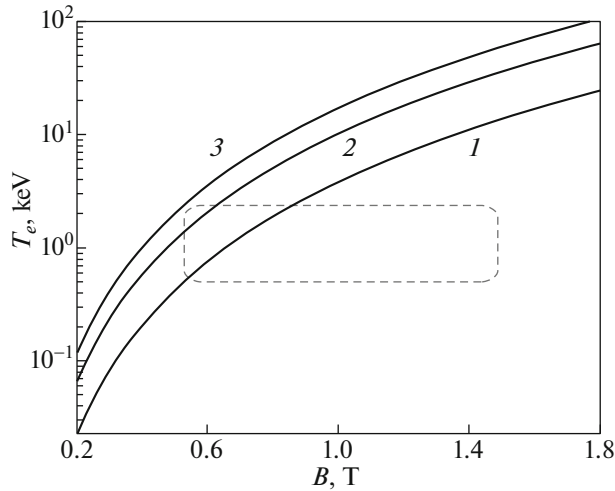


Fig. 16. Maximum operating electron temperature values in GDMT under vortex confinement as a function of the magnetic field at the center of the trap. Graphs are presented that take into account both criteria for different parameter values L_κ (which characterizes the length of a trap according to the curvature of field lines): $L_\kappa = 1$ m (curve 1), $L_\kappa = 3$ m (curve 2) and $L_\kappa = 10$ m (curve 3). Dotted line shows the zone of GDMT target parameters.

since the increment of the mode $m = 1$ is strongly suppressed by the end dissipation. After transformations, this criterion can be rewritten in the form

$$R_{\text{eff}} \left(\frac{T_e}{e\phi} \right) \left(\frac{\rho_*}{L_\kappa} \right)^{3/2} \frac{L_p}{a} \left(\frac{P_i}{P_e} + 1 \right)^{3/4} < 1.$$

This corresponds to the limiting temperature scaling of the form $T_e^{\text{max}} \propto B^{10/3}$. The condition on the vortex layer thickness: $m = 1$ and $\xi_a^2 \approx \kappa/H^2$ becomes softer (by a factor of 2π times) at the strong FLR effect, so after substitution, we have

$$2.5 R_{\text{eff}} \left(\frac{\rho_*}{a} \right)^2 \frac{L_p}{L_\kappa} \sqrt{\left(\frac{P_i}{P_e} + 1 \right)} < 1.$$

In this case, the temperature scaling is the same as for the weak FLR effect, $T_e^{\text{max}} \propto B^3$.

We use the vortex confinement criteria corresponding to the strong FLR effect and $e\phi/T_e = 1$ for the graphical presentation of the results. To estimate the gas-dynamic losses, we take the magnetic field value in the mirror as 12 T. The FLR effect corresponds to a large fraction of sloshing ions in the pressure, $P_i/P_e = 5$. Then it occurs that the criteria determine the maximum operating values of the electron temperature depending on the magnetic field in the center of the trap. The transition to the kinetic mode of longitudinal confinement at low density and high temperature of the background plasma *reduces* the

threshold of vortex confinement (compared to the plots presented) in proportion to the decrease in the longitudinal ion current of losses compared to the gas dynamic one. The results taking into account both criteria are shown in Fig. 16.

As can be seen from Fig. 16, in accordance with the theory, the vortex confinement mode is effective in most cases. Stability problems can arise at the attempts of the transition to the kinetic longitudinal confinement regime at a low target plasma density and a low magnetic field at the center of the trap. For a magnetic field higher than 0.5 T, confinement problems are not expected. Strong favorable scaling of the vortex confinement threshold with a magnetic field ($T_e^{\text{max}} \propto B^{3...4}$) makes it possible to consider this method as a potential fusion technology.

There are indications that convection in open traps can be suppressed by the shear flow beyond the boundaries of the vortex confinement regime as well, when the current coupling between the plasma and end electrodes is negligible [84–86]. This may become relevant for a complete GDMT version with multiple-mirror sections and strong longitudinal loss suppression. To maintain such a regime, the technology of radially nonuniform ECR heating, as in GAMMA-10, or other methods of maintaining the shear rotation are required.

3.4.2. Stabilization of ballooning modes by a conducting wall. An important component of the GDMT physics program is the implementation of the plasma confinement regime with maximum pressure $\beta \approx 1$, in which, presumably, the energy confinement time should increase (see Subsection 4.1). In this mode, as well as on the way to it at the start of the discharge from standard low-pressure operation modes, it is necessary to take into account the possibility of developing the ballooning instability.

Compared to standard conditions, two important effects should be taken into account in high-pressure plasma regimes: (1) the significant change in the equilibrium magnetic field including the curvature of its field lines compared to the vacuum configuration; (2) the possible curvature or modulation of the flutes during convection. The possibility of the flute modulation along the trap becomes especially pronounced in the limit of the relative plasma pressure $\beta \rightarrow 1$, so that any form of the line-tying stabilization, including the vortex confinement, should lose the effectiveness. Fortunately, in the same limit, the magnetic interaction of the plasma with the surrounding conductors becomes effective (through the eddy currents induced in them during the motion of the plasma). This interaction can be effectively used to stabilize large-scale modes such as the rigid mode $m = 1$, while the stability of higher modes is still provided by the FLR effects [79, 82].

It was shown in [82] that for a sufficiently smooth magnetic field at the center of a trap and at a suffi-

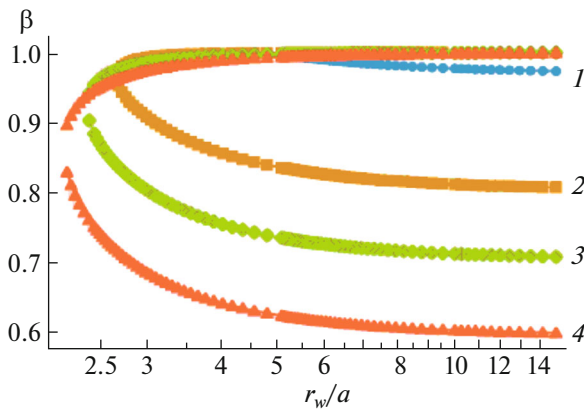


Fig. 17. Boundary of the linear MHD stability as a function of the relative distance from the plasma to the conducting wall at a mirror ratio $R = 24$ for various radial pressure profiles from [82]. It can be seen that stability can be ensured for all β at a sufficiently close wall ($r_w < 2a$).

ciently sharp plasma pressure gradient at the edge of the discharge, it is possible to ensure the ballooning stability of the system using a cylindrical conducting wall including transient regimes. The smooth shape of the equilibrium field lines provides a low energy gain during convection, and a large gradient at the edge contributes to the exit of the diamagnetic plasma field to the conducting wall.

An example of calculating the stability limit of ballooning modes from [82] is shown in Fig. 17. The dependence of the transverse plasma pressure p on the magnetic field flux Ψ in the form $p(\Psi) = p_0(1 - \Psi^k/\Psi_0^k)$ at $\Psi < \Psi_0$ and $p = 0$ at $\Psi > \Psi_0$ is used in the calculations. The variants of the curves for $k = (1, 2, 4, \infty)$ correspond to an increase in the pressure gradient towards the edge of the discharge. A sharp gradient at the edge (∞) improves the wall stabilization at high β while reducing stability at low pressure. The plasma stability at small β in the model is ensured by ideal line-tying, which is not implemented at the GDMT parameters. However, from the point of view of the stability of ballooning modes, it can be considered as a rough equivalent of the “vortex confinement,” since both are end effects that depend on the electrical contact of the plasma with the plasma absorber.

When designing the GDMT magnetic system, special care was taken to ensure that the high-pressure equilibrium field lines at the center of the trap remain sufficiently smooth up to the turning point of the fast ions (see Subsection 4.1). Beyond the turning point, there is a rapid drop in the plasma pressure, the discharge narrows, so that a large unfavorable curvature of the field lines becomes inevitable. Fortunately, the diamagnetic field lines emerge from the plasma in this zone (similarly to how a radial magnetic field is localized near the ends of a permanent magnet), so that the

local stabilization of ballooning modes by a conducting wall is possible exactly where necessary.

A large pressure gradient at the discharge edge in GDMT is also implemented, while in a natural way and only at high β . Indeed, it is shown in the calculations of the diamagnetic confinement regime (at a limiting pressure) that when the magnetic field is expelled from the plasma, the radial transport coefficients increase in the inner zone, so that the pressure gradient there is small (Subsection 4.1). The entire pressure drop is concentrated precisely on the boundary of the “diamagnetic bubble.”

It is impossible to provide a complete ideally conducting wall around the discharge as in theory. However, this is not required. As noted above, in the central part of the GDMT, the diamagnetic plasma field is concentrated inside the discharge, and the destabilization is small, so that a conducting wall plays no role, and it is not specifically provided for there. Behind the turning points of fast ions, where the danger of exciting ballooning modes is really great, and the plasma field “falls out” outward, it is planned to install massive conducting stabilizers with cuts.

It is well known that the stabilization method by a conductive wall is limited by its resistivity, since the eddy currents decay with time. Tokamaks have developed a way to overcome this shortcoming: spinning the plasma, so that the modes rotating with it become rapidly variable in terms of the wall conductivity, and the eddy currents do not decay. The rotation of the plasma and unstable modes fits very well with the “vortex confinement” support system. Indeed, in the case of vortex confinement with the help of electrodes and external current sources, fast rotation of the plasma is maintained in the layer located namely at the edge of the plasma. The flute modes observed in the GDT and in the simulation are indeed rotating, with characteristic frequencies between 5 and 20 kHz. The same frequencies are expected in the GDMT, which allows the use of copper stabilizers with a thickness of about 1 cm. The thickness and conductivity of the stabilizers also cannot be too large, since the magnetic field should penetrate into them in the characteristic time of the equilibrium pressure evolution on the order of 10 ms.

The problem of the stabilization of high-pressure modes similar to the stabilization of the rigid ballooning mode $m = 1$ in the GDMT by a conducting wall was previously successfully solved in the FRC C-2W facility [46]. Active magnetic coils and feedback circuits were installed as stabilizers there. However, the system showed operability in the passive mode, with shorted coils. There is a fundamental possibility of using similar approaches for the GDMT facility.

3.4.3. Stabilization methods in the GDMT. Thus, in order to maintain the MHD stability and suppress the plasma convection, the GDMT design includes a number of special measures:

1. The system for generating and maintaining differential plasma rotation using end electrodes, limiters and external current sources, which ensures the implementation of the “vortex confinement” mode at $\beta < 0.6$ and rotation of ballooning perturbations at higher pressures;

2. Magnetic system that provides a fairly smooth magnetic field in the central part of the trap, including at extreme plasma pressures;

3. External passive stabilizers of ballooning modes with a “conducting wall” function located near the turning points of sloshing ions.

With this in mind, the available experimental and theoretical data and their moderate extrapolations make it possible to hope for the successful operation of the GDMT facility in the target regimes. Since the most dangerous is the large-scale mode $m = 1$, in case of insufficiency of passive methods for suppressing the convection, it is possible in the future to develop and install active feedback stabilizers.

3.5. Kinetic Plasma Instabilities

In the two-component plasma regime, the distribution function of ions noticeably differs from the Maxwellian one in the central cell of the GDMT. This can provoke instabilities of relatively high-frequency and small-scale oscillations (kinetic instabilities). The interaction of plasma particles with these oscillations can lead to collisionless scattering and anomalous loss of particles from traps. Various kinetic instabilities can be developed in open traps (see, e.g., review [4]); however, in open traps with injection of powerful neutral beams, two instabilities are usually observed: Alfvén ion cyclotron (AICI), drift-cone (Drift-cone) Cyclotron Loss-Cone, DCLC) and double-humped (Double-Humped, DH) instabilities. It should be emphasized that this section considers the stability of a plasma with a finite but moderate relative pressure $\beta < 1$.

3.5.1. Alfvén ion-cyclotron instability. AICI is the electromagnetic instability, the excitation of which leads to the generation of waves with elliptical polarization propagating along the magnetic field [87]. The frequency of unstable perturbations ω is less than the cyclotron frequency of ions Ω_i . Since the excitation of the instability is accompanied by a perturbation of the magnetic field, AICI can be developed only when the ratio of the plasma pressure to the magnetic field pressure β exceeds the threshold value. Unstable perturbations receive the energy when interacting with resonant ions, the longitudinal velocity v_{\parallel} of which satisfies the cyclotron resonance condition

$$v_{\parallel} = v_{\text{res}} \equiv \frac{\omega - \Omega_i}{k_{\parallel}}, \quad (5)$$

where k_{\parallel} is the longitudinal component of the disturbance wave vector.

A necessary condition for the instability is the positiveness of the imaginary part of the ion contribution to the permittivity:

$$\text{Im}(\epsilon_+^{(i)}) \sim \frac{\omega_{\text{pi}}^2}{\omega^2} \int_0^{\infty} dv_{\perp} v_{\perp}^2 \left(v_{\perp} \frac{\partial f_i}{\partial v_{\parallel}} + \frac{\Omega_i}{k_{\parallel}} \frac{\partial f_i}{\partial v_{\perp}} \right) \Big|_{v_{\parallel}=v_{\text{res}}} > 0, \quad (6)$$

where $\epsilon_+^{(i)}$ is the contribution of ions to the dielectric response of the plasma for the circular component of the electric field in the direction of the cyclotron rotation of ions, the function $f_i(v_{\perp}, v_{\parallel})$ describes the ion distribution over the transverse v_{\perp} and longitudinal v_{\parallel} velocity components, $\omega_{\text{pi}} = (4\pi n_i e_i^2 / m_i)^{1/2}$ is the plasma frequency of ions. The condition Eq. (6) is the requirement that the derivative of the distribution function (inverse population) be positive along the invariant of motion along the perturbed trajectory $v_{\perp}^2 + (v_{\parallel} - \omega/k_{\parallel})^2 = \text{const}$ for resonant ions. Note that an increase in the angular width of the ion distribution function (e.g., due to an increase in the angular spread of the atomic injection) reduces the derivative of the distribution function along the trajectory of perturbed motion, which reduces the destabilizing contribution of resonant ions and contributes to the stabilization of AICI [88–91].

The experimental observation of AICI on the TMX [92, 93], GAMMA-10 [94] and GDT [95–97] facilities shows that a decrease in the ratio of the transverse to instability anomalous loss of fast ions. Thus, at the GAMMA-10 facility, the use of ICR heating leads to a strong anisotropy of the ion distribution function, which provokes the excitation of AICI [94]. The instability limits the anisotropy of the hot ions, which increases the longitudinal losses of the hot ions and limits the plasma density and pressure. Normal injection of atomic beams into the end mirror cells was used at the TMX facility for creating ambipolar barriers. Due to the high anisotropy of fast ions in the end mirror cells, AICI was excited [92], which led to heating of ions in the central cell and their loss through ambipolar barriers [93]. No AICI was observed on the TMX-U facility with oblique atomic injection into the end mirror cells [98]. The AICI-induced anomalous losses of fast ions in most regimes do not exceed the classical ones at the GDT facility, in whose plasma a population of fast ions is created by oblique atomic injection [96].

The strong influence of the injection angle on the anomalous loss of ions caused by AICI is apparently explained by the fact that in the case of oblique injection, only a small fraction of ions (with the energy close to the injection energy) can resonantly interact with an unstable perturbation. On the one hand, this leads to an increase in the critical β , at which the instability develops, and a decrease in the amplitude of unstable oscillations. On the other hand, as the frac-

tion of resonant ions in the plasma decreases, and the fraction of fast ions lost due to interaction with the wave decreases as well (the theoretical consideration shows that mainly the ions with a low transverse velocity and a longitudinal velocity close to the longitudinal velocity of the injected atoms are lost [99], the fraction of such ions is small). The main effect of the development of AICI in the plasma of open traps with oblique atomic injection is to increase the angular width of the ion distribution function, which has little effect on their confinement but can limit the height and minimum width of the fast ion density peaks (and, accordingly, the density neutron flux) at turning points.

The threshold β value, above which AICI is excited, depends significantly on the geometry of the vacuum magnetic field in the two-component plasma confinement mode at the GDMT facility under the planned parameters (hydrogen plasma, electron density $n_e \approx 5 \times 10^{13} \text{ cm}^{-3}$). If the bulk of the plasma is in the region of a long (about 4 m) uniform magnetic field, then there is no stabilization of the AICI by the longitudinal nonuniformity, since the wavelength of the unstable perturbation $2\pi V_A/\Omega_i \approx 2 \text{ m}$ is less than the length of the uniform field section. Direct numerical calculations using the methods described in [91] predict the AICI excitation with a frequency on the order of $0.5\Omega_i$ and an increment on the order of $10^{-2}\Omega_i$ in most operation modes with a uniform field section described in Section 3.2. At the same time, a change in the geometry of the magnetic field (replacement of a long section with a uniform field by a region with a magnetic field increasing from the center to the mirrors) seems to be an effective way to stabilize AICI if the characteristic scale of the magnetic field doubling is comparable with the perturbation wavelength. An operation mode with a nonuniform field in the main plasma confinement region is also provided in the GDMT project, see Fig. 3 in Section 2.1. The decrease in the density and reduction of the radius of the target plasma can also be used as stabilization methods.

The issue of the AICI effect on the confinement of fast ions in GDMT remains open at present. Because of the strong stabilization of AICI by longitudinal and transverse inhomogeneities, the β value achieved in the experiment at the GDT facility is close to the threshold value. Therefore, AICI is weak: the perturbation is almost monochromatic, and one spatial perturbation mode is observed [95]. In addition, the deceleration time of fast ions in the GDT (on the order of 1 ms) is relatively short: a fast ion has time to fly through the central region (where the resonant interaction with the wave occurs) only about thousand times. Under these conditions, many nonlinear effects have no time to be manifested, and the AICI effect on confinement of hot ions in the plasma is reduced to an increase in the angular spread of ions with an energy close to the injection energy, as well as diffusion along the pitch angle and anomalous longitudinal losses of

ions with a high longitudinal velocity and pitch angle close to the boundary of the loss cone [96, 99]. Since a higher electron temperature is expected in GDMT, the planned ratio of the deceleration time of a fast ion to the period of bounce oscillations is an order of magnitude larger than that in GDT. Under these conditions, AICI can become an important factor limiting the lifetime of fast ions. The study of anomalous losses of fast ions, optimization of the magnetic field configuration, target plasma parameters and injection are one of the scientific tasks of the GDMT operation.

The AICI effect on the loss during the transition to the diamagnetic confinement mode should be discussed separately in Section 4.1. On the one hand, the cyclotron resonance condition Eq. (5) cannot be satisfied at $\beta \approx 1$, and AICI apparently stabilizes. On the other hand, at the stage of accumulation of fast ions, AICI can provoke additional losses of fast ions and limit the maximum plasma pressure. We note that strong anomalous losses were one of the factors that limited the plasma pressure in the experiment with an attempt to reverse the field at the 2XIIB facility [100]. In addition, the stabilization by a longitudinal inhomogeneity is impossible in this regime, since a long section of a uniform field is important for the formation of a diamagnetic “bubble.” The need to reduce the anomalous losses caused by AICI during the transition to the diamagnetic confinement regime may require a decrease in the plasma radius to a value close to the Larmor radius of fast ions, and an increase in the angular spread of fast ions by varying the injection angle for different atomic injectors.

3.5.2. Drift-cyclotron-loss-cone and double hump instabilities. Drift-cyclotron-loss-cone (DCLC) and double hump (DH) instabilities are quasi-potential kinetic instabilities, the excitation of which leads to the generation of potential waves propagating in the azimuthal direction [101, 102]. The frequency of such oscillations ω is on the order of the ion-cyclotron frequency Ω_i , the transverse wavelength is small compared to the Larmor radius of ions (respectively, the dependence of the potential perturbation on the azimuthal angle is described by the expression $\exp(im\theta - i\omega t)$ with large azimuth numbers $|m| \sim 10-100$). Since the perturbation frequency is small compared to the electron plasma frequency, the potential perturbation levels off along the field line and a quasi-flute spatial structure of unstable oscillations is formed. The linear stage of DCLC and DH instabilities is described by a common dispersion relation, and formally they differ only in the excitation mechanism: DCLC develops due to the depletion of the distribution of ions in the low-energy region (e.g., due to the presence of a loss cone) and transverse plasma nonuniformity, and DH instability develops due to the difference in the average transverse velocities of fast and target ions, similarly to two-stream instability (and therefore can oscillate even in a uniform plasma).

If the distribution of fast ions is depleted at low energies and there are no warm Maxwellian ions, i.e., $F_i(v=0) = 0$, the DCLC instability develops already at a very weak transverse nonuniformity, when the plasma radius is equal to several hundred Larmor radii of ions, and the instability increment can exceed the cyclotron frequency of the ions. The addition of warm Maxwellian ions stabilizes the DCLC when their density reaches a few percent. However, if the temperature of the warm ions is too low, their addition may provoke the DH instability. An increase in the temperature of warm ions “covers up” the dip in the distribution of ions at low energies and contributes to the stabilization of the DH instability. In general, at a fraction of warm Maxwellian ions of a few tenths of the density of fast ions and at a temperature exceeding a few percent of the average energy of fast ions, the DCLC and DH instabilities are stabilized [103, 104].

The effects of finite β make it possible to increase the critical plasma gradient, at which DCLC develops, by several times [105]. The longitudinal plasma nonuniformity reduces the size of the region, in which unstable perturbations efficiently exchange energy with ions and contributes to the stabilization of DCLC and DH instabilities. An additional stabilizing factor can be absorption of the vibrational energy in the regions of the trap filled with cold Maxwellian ions, e.g., in expanders [101, 106]. Since unstable perturbations are extended along field lines, DCLC and DH instabilities can be stabilized by the shear of the magnetic field [101].

In general, the stability limit for DCLC and DH instabilities is sensitive to the low-energy ion distribution and, as a consequence, to the spatial distribution of the electrostatic potential in the plasma. (The strong dependence of the amplitude of unstable oscillations on the plasma potential was repeatedly noted in experimental works; see, e.g., [107].) The elongation of unstable disturbances along the magnetic field lines leads to the need in the stability analysis to take into account the plasma parameters along the entire traps, and not only in the central part. To obtain the sufficient stability conditions, one can use the dispersion relation for perturbations in a longitudinally uniform plasma (given, e.g., in [103, 104]).

The excitation of DCLC leads to collisionless scattering of ions, their diffusion along the pitch angle and radial coordinate. The anomalous longitudinal losses of ions during DCLC flashes observed at the PR-6 [107, 108] and 2XIIB [100] facilities, exceeded the classical ones. At the same time, no noticeable anomalous losses were observed in the central cell of the TMX-U facility, where DCLC is developed due to the displacement of the target plasma from turning points of the fast ions [98]. Apparently, this was due to the small amplitude of the unstable oscillations caused by the smallness of the region of space, in which the oscillations could effectively exchange energy with fast

ions. The quasi-linear theory predicts that the excitation of the DCLC instability leads to a partial filling of the loss cone of ions due to diffusion over the pitch angle, with the derivative of the distribution function of ions $\partial F_i / \partial v_{\perp}$ decreases in the low-energy region, which leads to the self-limitation of the amplitude of unstable oscillations [109].

Calculations using the DOL code (see Subsection 3.2) and the dispersion relation for waves in the longitudinally homogeneous plasma show that DH instability can develop in GDMT in low temperature target ions due to the nonequilibrium distribution function of fast ions. However, it stabilizes as the target plasma temperature increases (such an increase is also beneficial for increasing the power gain Q). At the same time, an increase in the temperature of the target ions leads to the fact that they begin to be contained not in the gas-dynamic (loss cone is filled) but in the kinetic (loss cone is empty) mode. An increase in the electron temperature of the plasma, which is important for increasing Q , also reduces the fraction of low-energy ions, because, firstly, it increases the ambipolar potential at the center of traps and, secondly, it increases the angular width of the distribution of fast ions and greatly reduces the peaks of the ambipolar potential at points stops between which warm ions might be trapped. An analysis using the dispersion relation [104] shows that the transition to confinement of target ions in the kinetic regime should be accompanied by the excitation of a small-scale (with a wavelength hundreds of times smaller than the Larmor radius of fast ions) DCLC instability, which develops due to emptying of the loss cone of target ions [110]. Such an instability, apparently, does not affect confinement of fast ions, but it can increase the loss of particles and energy from the target plasma in the kinetic regime to a level corresponding to gas-dynamic losses.

4. IMPROVING THE PLASMA CONFINEMENT IN GDMT

4.1. Diamagnetic Plasma Confinement Mode

One of the goals of the GDMT project is to experimentally study the regime of diamagnetic plasma confinement, also otherwise called diamagnetic bubble [9]. The idea of diamagnetic confinement can be formulated on the basis of the following reasoning. Imagine that we can somehow, e.g., by increasing the input heating power, gradually increase the equilibrium energy content of the plasma in a gas-dynamic trap. The vacuum magnetic field, which is created by currents in external conductors, is considered to be fixed. At the initial stage, the increase in the energy content occurs due to an increase in the plasma pressure in the axial region, and the plasma radius does not increase significantly, since the transverse transport in the magnetic field is significantly suppressed in com-

parison with the longitudinal losses. The relative plasma pressure is limited by the theoretical equilibrium limit $\beta \leq 1$. When the plasma pressure reaches the pressure of the vacuum magnetic field, a region is formed filled with plasma, from which the magnetic field is forced out (the so-called diamagnetic bubble). A transition layer is formed at the boundary of the diamagnetic bubble, in which the magnetic field increases and the plasma pressure decreases. Theoretical estimates [9] show that in the approximation of single-fluid magnetohydrodynamics (similar to estimates for the width of a viscous-resistive layer in cusps [111]), the lifetime of particles in a diamagnetic bubble is

$$\tau_n \sim \sqrt{\tau_{\perp} \tau_{\text{gdt}}},$$

where $\tau_{\text{gdt}} = LR/2v_m$ is the confinement time in a classical gas-dynamic trap [33] (see also Subsection 3.1, Eq. (2)), $\tau_{\perp} = a^2/\mathcal{D}$ is the characteristic time of plasma transverse diffusion, \mathcal{D} is the plasma diffusion coefficient across the magnetic field. The width of the transition layer in the MHD approximation is determined by the balance between diffusion across the magnetic field and plasma losses along the field, $\lambda \sim (D\tau_{\text{gdt}})^{1/2}$. As a rule, transverse transport in a magnetic field is largely suppressed and $\tau_{\perp} \gg \tau_{\text{gdt}}$, hence, it can be expected that the particle confinement time in the bubble τ_n can increase significantly compared to the classical gas-dynamic time τ_{gdt} (more realistic estimates that take into account kinetic effects are given below).

Plasma confinement with $\beta \approx 1$ in open traps was previously theoretically considered in [112–117]. Efficient plasma confinement with $\beta \approx 1$ in a gas dynamic system was experimentally demonstrated on the 2MK-200 test bench [118]. Structures similar to a diamagnetic bubble, also called magnetic holes, are observed in cosmic plasma [119–122]. Regimes with $\beta \approx 1$ were theoretically and experimentally studied in antimirror cells (see reviews [111, 123]). It is noted in [124] that traps with conductors immersed in the plasma (“Galateas”) make it possible to implement configurations that the authors called “magnetic balloons” with $\beta \approx 1$.

A steady-state hydrodynamic equilibrium model of diamagnetic confinement was constructed in the cylindrical approximation and an equilibrium plasma pressure profile at the bubble boundary was obtained (Fig. 18) [9]. The possibility of transition to the diamagnetic regime and methods for stabilizing instabilities in a diamagnetic bubble were also discussed.

The hydrodynamic model of plasma equilibrium constructed in [9] was extended to the case of non-paraxial axisymmetric traps [125, 126]. In particular, bubble equilibria were constructed for the GDMT design configuration (Fig. 19). The effect of magnetic field corrugation on the plasma equilibrium in the dia-

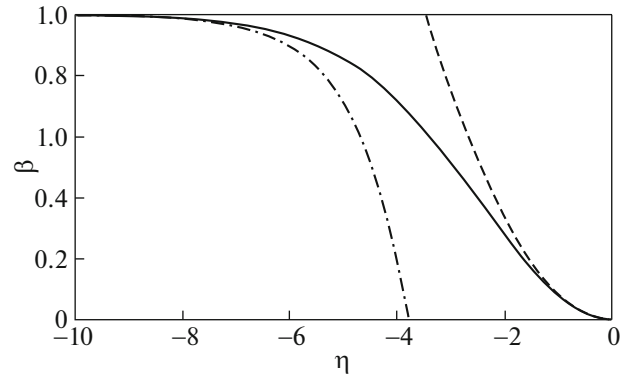


Fig. 18. Equilibrium plasma pressure profile at the boundary of the diamagnetic bubble (solid curve) and asymptotics near the boundary ($\beta \approx \eta^2/12$, dotted line) and far from the boundary ($\beta \approx 1 - \exp(1.03(\eta + 3.8))$, dash-dotted line). Dimensionless variable $\eta = (r - a)/\lambda$.

magnetic confinement regime was also studied. An analytical dependence of the corrugation depth of the bubble boundary $\delta a_0/a_0$ on the initial corrugation depth of the vacuum magnetic field at the bubble boundary $\delta B_{v0}/B_{v0}$ and corrugation step h was obtained

$$\frac{\delta a_0}{a_0} \approx \frac{\delta B_{v0}}{B_{v0}} \mathcal{H} \left(\frac{2\pi a_0}{h} \right), \quad \mathcal{H}(x) = \frac{1}{x^2} \frac{1}{I_0(x) K_0(x)},$$

where $I_0(x)$ and $K_0(x)$ are modified Bessel functions. The same dependence was obtained in a series of numerical calculations. The possibility of the plasma stabilization in a diamagnetic bubble by a combination of vortex confinement [22, 36, 127] and conducting wall [82, 128, 129] is also briefly discussed in [126].

As noted earlier, the magnetic field inside the bubble is close to zero. In this case, the Larmor radius and mean free path of sufficiently high-energy particles can be comparable to or larger than the characteristic scale of magnetic field inhomogeneities. This is especially true for the GDMT, where the injection of high-energy neutral beams is planned. Thus, there is a need for a detailed kinetic model of high-energy particles in a diamagnetic bubble. A fully kinetic model of the equilibrium of a diamagnetic bubble in a cylindrical geometry with a distribution function isotropic in the transverse plane is presented in [130]. Collisionless dynamics of individual particles and its effect on the plasma equilibrium and particle and energy transport in the diamagnetic confinement regime were studied in [30, 131]. During the collisionless motion of a particle in a steady-state axisymmetric field, the energy E and the azimuthal component of the angular momentum are conserved $P_\theta = mrv_\theta + eA_\theta/c$, here, $A_\theta(r, z)$ is the azimuthal component of the magnetic field vector potential. The particle dynamics essentially depends on the sign and absolute value of the azimuthal

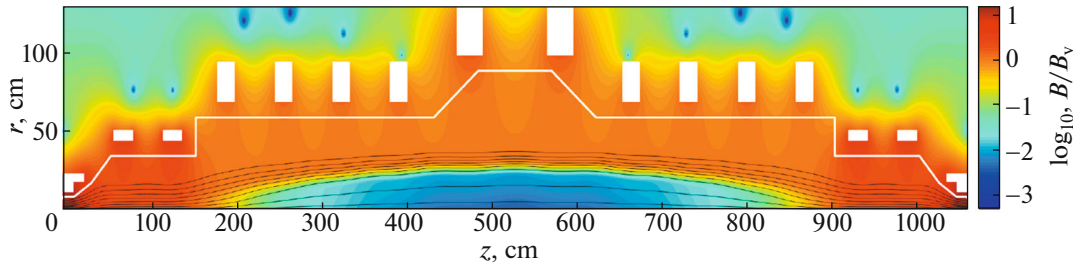


Fig. 19. Example of the magnetic field distribution in GDMT in the diamagnetic confinement mode. The magnetic field lines are shown in black. Vacuum chamber and magnetic system are shown in white. The calculations were carried out by the method described in [125, 126].

moment P_θ . Following [124], it is convenient to call particles with $\Omega P_\theta < 0$ co-particles, and particles with $\Omega P_\theta > 0$ counter-particles (here, Ω is the cyclotron frequency); for the former, the direction of rotation around the traps axis coincides with the direction of cyclotron rotation in a magnetic field outside the bubble, in the latter it is opposite to it. In axisymmetric magnetic traps with a smooth magnetic field, in the case of collisionless motion of particles, the adiabatic invariant $I_r = \oint p_r dr$ is preserved, which is associated with the difference in the period of radial and longitudinal oscillations (see, e.g., [124, 132–134]); this invariant is proportional to the magnetic field flow through the particle orbit in the reference frame, where the particle trajectory is closed and when the particle moves in a uniform magnetic field, this invariant is proportional to the sum of the magnetic moment and P_θ . In a diamagnetic trap, the invariant is preserved for particles with a sufficiently low longitudinal velocity (for the conservation of I_r , it is required that the transverse structure of the electromagnetic field in the bubble during the longitudinal motion of the particle changes slightly over time on the order of the period of radial oscillations). The period of radial oscillations is the least for counter-particles moving in a region with a strong magnetic field outside the bubble (the period is approximately equal to the period of cyclotron oscillations) and for co-particles with low radial velocity (rotating along betatron orbits near the bubble boundary); for these groups of particles, the adiabatic invariant is destroyed last of all. Apparently, the main role in the destruction of the adiabatic invariant is played by small-scale corrugation of the magnetic field, which arises due to the discrete structure of the magnetic system of the facility; conditions for the adiabaticity of the motion for several groups of particles with different types of trajectories were found in [30]. In general, the adiabaticity condition is reduced to the fact that the longitudinal component of the particle velocity should not exceed the threshold value, which depends on the energy and azimuthal momentum of the particle, the radius of the diamagnetic bubble, and the structure of the magnetic field.

The condition of the confinement of adiabatically moving particles in a trap has a similar form; in a diamagnetic trap with a smooth vacuum field with a corrugation amplitude of less than a percent, ions with a ratio of the longitudinal to the transverse velocity component on the order of a hundred can be confined in the adiabatic regime.

It is important to note that most of the co-particles are confined in an axisymmetric trap absolutely, even if they move along chaotic trajectories. The mechanism of absolute confinement is associated with centrifugal force, which throws co-particles rotating around the axis along the radius and prevents particles from penetrating into regions with a smaller transition layer radius near the mirrors. Chaotically moving particles that are not absolutely confined leave the trap in a time on the order of [30, 131]

$$\tau_n \sim \frac{a}{\rho_v} \tau_{\text{gdt}},$$

where ρ_v is the Larmor radius of particles calculated from the vacuum field at the center.

When considering the plasma lifetime in a diamagnetic trap, it should be taken into account that due to the conservation of the azimuthal moment and the huge difference in the masses of ions and electrons in the mirrors and in the transition layer, the regions can be formed where ions but not electrons from the diamagnetic bubble can enter. To maintain plasma quasi-neutrality, electrostatic potentials are formed in these regions, which suppress the flow of ions. In the simplest case of the plasma outflow with a Maxwellian distribution, the outflow time is on the order $\tau_{\text{loss}} = \tau_{\text{gdt}} a / \Delta r$, where Δr is the transition layer width [30]. The width of the transition layer certainly cannot be less than the Larmor radius of the electron; various processes, e.g., instabilities, in the transition layer lead to its smearing. The smearing of the transition layer in cusps has been studied experimentally and theoretically in detail [111, 123]. In particular, it was shown on the ATOLL magnetoelectrostatic trap [123] that, due to the transverse electric field introduced into the layer (the potential drop across the layer width is about

1 kV), kinetic instabilities are excited in the plasma (including the long-wavelength ion-acoustic instability [135, 136]), the source of energy for which is the difference in the drift velocities of ions and electrons. These instabilities determined the structure of the transition layer and led to anomalous losses hundreds of times higher than the classical ones (those that would be in a magnetoelectrostatic trap if only Coulomb collisions were taken into account) [123]. The excitation of kinetic instabilities in the plasma at the ATOLL facility led to the broadening of the transition layer to a value on the order of the Larmor radius of the ion.

Systematic experimental data on the structure of the transition plasma layer in open traps with $\beta \approx 1$ are currently lacking. For estimates of the lifetime of warm plasma in GDMT, the “pessimistic” estimate is further used, when the width of the transition layer is on the order of the Larmor radius of warm ions ρ_i , while there is no electrostatic potential blocking the flow of ions in the transition layer and in the mirrors (unlike magnetoelectrostatic traps). In fact, we neglect the possibility of additional blocking of the plasma flow by the electrostatic potential, which played an important role in the ATOLL facility. This estimate agrees with the experimentally measured layer width in cusps [123].

In the case when the transverse transport of warm plasma outside the bubble is determined by Coulomb collisions (and is small compared to the longitudinal transport), and the Larmor radius of warm ions is small, a simple zero-dimensional model of the plasma energy balance in the GDMT in the diamagnetic confinement regime can be constructed. The energy is introduced into the diamagnetic bubble by means of neutral injection, fast ions transfer their energy to the target plasma during the time on the order of the deceleration time of fast ions on electrons τ_d Eq. (4), the target plasma is lost from the trap in a time on the order of τ_{loss} , and each ion–electron pair carries out an energy on the order of $8T_e$, where T_e is the electron temperature of the target plasma. The temperature of the target plasma is determined by the balance between the input power P_{inj} and the power carried by the outflowing target plasma $8T_e J_{\text{src}}$, where J_{src} is the rate of the input of warm atoms into the bubble (as a result of gas injection or pellet injection). The density of target ions is determined by the balance between the input J_{src} and losses $\pi a^2 L n_i / \tau_{\text{loss}}$. The temperature and density of target ions are on the order of

$$T_i \sim T_e \sim \frac{1}{8} \frac{k_{\text{inj}} P_{\text{inj}}}{J_{\text{src}}}, \quad n_i \sim \frac{1}{2\pi} \frac{e B_{\text{max}} J_{\text{src}}}{c T_e a}, \quad (7)$$

where B_{max} is the magnetic field in the mirror, a is the radius of the diamagnetic bubble, k_{inj} is the beam capture efficiency factor. Estimation Eq. (7) neglects losses due to ionization and heating of the introduced

atoms and it is assumed that the target ions and electrons have the same temperature. The ratio of the total energy of the target plasma to the total energy of fast ions is on the order of $\tau_{\text{loss}}/\tau_d \ll 1$.

The plasma energy density inside the bubble is $B_v^2/8\pi$ and approximately coincides with the pressure of fast ions. On the other hand, the total energy content of fast ions is determined by the balance between the input power $k_{\text{inj}} P_{\text{inj}}$ and transfer of energy to the target plasma via deceleration of ions on electrons

$$\frac{B_v^2}{8\pi} \pi a^2 L \sim k_{\text{inj}} P_{\text{inj}} \tau_d, \quad (8)$$

where L is the distance between mirrors and B_v is the vacuum magnetic field. Combining Eqs. (7) and (8), one can estimate the diamagnetic bubble radius for a given magnetic field, injection power and gas injection

$$a \sim 6\sqrt{\pi} \frac{1}{\Lambda L} \frac{B_v}{B_{\text{max}}} \left(\frac{m_i}{m_e}\right)^{3/2} \left(\frac{m_i c}{e B_v}\right)^3 \frac{m_e c^2}{e^2} \frac{1}{c^4} \left(\frac{2T_e}{m_i}\right)^{7/2},$$

$$T_e \sim \frac{1}{8} \frac{k_{\text{inj}} P_{\text{inj}}}{J_{\text{src}}}.$$

Here, Λ is the Coulomb logarithm. We note that $e^2/m_e c^2 \approx 3 \times 10^{-13}$ cm is the classical electron radius.

The capture efficiency satisfies the equation

$$k_{\text{inj}} = 1 - \exp(-\sigma n_i a) \sim 1 - \exp\left(-\frac{\sigma}{2\pi} \frac{e B_{\text{max}}}{c} \frac{8 J_{\text{src}}^2}{k_{\text{inj}} P_{\text{inj}}}\right),$$

where $\sigma = \sigma_{\text{ex}} + \sigma_{v_e}/v_a + \sigma_{ii}$, here, σ_{ex} is the resonant charge exchange cross section of fast neutrals on target ions, σ_{v_e} is the electron impact ionization rate constant, σ_{ii} is the ionization cross section in ion-ion collisions, v_a is the velocity of injected neutral atoms.

Figure 20 shows an example of the dependence of the diamagnetic bubble radius and target ion density on the target plasma injection rate for a given injection power. There is a strong dependence of the bubble radius and target plasma density on the puffing power. As J_{src} increases, the density of the target plasma increases, while the deceleration of fast ions on electrons increases and the longitudinal losses increase, so the total energy content decreases. Note that when $B_v = 0.5$ T and the injection energy of 30 keV, the density of fast ions in the diamagnetic confinement mode is on the order of 5×10^{13} cm $^{-3}$, and the Larmor radius of fast ions is approximately 4 cm. In this case, the assumptions of the zero-dimensional model that the density of target ions is much higher than the density of fast ions and the bubble radius is larger than the Larmor radius of a fast ion are obviously violated at $n_i < 10^{14}$ cm $^{-3}$ and $a < 4$ cm.

In the transition layer at the plasma–vacuum interface, the average velocities of ions and electrons are different (since the diamagnetic current flows), and

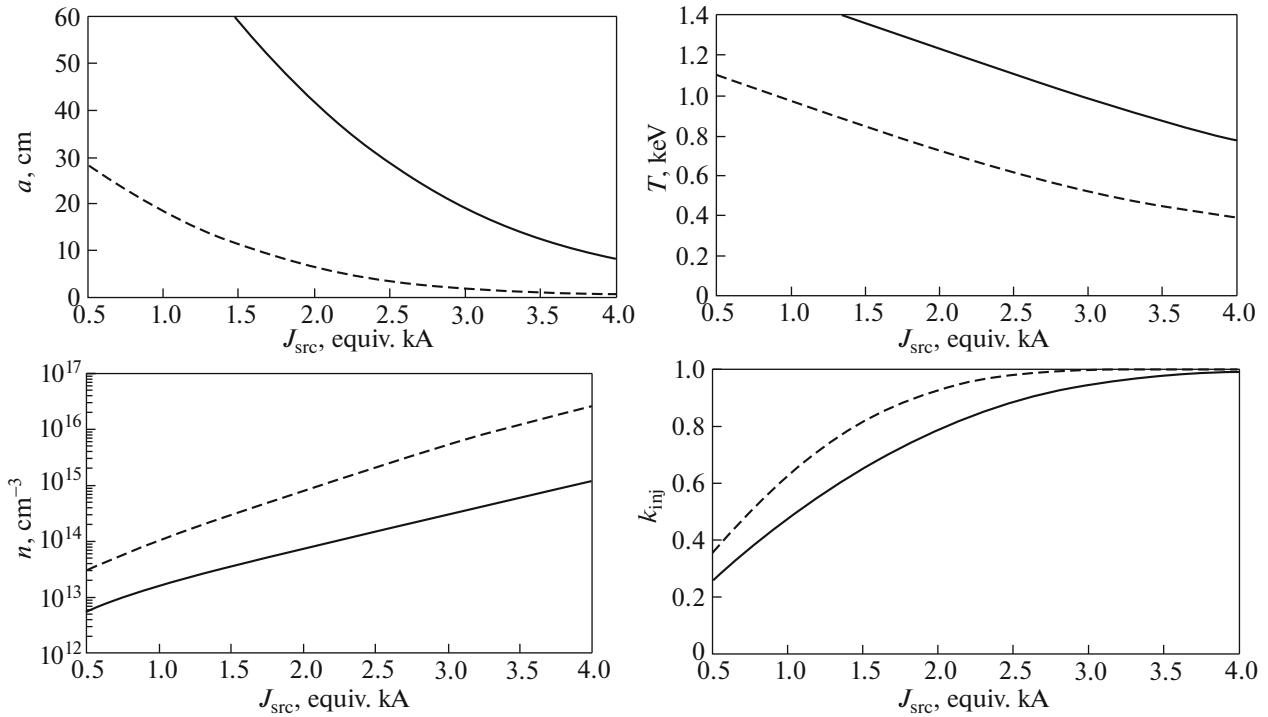


Fig. 20. Example of the dependence of the diamagnetic bubble radius, target plasma density and electron temperature, and capture efficiency on the target ion injection rate. Parameters: magnetic field in the mirror and central section $B_{\text{max}} = 20$ T and $B_z = 0.5$ T, distance between the mirrors $L = 8$ m, neutral injection power $P_{\text{inj}} = 24$ MW (solid curves) and 12 MW (dashed line), injection energy 30 keV. When calculating the capture coefficient, the following cross sections were used [76]: $\sigma_{\text{ex}} = 2.79 \times 10^{-16}$ cm², $\sigma_{v_e/v_a} \approx 10^{-16}$ cm², $\sigma_{ii} \approx 10^{-16}$ cm², $\sigma_{ii} \approx 5 \times 10^{-16}$ cm².

there are significant density and pressure gradients of the plasma. In addition, the ion distribution function in the GDMT differs significantly from the Maxwellian one due to the use of atomic injection to create and maintain a discharge. All this can provoke the excitation of kinetic instabilities and anomalous losses in addition to the “classical” losses described above. Systematic data on kinetic instabilities in axisymmetric open traps with powerful atomic injection and $\beta \approx 1$ are not currently available; the main data were obtained at the C-2W facility. At this facility, off-axis injection of atomic beams with an energy of 15–40 keV and a total power of 13 MW into a plasma is performed in a preliminarily created configuration with a reversed field [47]. Basically, small-scale drift instabilities with a wide spatial spectrum, concentrated near the separatrix and traveling in the azimuthal direction, are observed in the plasma at this facility. It is noted that drift instabilities do not affect the dynamics of fast ions, since the orbital radius of ions significantly exceeds the azimuthal wavelength of the instabilities. In addition, at the C2-W facility, electromagnetic instabilities are observed in the plasma with a frequency on the order of the ion-cyclotron, presumably associated with the excitation of Alfvén [137] or Bernstein [138] waves, while these waves do not affect the

energy content of the fast ions population. The absence of anomalous losses of fast ions in the plasma may be due to the fact that, when using off-axis atomic injection, most of the fast ions are confined absolutely, while the angular scattering should have little effect on their loss rate (in contrast to the experiment on an attempt to reverse the field at the 2XIIB facility [100], where there was no axial symmetry due to the use of quadrupole MHD stabilizers). The currently available data suggest that, in an axisymmetric diamagnetic trap, the anomalous losses associated with plasma microinstabilities can be reduced to an acceptable level. A detailed study of kinetic instabilities in plasma with $\beta \sim 1$ and methods for their stabilization is planned during supporting experiments at the GDT and CAT facilities [8].

An experimental study of the diamagnetic confinement regime is one of the tasks of the first stage of the GDMT. The DOL code calculations show (see Subsection 3.2) the possibility of achieving $\beta > 0.7$ in modes with low gas injection and moderate magnetic field (about 0.3 T), which can be interpreted as a transition to diamagnetic confinement. To increase the power density of the neutral injection into plasma, it is possible to rotate the injectors in the vertical plane (see Subsection 2.2) to perform off-axis injection, when

the center of the Larmor orbit of a fast ion approximately coincides with the traps axis. The GDMT also provides for a stepwise magnetic field rise mode (see Subsection 2.1), in which it is planned to switch to the diamagnetic confinement mode at a moderate magnetic field (about 0.3 T) followed by a field rise to 1.5 T; as the field rises, an increase in the energy stored in the plasma is expected. The transition to the diamagnetic confinement mode, apparently, requires solving the problems associated with MHD stability and anomalous transport in the transition layer. For MHD stabilization, it is planned to use a combination of vortex confinement and line-tying of the magnetic field into a conducting wall (see Subsection 3.4). The suppression of anomalous transport probably requires the control of the vacuum magnetic field profile, potential distribution in the transition plasma layer and gas puffing. Estimates show that upon transition to the diamagnetic confinement regime of the plasma, one can expect an increase in the particle lifetime (and the energy stored in the plasma) by an order of magnitude.

4.2. Multiple-Mirror and Helical Plasma Confinement

The modular design of open plasma traps allows the use of additional sections of the magnetic system specially designed to reduce longitudinal losses. This section considers proposals for using sections with a periodic magnetic field to suppress longitudinal particle and energy losses in a new generation open traps project. In this case, the central part (gas-dynamic or diamagnetic trap, in which the plasma is heated) remains unchanged. Thus, it is expected that the plasma parameters in a trap gradually improve as the magnetic system is developed and new specialized modules are added.

In this section, for simplicity, we assume that a quasi-neutral flow of thermodynamically equilibrium plasma flies out into the mirrors of the central traps. Such an assumption is valid for the regime of a purely gas-dynamic plasma outflow. With an increase in the plasma temperature and a corresponding increase in the mean free path of ions (transition to the kinetic confinement regime), depopulation of the distribution function in the region of low transverse velocities is observed, since the exit of particles from traps corresponds to weak diffusion inside the loss cone in the velocity space.

When considering the operation of the central trap in the mode of simulating a neutron source with a two-component plasma, we assume that fast ions have time to thermalize before they are scattered before they escape into the loss cone. Further in this section, fast ions in the central trap is ignored; accordingly, only the value related to the warm plasma flow is taken into account as the relative pressure parameter β . An increase in the anisotropy of the ion distribution function in the velocity space upon transition to the kinetic

confinement regime in the central trap undoubtedly affects the efficiency of the longitudinal loss suppression. An accurate prediction of the magnitude of such an effect in a magnetic system of finite length is possible only as a result of numerical simulation using a specialized code that has yet to be developed. Therefore, in this section we restrict ourselves to simple numerical estimates for understanding the physics of the operation of multiple-mirror and helical magnetic sections.

4.2.1. Principles of multiple-mirror confinement plasma. The multiple-mirror scheme of plasma magnetic confinement as applied to the problem of controlled thermonuclear fusion was first proposed in early 1970s [11, 12]. A detailed review of the multiple-mirror confinement research, experimental results and proposals for reactors based on this scheme is given in reviews [34, 139]. In a multiple-mirror trap, the magnetic field periodically changes along the axis, forming a kind of chain of elementary mirror cells (multiple-mirror traps cells). We introduce the field corrugation value (the mirror ratio of multiple-mirror traps cells) as $R_{\text{mm}} = B_{\text{max}}/B_{\text{min}}$, where B_{max} and B_{min} are the maximum and minimum magnetic induction in each cell. Depending on the corrugation depth, traps with weak corrugation $R_{\text{mm}} - 1 \ll 1$, traps with moderate corrugation $R_{\text{mm}} - 1 \sim 1$, and traps with strong corrugation $R_{\text{mm}} \gg 1$ are conventionally distinguished. Note that for the purposes of this work, only the last two cases are of interest.

In each cell of the multiple-mirror plasma trap, there are two ion populations: transient, in which the pitch angle with respect to the magnetic field is small, and locked in local mirror cells, in which the pitch angle is large enough. Transient particles become trapped during scattering and begin to oscillate being reflected from magnetic mirrors. By the time of the next scattering, they fly out with equal probability in both directions. As a result, the longitudinal motion of ions becomes diffusion instead of a simple expansion along the magnetic field, and the lifetime of particles under optimal conditions increases significantly compared to the free expansion time of the plasma along the solenoid

$$t \sim \frac{L^2}{v_{Ti} l} (R_{\text{mm}} - 1)^2 = N (R_{\text{mm}} - 1)^2 \tau_0, \quad (9)$$

where v_{Ti} is the thermal velocity of ions, l is the period of the multiple-mirror system, N is the number of periods of the multiple-mirror system, and τ_0 is the time of flight of the system with the thermal velocity.

The multiple-mirror trap works effectively in a relatively small space of plasma parameters. The optimal condition is the proportionality of the effective length of the elementary mirror cell and the free path of the ion. For the case of moderate corrugation, this reduces to a simple condition $\lambda = l$ (for the transition of a tran-

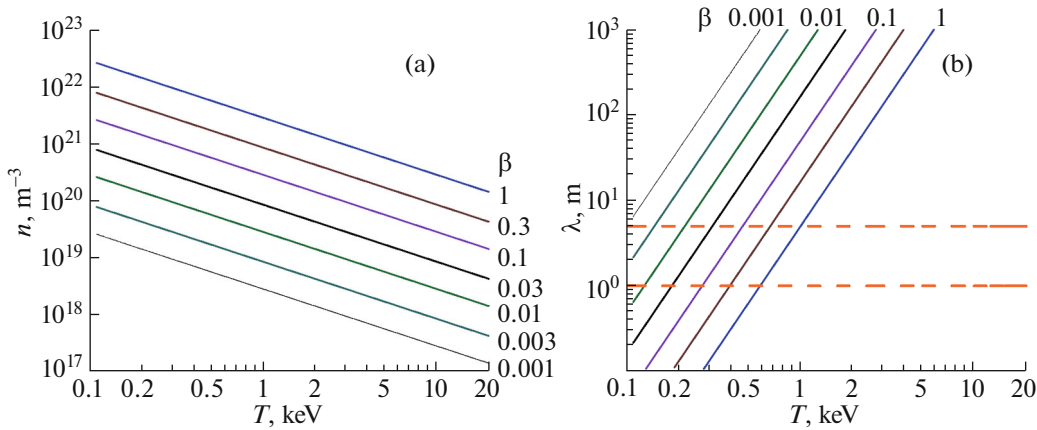


Fig. 21. Temperature dependences of the density (a) and classical free path (b) for the plasma with a fixed β value. The calculation was carried out for the equilibrium plasma confined in a magnetic field $B = 1.5$ T. The β values are indicated next to the corresponding curves. The dotted lines indicate the values $\lambda = 1$ m (optimal at $l = 1$ m and $R_{\text{mm}} - 1 = 1$) and $\lambda = 5$ m (optimal at $l = 1$ m and $R_{\text{mm}} = 5$).

sient particle to trapped ones and its temporary capture in some cell of the multiple-mirror system, scattering by an angle on the order of units is required), for the case of strong corrugation, to the condition $\lambda = R_{\text{mm}}l$ (scattering per angle on the order of the loss cone angle is sufficient for trapping a transient particle).

A feature of the multiple-mirror confinement scheme is that the useful effect (friction of transient ions against locally trapped ones) is determined by the ion scattering rate over the pitch angle. Any process leading to an increase in the frequency of collisions of ions in the plasma is beneficial from the point of view of the feasibility of a multiple-mirror thermonuclear reactor. This topic is discussed in more detail in Section 4.2.3.

4.2.2. Choice of parameters of the multiple-mirror system. A significant complication of the facility design when sections with a multiple-mirror magnetic field are added to its composition can be justified if such sections can reduce the longitudinal losses of particles and plasma energy by a factor of 3–10 compared to the lifetime provided by the central trap itself. Considering that in a finite length system, only a part of the corrugated field cells can operate under conditions close to optimal, it is reasonable to consider the total number of corrugation periods in each section $N = 10\text{--}20$. In this case, the total length of sections of the corrugated field should be commensurate with the length of the central traps. From these two requirements, indicative parameters of multiple-mirror sections are obtained: the corrugation period $l \approx 1$ m, and the total length $L_{\text{mm}} \approx 15$ m. These parameters should be specified during the direct design of multiple-mirror sections.

The list of physical problems solved at different stages of the development of a new generation of a modular open trap suggests the possibility of varying

the plasma parameters over a wide range. Figure 21 shows the temperature dependences of the plasma density (Fig. 21a) and the classical free path of ions (Fig. 21b) calculated for a plasma with a fixed relative pressure β held in a central trap in a leading magnetic field of 1.5 T. Therefore, the parameter β in this figure applies only to the pressure of the warm component, the pressure of fast ions here is not taken into account. The calculation was carried out according to formulas from [140]. At the first stage of operation, the GDMT magnetic field in the central trap may be smaller. Plots for $\beta \approx 0.01$ at $B = 1.5$ T correspond to $\beta \approx 0.1$ at $B = 0.5$ T and $\beta \approx 0.3$ at $B = 0.3$ T; respectively, and dependences for other parameters can be recalculated.

An analysis (Fig. 21) shows that the benefit of using sections with a multiple-mirror magnetic field depends significantly on the experimental scenario. In the main scenario for simulating the parameters of a neutron source with a two-component plasma, it is assumed to work with the warm plasma parameters of $n \sim 3 \times 10^{13} \text{ cm}^{-3}$ and $T \sim 1$ keV (corresponds to the relative pressure of the warm component $\beta \sim 0.3$ at $B = 0.3$ T). The classical ion scattering length in this mode is hundreds of meters. Thus, deceleration of the flow by a multiple-mirror section at moderate ($R_{\text{mm}} - 1 \sim 1$) and strong ($R_{\text{mm}} = 5$) corrugation requires anomalous ion scattering.

From the point of view of reactor prospects for an open plasma trap operating in the diamagnetic confinement mode, it is important to ensure the transition from gas dynamic confinement with $\beta \sim 0.3$ to the diamagnetic bubble mode with $\beta \approx 1$ at a reasonable injection power. A possible scenario for this case is the creation of a dense one-component plasma, the parameters of which fall within the range of effective operation of multiple-mirror sections (e.g., $n \sim 3 \times 10^{14} \text{ cm}^{-3}$ and $T \sim 200$ eV at $B = 0.3$ T), in the first

phase of the experiment. Then, in the second phase, there is a synchronous increase in the density and temperature of the plasma in the central trap until the diamagnetic plasma expansion is completed, and only after that, in the third phase, the transition to the confinement of two-component plasma occurs with a gradual synchronous decrease in density and increase in temperature at a constant β value. Without taking into account the anomalous collision in the third phase, the multiple-mirror sections gradually lose efficiency due to an increase in the mean free path of warm plasma ions, however, the longitudinal losses already have an acceptable value without multiple-mirror sections due to the increased effective mirror ratio in the diamagnetic trap. The emerging issue of the need for a system to accurately control the balance between the supply of matter and the power deposited in the plasma, in any case, should be resolved for the successful implementation of the idea of the diamagnetic trap.

The physics of the operation of multiple-mirror sections is to temporarily capture the transient particle in the local mirror cell due to ion scattering in a small angle, and return it with a 50% probability towards the central trap at the next collision. An important technical requirement follows from this: the magnetic induction in the mirrors of the multiple-mirror system should be no less than that in the main mirrors of the central traps. The mirror ratio in the corrugated part should be chosen as high as possible (taking into account the negative impact on stability) in order to extend the performance of multiple-mirror sections to the region of high plasma temperatures for a given corrugation period. In this case, the natural minimum of the field is the same induction as in the center of the main trap. This solution, however, may not be optimal in a real design due to the degradation of the plasma stability (see Subsection 4.2.4).

The specified requirements for the magnetic field make it possible to use coils with a design close to the design of the central trap mirror units in multiple-mirror sections with a fixed mirror ratio, which are to be created at the first stage of construction of a new facility.

4.2.3. Ways to expand the available range of plasma parameters. In the previous section, we discussed the prospects for using multiple-mirror sections in classical scattering of plasma particles. When the plasma temperature rises to several hundreds of electron-volts for the condition $\lambda = R_{\text{mm}}l$ to be satisfied, the cell length of the multiple-mirror system becomes unacceptably large. However, it is possible to make multiple-mirror sections efficient enough for rare hot plasma. To this end, it should be done so that ion scattering in these sections is faster compared to that in Fig. 21. Scattering can occur due to Coulomb collisions in a plasma with changed parameters, and due to the interaction of transient ions with electromagnetic

waves in a plasma. The frequency of Coulomb collisions can be changed as follows:

1. Gas outlet at the end of the multiple-mirror section. Forcibly the plasma density is increased and the plasma temperature is decreased on the part of the multiple-mirror system. The disadvantage of the method is cooling of the plasma electrons in the central part and, thereby, the decrease in the plasma gain Q .

2. Injection of a small amount of impurities with an average atomic number Z (neon, silicon) into the multiple-mirror section. In this case, the frequency of collisions increases as $\nu \sim \sum n_z Z_i^2$, where n_z and Z_i are densities and charge numbers of the respective impurities. The decrease in the mean free path λ from ~ 300 to $\sim 1-5$ m requires an increase in the collision frequency by a factor of 60–300 compared to pure hydrogen plasma. At the impurity ion charge number $Z = 14$ (fully ionized silicon), the local relative density of the impurity should reach $n_z/n_H \approx 0.3$. Such a proposal was numerically studied in [141] as applied to a multiple-mirror reactor. There is no experimental confirmation. The disadvantage of the method is also cooling of the plasma electrons in the central part and, thereby, the decrease in the plasma gain Q .

Anomalous scattering of particles is possible when turbulence develops in the plasma with a sufficiently high root-mean-square value of the electric field. Experimental observations of anomalous scattering of particles were carried out only for certain types of waves and sources of their excitation. In previous experiments, anomalous collisions were studied in detail only at extremely high levels of turbulence pumping power. It follows that an important experimental task of the multiple-mirror GDMT program is to study the mechanisms of anomalous ion scattering at a moderate pump power.

For the maximum efficiency of multiple-mirror sections, a collision rate is needed to ensure that the length of the free path and the period of the multiple-mirror field are

$$v_{\text{eff}} = v_{Ti}/l.$$

Here, v_{eff} is the effective collision rate, v_{Ti} is the thermal velocity of ions.

This ion scattering frequency is small compared to the ion cyclotron frequency Ω_i ; for $T = 1$ keV, $l = 1$ m the scattering frequency is $v_{\text{eff}} \approx 5 \times 10^5 \text{ s}^{-1} < 10^{-2} \omega_{Bi}$. The average power transferred to one scattered ion can be estimated as:

$$P_i \sim m_i (1 - \kappa) v_{\text{eff}} v_{Ti} \delta v \sim m_i (1 - \kappa) v_{\text{eff}} v_{Ti}^2, \quad (9a)$$

here, κ is the fraction of trapped particles in the multiple-mirror field.

Formally, the power Eq. (9a) can be large, on the order of the power of longitudinal losses from the cen-

tral section. However, this power is used to heat the ions and, in the case of the effective loss suppression by the multiple-mirror sections, is returned to the central section. It is useful to compare the power Eq. (9a) with the characteristic pump power of the oscillations leading to ion scattering. Since the mechanisms of these fluctuations may be different, let us dwell for definiteness on the case of a helical trap (see Subsection 4.2.4). The main difference between “running” corrugation and systems with a steady-state magnetic field is a fraction of trapped particles moving towards the plasma flow at a velocity v_z . In the case of a helical trap, this speed is proportional to the pitch l and the rotational speed in crossed fields: $v_z = l\omega E \times B/2\pi$. In general, this speed can be chosen arbitrarily.

For a rotating plasma in a helical magnetic field, the energy source is a radial electric field that causes rotation. The energy of an external source is transferred to the scattered ions through trapped ions and an alternating electric field. The energy contained in trapped particles is proportional to their fraction and the kinetic energy of an ion moving at the velocity of the motion of magnetic disturbances

$$W_{\text{trapped}} \sim \kappa v_z^2.$$

Then the inverse characteristic time during which the energy should be transferred from the trapped ions to the wave is

$$\tau \sim \frac{W_{\text{trapped}}}{P_i} \sim v_{\text{eff}}^{-1} \frac{\kappa}{1 - \kappa v_{Ti}^2} \frac{v_z^2}{v_{Ti}^2}.$$

Let us make this time dimensionless with respect to the ion cyclotron frequency

$$\tau \Omega_i \sim \frac{\Omega_i}{v_{\text{eff}}} \frac{\kappa}{1 - \kappa v_{Ti}^2} \frac{v_z^2}{v_{Ti}^2}.$$

This quantity has the meaning of the number of ion cyclotron periods during which the trapped ion should give energy to the wave. A reasonable estimate for the square of the ratio of velocities is

$$v_z^2/v_{Ti}^2 \sim 5-10.$$

Thus, the energy transfer should be rather slow, and scattering is not forbidden from the energetic point of view at the fraction of trapped particles of $\kappa \sim 10^{-2}$. Anomalous scattering leads to an increase in the fraction of trapped particles and increase its own efficiency, which forms a positive feedback for this process.

It should be noted that for the effective transfer of energy to the transverse component of the velocity of transient ions, the growth rate and the spatial spectrum of the most unstable oscillation are important for the chosen anomalous scattering mechanism. These issues require an experimental answer obtained under conditions relevant to the GDMT parameters.

To date, two methods for the excitation of anomalous collisions have been experimentally shown:

1. Excitation of the small-scale Langmuir turbulence during electron beam injection. As was shown in [142, 143], such a process results in the turbulent suppression of the longitudinal electron heat conduction. This means, in addition to high-frequency Langmuir oscillations, the presence of rather low-frequency electric fields, which are most likely caused by density fluctuations arising during turbulence. These fields can lead to additional ion scattering. There are two difficulties in this method. First, this method of the excitation of strong Langmuir turbulence was demonstrated for sufficiently powerful pulsed electron beams. An experimental study of the possibility of achieving intense beam-plasma interaction at a reasonable power of quasi-steady-state electron beams is required. Secondly, it is necessary to search for such a beam injection regime, in which the beam-plasma interaction would be localized only in multiple-mirror sections, without capturing the central trap, in which additional ion scattering is unacceptable. Thirdly, the creation of a technology for generating electron beams that is operable under conditions of a powerful oncoming plasma flow is a separate and non-obvious scientific and technical task.

2. Excitation of large-scale bounce instability on weakly trapped ions in the multiple-mirror section cells. Such an instability was first discovered experimentally at the GOL-3 facility [31] and then studied theoretically in [144]. A spontaneous occurrence of bounce instability was observed in regions with a large plasma pressure gradient at the GOL-3 facility. In this case, the plasma expansion rate apparently exceeded the instability development threshold, and the instability was maintained during the entire time that a sufficiently large longitudinal plasma flow existed. It is possible that the threshold of the spontaneous development of the bounce instability is too high for this effect to be used in the form, in which it was observed at the GOL-3 facility. However, there is the possibility of forced buildup of bounce oscillations at the resonant frequency using an antenna. To this end, not only the creation of an appropriate experimental technique is required, but also a sufficiently accurate control of the plasma parameters in multiple-mirror sections for their transfer to the automatic tuning system of the RF generator.

Thus, methods for reducing the effective mean free path of ions exist, but none of them is currently fully confirmed. An experimental study of these methods is required, which should be one of the scientific objectives of the GDMT project.

4.2.4. Effect of multiple-mirror sections on the plasma stability. In addition to a positive effect on the longitudinal confinement time of the plasma, sections with a multiple-mirror magnetic field simultaneously worsen the overall MHD stability of the plasma in the

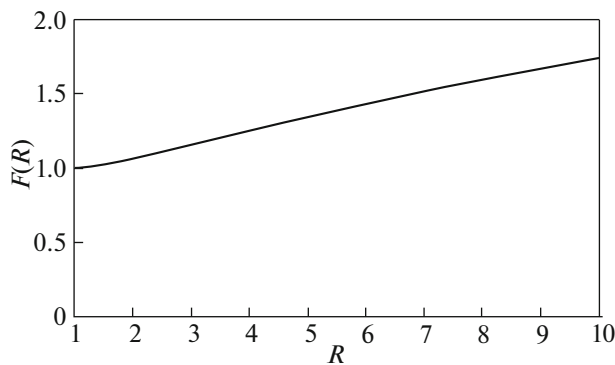


Fig. 22. Plot of function Eq. (12).

trap. Each multiple-mirror section is a set of a large number of elementary simplest mirror cells, which are known to be MHD unstable [145]. Moreover, with strong corrugation with $R_{\text{mm}} \gg 1$, approaching the value of the mirror ratio in the central trap, the average curvature of the field line in the multiple-mirror section and, consequently, the negative contribution of these sections to the overall stability integral is significantly larger than the contribution from the central trap.

To estimate the MHD stability of the confinement region, we use the Rosenbluth–Longmeyer criterion [145]

$$\int \frac{\kappa(p_{\perp} + p_{\parallel})}{rB^2} dl = \frac{1}{8\pi} \int (\kappa/r)(\beta_{\perp} + \beta_{\parallel}) dl > 0.$$

In the paraxial approximation $r = r_0(B_0/B)^{1/2}$ and $\kappa = d^2r/dz^2$, in this case, $\kappa/r = (3/4)((B'/B)^2 - 2B''/B)$. Thus, in the paraxial approximation, the criterion can be rewritten as

$$\begin{aligned} & -\frac{1}{8\pi} \int \frac{2}{\sqrt{B}} \frac{3}{4} \left(\frac{B'}{\sqrt{B}} \right)' (\beta_{\perp} + \beta_{\parallel}) dl \\ & = \frac{1}{8\pi} \int \sqrt{B} (1/\sqrt{B})'' (\beta_{\perp} + \beta_{\parallel}) dl > 0. \end{aligned} \quad (10)$$

The field in the multiple-mirror section is approximated by the function $B(z) = (B_{\text{max}} + B_{\text{min}})/2 + (B_{\text{max}} - B_{\text{min}})\cos(2\pi z/L)/2$. Then the integral Eq. (10) in the multiple-mirror section can be written in the form (we assume that the pressure is constant)

$$\begin{aligned} & \int \frac{\kappa(p_{\perp} + p_{\parallel})}{rB^2} dl \\ & \approx N \frac{p_{\perp} + p_{\parallel}}{B_{\text{max}}^2} \int_0^l \sqrt{B} (1/\sqrt{B})'' \frac{dl}{B^2/B_{\text{max}}^2} \\ & = N \frac{p_{\perp} + p_{\parallel}}{lB_{\text{max}}^2} \int_0^1 \sqrt{b} (1/\sqrt{b})'' \frac{dl}{b(x, R_{\text{mm}})^2}, \end{aligned} \quad (11)$$

here, N is the number of cells, l is the cell length, $R_{\text{mm}} = B_{\text{max}}/B_{\text{min}}$ is the mirror ratio, $b(x, R) = (1 + 1/R)/2 + (1 - 1/R)\cos(2\pi x)/2$. At $R_{\text{mm}} - 1 \ll 1$ the integral is approximately $-(3\pi^2/32)(R_{\text{mm}} - 1)^2 \approx -(R_{\text{mm}} - 1)^2$, so it is convenient to introduce the function

$$F(R) = -\frac{32}{3\pi^2} \frac{1}{(R-1)^2} \int_0^1 \sqrt{b} (1/\sqrt{b})'' \frac{dl}{b(x, R)^2}. \quad (12)$$

The graph of the function $F(R)$ is shown in Fig. 22. It can be seen that this function is on the order of unity and changes slightly when changing the mirror ratio.

Finally, integral Eq. (11) can be written as

$$\begin{aligned} \int \frac{\kappa(p_{\perp} + p_{\parallel})}{rB^2} dl & \approx -\frac{\beta_{\perp} + \beta_{\parallel}}{8\pi} \frac{N}{l} \frac{3\pi^2}{32} (R_{\text{mm}} - 1)^2 F(R) \\ & \approx -\frac{\beta_{\perp} + \beta_{\parallel}}{8\pi} \frac{N}{l} (R_{\text{mm}} - 1)^2. \end{aligned} \quad (13)$$

To take into account the contribution of the second multiple-mirror section, its value should be multiple-mirror by two. Since the purpose of creating multiple-mirror sections of the magnetic system is to suppress the plasma flow along the magnetic field, the estimate Eq. (13) is obviously overestimated and can be used as a pessimistic guideline. The origin is that the plasma pressure gradually decreases from the center to the end of the facility and, thus, the contribution of the end sections to the stability integral is significantly less than that accepted for Eq. (13). Under the optimal operation mode of the multiple-mirror system, the expected pressure distribution along the length is similar to a ladder, in which the plasma pressure varies slightly within each period of corrugation, and jumps in density and ambipolar potential are localized near the mirrors [146, 147].

We estimate the length of multiple-mirror sections at which their destabilizing contribution to integral Eq. (13) becomes equal to the contribution from the central section of the trap. At a gas injection rate with an equivalent current of 2.4 kA, a relative plasma pressure $\beta = 0.1$, and a warm plasma density in the mirror of $6 \times 10^{19} \text{ m}^{-3}$ the integral Eq. (10) is $3 \times 10^{-3} \text{ cm}^{-1}$. With a mirror ratio $R_{\text{mm}} = 2$ and a distance between the mirrors of 1 m, the contribution of multiple-mirror sections Eq. (13) is compared with the contribution of the confinement region with the number of cells $N \approx 400$. Even with strong corrugation $R_{\text{mm}} = 5$, the allowable number of multiple-mirror cells is $N \approx 25$, which seems sufficient for pilot program objectives.

4.2.5. Confinement with helical mirrors. The helical confinement scheme involves the creation of a leading magnetic field with helical symmetry. In such a geometry, periodic maxima of the magnetic field appear along each field line forming a multiple-mirror system. As noted earlier, when using the vortex confinement technique to limit lateral losses, the plasma

rotates around an axis in crossed electric and magnetic fields. The use of multiple-mirror sections with helical magnetic field symmetry makes it possible to increase the confinement efficiency by creating an additional force depending on the mutual direction of plasma rotation and magnetic field helicity. Similarly to classical multiple-mirror confinement, a population of trapped particles appears between the magnetic field maxima. The magnetic mirrors are displaced along the longitudinal coordinate on neighboring field lines. In the reference frame rotating synchronously with the plasma, the magnetic field maxima move along the axis of the facility at a velocity that depends on the helix pitch [35, 148]

$$v_z = \frac{hcE_r}{2\pi a B_z},$$

where h is the helix pitch, E_r is the radial electric field, a is the radius of the plasma column, B_z is the leading magnetic field. At reasonable geometric parameters and electric field $E_r \sim T_e/a$ the velocity of the motion of magnetic disturbances can be comparable with the ion-sound speed. If the length of the free path of a particle with respect to scattering into the loss cone is small compared to the length of the system, the loss cone of each individual cell of the multiple-mirror field is filled. Field variations impart momentum to trapped particles; these, in turn, produce a deceleration force acting on the plasma as a whole.

The direction of the force is determined by three independent parameters: the directions of the leading magnetic and radial electric fields and the right or left symmetry of the helical field. Thus, the choice of symmetry allows the plasma to be pumped towards the central trap in both end sections.

The corrugation depth of the magnetic field in a system with helical symmetry is variable over the radius. There is no corrugation on the magnetic axis and increases squared with the radius in the optimal case [149].

The trap length required for the loss suppression in the multiple-mirror trap by moving mirrors in e times is estimated in [13] as

$$\Lambda = \frac{D}{kv_z} \approx \frac{\lambda v_{Ti}}{\kappa v_{ii}} \left(\frac{4\pi a^2}{\rho_u h} \right),$$

where D is the effective diffusion coefficient for the longitudinal propagation of the plasma in a multiple-mirror trap, $\kappa \propto \sqrt{R_{\text{mm}}}$ is the fraction of trapped particles, R_{mm} is the corrugation depth, λ is the mean free path, ρ_u is the Larmor radius calculated from the applied radial stress.

An analytical model of longitudinal and radial transport of particles is presented in [13]. An estimate of the radial electric field required for the required efficiency of suppression of the longitudinal plasma flow is given in [150]. The above estimates show that

the required electric field value is $E_r \sim (3-4)T_e/ea$ for practically significant parameters for $\kappa \neq 0$. The potential difference between the plasma axis and periphery $U \sim 4T_e$ appears feasible under GDMT conditions and compatible with the vortex confinement mode.

It was also shown in [13] that, a neoclassical transport of ions occurs at a negative potential on the axis of the plasma column, which is necessary for closing currents leading to a decrease in the average radius of the plasma column (plasma pinching). The nonuniformity of the corrugation depth over the plasma cross section is manifested similarly. These effects make it possible to counteract plasma expansion due to transverse diffusion. At the same time, plasma contraction to the center, where there is no population of trapped particles, limits the maximum achievable efficiency of this scheme and may require additional measures to improve the longitudinal confinement.

The results of an experimental verification of the helical confinement theory are given in [14, 151, 152]. The suppression of the longitudinal plasma flow in the section with a helical magnetic field is experimentally shown, which corresponds to the effective mirror ratio $R_{\text{eff}} > 10$. The observed plasma density distribution corresponds to the calculations performed on the basis of the model of longitudinal and transverse transport [13]. A decrease in the maximum density and the above-described decrease in the average radius of the plasma jet were found. At the maximum rotation speed and corrugation depth, the formation of a reverse (i.e., moving in the direction of the density gradient) flux of ions in the paraxial region of the plasma column was detected.

The analytical estimate given in [35] predicts a higher efficiency of helical confinement compared to classical multiple-mirror confinement for any length of the section. At the same time, this estimate is not applicable for comparing systems with similar engineering parameters, since it assumes the equality of cross-section-averaged mirror ratios. Since the local mirror ratio in a magnetic system with helical symmetry falls off towards the axis, a more practical comparison would be a comparison of systems with an equal local mirror ratio at the boundary of the plasma column. Figure 23 compares the efficiency of the multiple-mirror confinement calculated from Eq. (9) and the efficiency of helical confinement calculated based on the transport equations from [13]. The electron temperature is taken as $T_e = 1$ keV, the leading magnetic field $B_z = 10$ T, the angular velocity of plasma rotation in the helical system is assumed to be constant along the radius and corresponds to the potential difference between the axis and the periphery $U = 4T_e$. The local mirror ratio at the plasma periphery is assumed to be $R(a) = 2$ or $R(a) = 5$, that corresponds to $R_{\text{mm}} = 2$ or $R_{\text{mm}} = 5$ in a multiple-mirror system and

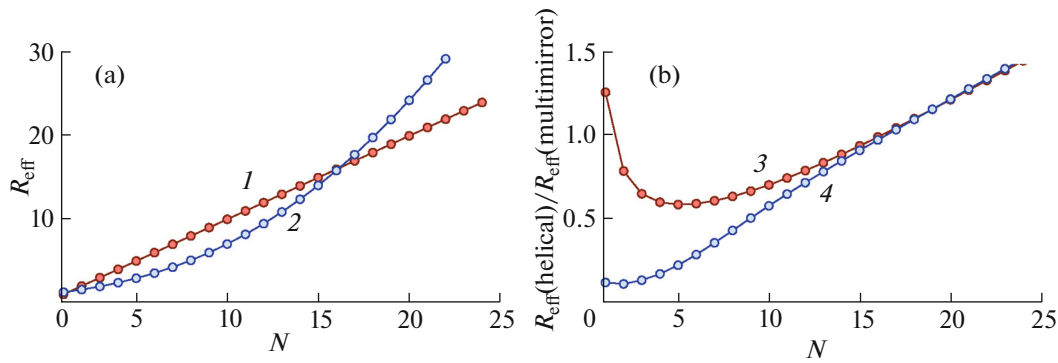


Fig. 23. (a): Calculated dependence of the effective mirror ratio of (1) multiple-mirror and (2) helical sections on the number of periods of the magnetic field at the depth of corrugation at the edge $R(a) = 2$. (b) Dependence of the efficiency ratio of helical and multiple-mirror sections on the number of periods of the magnetic field at the depth of corrugation at the edge $R(a) =$ (3) 2 and (4) 5.

$R_{\text{mean}} = 1.5$ or $R_{\text{mean}} = 3$ in a helical system. The mean free path was assumed to be equal to the period of the magnetic field (Subsection 4.2.3). For small-length systems, multiple-mirror sections are more efficient due to the larger mirror ratio; for larger lengths, helical sections are more efficient. Equal system efficiency corresponds to the length $L = 10\text{--}20 l$, where l is the length of the period of the multiple-mirror system.

The fulfillment of the condition of smallness of the mean free path in comparison with the length of the system due to only paired Coulomb collisions, similarly to the classical multiple-mirror confinement, is impossible. At the same time, if the relative velocity of trapped and passing particles in a system with moving mirrors exceeds the speed of sound c_s , conditions arise for the excitation of the two-flow instability, which can be a way to reduce the effective mean free path to the required values [13]. This anomalous collision mechanism is currently being studied at the SMOLA facility [152]. An indirect sign of its presence can be the effective confinement observed in experiments at a classical mean free path with respect to Coulomb collisions, which is comparable to the facility length [152]. Another theoretical possibility of reducing the effective mean free path is the stochastization of the motion of ions proposed in [153]. This method is also supposed to be verified in the experiment.

4.2.6. Conclusions on the multiple-mirror and helical plasma confinement in GDMT. In this section, two methods have been considered to improve longitudinal plasma confinement in a trap using additional sections of the magnetic system. Both of the technologies discussed, multiple-mirror confinement and helical confinement, use a magnetic field that varies periodically along the axis of the system. In a multiple-mirror system, this field is axially symmetrical; such a system is completely passive, i.e., it does not require additional action on the plasma. In a helical system, the magnetic field has helical symmetry with a spatial axis. The field modulation depth is maximum at the

periphery and tends to zero on the magnetic axis. Therefore, such a system has a stronger efficiency of suppressing the longitudinal plasma flow at the periphery. In addition, for helical confinement to function, it is required to ensure the rotation of the plasma. It is assumed that the same electrodes and power systems are to be used for this as those needed to stabilize the plasma in the trap by the vortex confinement method. An additional bonus of the helical system is that it should provide plasma pinching to the axis, i.e., it is a way to counteract the diffusion expansion of the plasma.

From a technical point of view, the classic multiple-mirror magnet system uses simple axisymmetric coils, which can be manufactured using almost the same technologies as the main mirror coils of the central trap. The multiple-mirror system is easily modularized. Sections with a helical field are more complex in terms of the production technology and operating conditions of current-carrying windings. In principle, sections with a helical field can be considered as part of the magnetic system of a straightened stellarator, e.g., having two helical windings similar to the LHD stellarator. The production of sections with a helical field with magnetic induction about 5 T with a length of several meters seems to be a feasible task.

Considering features of the operation and parameters of the magnetic systems of multiple-mirror and helical traps, it seems appropriate to consider the following facility structure. The main trap of the gas-dynamic or diamagnetic type, in which the plasma is heated, is in the center. The leading field in this trap can vary within 0.3–1.5 T. Sections with a helical field are located between the central trap and the first magnetic mirrors; the magnetic induction in them is chosen to be the maximum possible according to the available technology so that the turning points of fast ions remain in the central trap until the transition to the helical section. Then the mirror unit is located followed by a regular multiple-mirror structure, after which a magnetic flux expander and plasma absorbers

are located. In this scheme, the section with a helical field most strongly decelerates the plasma losses from the transition layers of the diamagnetic bubble (in which the main longitudinal losses occur) and shift the reverse plasma flow closer to the axis, and the multiple-mirror sections additionally reduce the longitudinal losses, returning back some particles ejected into mirrors.

The physics of the operation of sections with classical multiple-mirror and helical magnetic fields is developed quite well theoretically. At the same time, for a number of reasons, there is still no independent experimental verification in the range of dimensionless parameters corresponding to the expected operating modes of new-generation open traps. Therefore, parallel experimental programs are being performed at the Budker Institute of Nuclear Physics, Siberian Branch, Russian Academy of Sciences aimed at developing an appropriate physical knowledge base and new plasma confinement technologies.

The physics of multiple-mirror confinement in a magnetic configuration, for the first time consisting of a central gas-dynamic trap with multiple-mirror sections to reduce longitudinal losses, is to be studied at the GOL-NB facility. Heating using plasma with the density of about $n \sim 3 \times 10^{19} \text{ m}^{-3}$ is carried out by the atomic injection method with a total power of two beams of up to 1.5 MW. The description of the physical tasks of the project, achievable parameters and design of the facility is given in [154–156]. The prediction of the theory [159] that there are no significant differences in the transport of a highly collisional plasma flow through a strong field section in solenoidal and multiple-mirror configurations was first experimentally confirmed in [157, 158]. At present, plasma accumulation, heating, and confinement in the central trap are being studied in the case of solenoidal switching on of strong field sections [160, 161]. The work program at the GOL-NB facility provides for testing the ideas outlined in Subsection 4.2.3.

The helical confinement concept is being tested at the SMOLA facility launched at the Budker Institute of Nuclear Physics, Siberian Branch, Russian Academy of Sciences in 2017 [149, 150]. Experiments have shown the helical confinement effect, which is manifested in a significant decrease in the integral flux and a decrease in the average radius of the rotating plasma along the section with the helical field [151]. It has been shown that the efficiency of the helical section increases with increasing magnetic field, average corrugation depth and rotation speed [14], which is consistent with theoretical assumptions. The suppression of the longitudinal plasma flow in the section with a helical magnetic field is shown experimentally, which corresponds to the effective mirror ratio $R_{\text{eff}} > 10$ [152]. The observed plasma density distribution is in good agreement with the theory.

5. CONCLUSIONS

The new-generation GDMT trap described in this work is a natural next step in the program of linear magnetic traps being developed at the Budker Institute of Nuclear Physics, Siberian Branch, Russian Academy of Sciences. The GDMT is based on the principles of fusion plasma confinement successfully implemented at the GDT and GOL-3 facilities.

Being close to the existing GDT facility in terms of design and a number of parameters (such as linear dimensions and energy of fast ions), the starting GDMT configuration differs dramatically in the discharge duration (1–2 s versus 10 ms in GDT), atomic injection power (24 MW versus 5.4 MW) and magnetic field strength in the central section (up to 1.5 T versus 0.35 T in GDT). A relatively long discharge duration allows studying steady-state regimes (unlike GDT, where the energy stored in the plasma increases monotonically during the shot). The higher field strength and the power of atomic injection make it possible to count on plasma confinement with a stored energy on the order of 200 kJ, which is hundreds of times higher than the stored energy in the GDT plasma even in regimes with moderate parameters. The plasma parameters in GDMT in these modes are close to the plasma parameters in a fusion neutron source suitable for testing structural materials.

At the GDMT facility, it is planned to test a number of thermonuclear technologies, such as methods for replenishing the plasma with matter, MHD plasma stabilization with a high relative pressure, and the creation of strong constant magnetic fields using coils based on modern HTSC tapes. A radical increase in the energy stored in the plasma and the discharge duration leads to a significant heat flux to the surfaces in contact with the plasma (thus, according to estimates made on the basis of the DOL code, power densities of about 10 MW/m² are expected in certain modes on the surface of the plasma absorber), which makes it possible to study in detail the issues related to the plasma–surface interaction.

In the case of the successful development of additional methods for suppressing longitudinal losses, such as multiple-mirror end sections and diamagnetic confinement in the central cell, it is expected to increase the particle confinement time and energy in the trap by at least an order of magnitude. This makes it possible to simulate a neutron source suitable for use as a driver of a subcritical nuclear reactor and to consider the prospects for creating a fusion reactor based on linear magnetic traps.

FUNDING

The results presented in this paper were obtained mainly as part of the implementation of the work plan for the event “Experimental verification of effective methods for confining plasma in existing and promising linear systems” of the

Federal project “Development of controlled thermonuclear fusion technologies and innovative plasma technologies” of the integrated program “Development of technology, technologies and scientific research in the field of the use of atomic energy in the Russian Federation for the period up to 2024.” Some studies at the GDT, GOL-NB, CAT and SMOLA facilities were supported in part by the Ministry of Science and Higher Education of the Russian Federation within the State research plan. The study of the plasma stability in a multiple-mirror trap (Subsection 4.2.4) was supported by the Russian Science Foundation (project no. 21-12-00133; <https://rscf.ru/en/project/21-12-00133/>). The study of the improved longitudinal plasma confinement in linear open traps with a helical magnetic field (Subsection 4.2.5) was supported by the Russian Science Foundation (project no. 22-12-00133; <https://rscf.ru/en/project/22-12-00133/>).

CONFLICT OF INTEREST

The authors declare that they have no conflicts of interest.

REFERENCES

- G. I. Budker, in *Plasma Physics and Problem of Controlled Fusion Reactions*, Ed. by M. A. Leontovich (Akad. Nauk SSSR, Moscow, 1958), Vol. 3, p. 1 [in Russian].
- R. F. Post, in *Proceedings of the 2nd United Nations International Conference on the Peaceful Uses of Atomic Energy, Geneva, 1958*, Vol. 32: *Controlled Fusion Devices* (United Nations, Geneva, 1958), p. 245.
- D. D. Ryutov, *Sov. Phys.—Usp.* **31**, 300 (1988). <https://doi.org/10.1070/PU1988v031n04ABEH005747>
- R. F. Post, *Nucl. Fusion* **27**, 1579 (1987). <https://doi.org/10.1088/0029-5515/27/10/001>
- I. N. Golovin and B. B. Kadomtsev, *At. Energy* **81**, 793 (1996). <https://doi.org/10.1007/BF02408179>
- A. Beklemishev, A. Anikeev, V. Astrelin, P. Bagryansky, A. Burdakov, V. Davydenko, D. Gavrilenko, A. Ivanov, I. Ivanov, M. Ivantsivsky, I. Kandaurov, S. Polosatkin, V. Postupaev, S. Sinitsky, A. Shoshin, et al., *Fusion Sci. Technol.* **63**, 46 (2013). <https://doi.org/10.13182/FST13-A16872>
- A. Beklemishev, A. Anikeev, A. Burdakov, A. Ivanov, I. Ivanov, V. Postupaev, and S. Sinitsky, *AIP Conf. Proc.* **1442**, 147 (2012). <https://doi.org/10.1063/1.4706862>
- P. A. Bagryansky, A. D. Beklemishev, and V. V. Postupaev, *J. Fusion Energy* **38**, 162 (2019). <https://doi.org/10.1007/s10894-018-0174-1>
- A. D. Beklemishev, *Phys. Plasmas* **23**, 082506 (2016). <https://doi.org/10.1063/1.4960129>
- A. D. Beklemishev, *AIP Conf. Proc.* **1771**, 030001 (2016). <https://doi.org/10.1063/1.4964157>
- G. I. Budker, V. V. Mirnov, and D. D. Ryutov, *JETP Lett.* **14**, 212 (1971).
- B. G. Logan, A. J. Lichtenberg, M. A. Lieberman, and A. Makhijani, *Phys. Rev. Lett.* **28**, 144 (1972). <https://doi.org/10.1103/PhysRevLett.28.144>
- A. D. Beklemishev, *AIP Conf. Proc.* **1771**, 040006 (2016). <https://doi.org/10.1063/1.4964191>
- A. V. Sudnikov, A. D. Beklemishev, A. A. Inzhevatkina, I. A. Ivanov, V. V. Postupaev, A. V. Burdakov, V. V. Glinskiy, K. N. Kuklin, A. F. Rovenskikh, and V. O. Ustyuzhanin, *J. Plasma Phys.* **86**, 905860515 (2020). <https://doi.org/10.1017/S0022377820001245>
- I. A. Kotelnikov, V. V. Mirnov, V. P. Nagornyy, and D. D. Ryutov, in *Plasma Physics and Controlled Nuclear Fusion Research, 1984: 10th Conference Proceedings, London, 1984/Isp670-1 (Nuclear Fusion Suppl 198)* (IAEA, Vienna, 1985), Vol. 2, p. 309.
- A. A. Ivanov, E. P. Kruglyakov, Yu. A. Tsidulko, V. G. Krasnoperov, and V. V. Korshakov, in *Proceedings of the 16th IEEE/NPSS Symposium on Fusion Engineering, Champaign, IL, 1995*, Vol. 1, p. 66. <https://doi.org/10.1109/FUSION.1995.534176>
- P. A. Bagryansky, A. A. Ivanov, E. P. Kruglyakov, A. M. Kudryavtsev, Yu. A. Tsidulko, A. V. Andriyash, A. L. Lukin, and Yu. N. Zouev, *Fusion Eng. Des.* **70**, 13 (2004). <https://doi.org/10.1016/j.fusengdes.2003.08.002>
- P. A. Bagryansky, Z. Chen, I. A. Kotelnikov, D. V. Yakovlev, V. V. Prikhodko, Q. Zeng, Y. Bai, J. Yu, A. A. Ivanov, and Y. Wu, *Nucl. Fusion* **60**, 036005 (2020). <https://doi.org/10.1088/1741-4326/ab668d>
- D. V. Yurov and V. V. Prikhodko, *Phys.—Usp.* **57**, 1118 (2014). <https://doi.org/10.3367/UFNe.0184.201411f.1237>
- B. V. Kuteev and P. R. Goncharov, *Fusion Sci. Technol.* **76**, 836 (2020). <https://doi.org/10.1080/15361055.2020.1817701>
- P. A. Bagryansky, E. D. Gospodchikov, A. A. Ivanov, A. A. Lizunov, E. Yu. Kolesnikov, Z. E. Konshin, O. A. Korobeynikova, Y. V. Kovalenko, V. V. Maximov, S. V. Murakhtin, E. I. Pinzhenin, V. V. Prikhodko, V. Ya. Savkin, A. G. Shalashov, D. I. Skovorodin, et al., *Plasma Fusion Res.* **14**, 2402030 (2019). <https://doi.org/10.1585/pfr.14.2402030>
- P. A. Bagryansky, A. V. Anikeev, A. D. Beklemishev, A. S. Donin, A. A. Ivanov, M. S. Korzhavina, Yu. V. Kovalenko, E. P. Kruglyakov, A. A. Lizunov, V. V. Maximov, S. V. Murakhtin, V. V. Prikhodko, E. I. Pinzhenin, A. N. Pushkareva, V. Ya. Savkin, et al., *Fusion Sci. Technol.* **59**, 31 (2011). <https://doi.org/10.13182/FST11-A11568>
- P. A. Bagryansky, A. G. Shalashov, E. D. Gospodchikov, A. A. Lizunov, V. V. Maximov, V. V. Prikhodko, E. I. Soldatkina, A. L. Solomakhin, and D. V. Yakovlev, *Phys. Rev. Lett.* **114**, 205001 (2015). <https://doi.org/10.1103/PhysRevLett.114.205001>
- P. A. Bagryansky, A. V. Anikeev, G. G. Denisov, E. D. Gospodchikov, A. A. Ivanov, A. A. Lizunov, Yu. V. Kovalenko, V. I. Malygin, V. V. Maximov, O. A. Korobeynikova, S. V. Murakhtin, E. I. Pinzhenin, V. V. Prikhodko, V. Ya. Savkin, A. G. Shalashov, et al., *Nucl. Fusion* **55**, 053009 (2015). <https://doi.org/10.1088/0029-5515/55/5/053009>

25. P. A. Bagryansky, E. D. Gospodchikov, Yu. V. Kovalenko, A. A. Lizunov, V. V. Maximov, S. V. Murakhtin, E. I. Pinzhenin, V. V. Prikhodko, V. Ya. Savkin, A. G. Shalashov, E. I. Soldatkina, A. L. Solomakhin, and D. V. Yakovlev, *Fusion Sci. Technol.* **68**, 87 (2015). <https://doi.org/10.13182/FST14-864>
26. A. V. Arzhannikov, V. T. Astrelin, A. V. Burdakov, V. G. Ivanenko, V. S. Koidan, V. V. Konyukhov, A. G. Makarov, K. I. Mekler, P. I. Melnikov, V. S. Nikolaev, S. S. Perin, S. V. Polosatkin, V. V. Postupaev, A. F. Rovenskikh, and S. L. Sinitsky, *Fusion Technol.* **35**, 112 (1999). <https://doi.org/10.13182/FST99-A11963834>
27. I. Kotelnikov, Z. Chen, P. Bagryansky, A. Sudnikov, Q. Zeng, D. Yakovlev, F. Wang, A. Ivanov, and Y. Wu, *Nucl. Fusion* **60**, 067001 (2020). <https://doi.org/10.1088/1741-4326/ab81ab>
28. M. Yu, K. Sanwalka, T. Bohm, C. Forest, J. Anderson, and WHAM Collaboration Team, in *Proceedings of the 63rd Annual Meeting of the APS Division of Plasma Physics, Pittsburgh, PA, 2021*, Paper TP11.00073. <https://meetings.aps.org/Meeting/DPP21/Session/TP11.73>
29. H. Gota, M. W. Binderbauer, T. Tajima, S. Putvinski, M. Tuszewski, S. Dettrick, E. Garate, S. Korepanov, A. Smirnov, M. C. Thompson, E. Trask, X. Yang, L. Schmitz, Z. Lin, A. A. Ivanov, et al., *Nucl. Fusion* **57**, 116021 (2017). <https://doi.org/10.1088/1741-4326/aa7d7b>
30. I. S. Chernoshtanov, *Plasma Phys. Rep.* **48**, 79 (2022). <https://doi.org/10.1134/S1063780X22020052>
31. A. Burdakov, A. Azhannikov, V. Astrelin, A. Beklemishev, V. Burmasov, G. Derevyankin, V. Ivanenko, I. Ivanov, M. Ivantsivsky, I. Kandaurov, V. Konyukhov, I. Kotelnikov, V. Kovenya, T. Kozlinskaya, K. Kuklin, et al., *Fusion Sci. Technol.* **51**, 106 (2007). <https://doi.org/10.13182/FST07-A1327>
32. A. V. Burdakov, A. V. Arzhannikov, V. T. Astrelin, A. D. Beklemishev, A. A. Ivanov, I. A. Kotelnikov, E. P. Kruglyakov, S. V. Polosatkin, V. V. Postupaev, S. L. Sinitsky, I. V. Timofeev, and V. P. Zhukov, *Fusion Sci. Technol.* **59**, 9 (2011). <https://doi.org/10.13182/FST11-A11564>
33. A. A. Ivanov and V. V. Prikhodko, *Phys.—Usp.* **60**, 509 (2017). <https://doi.org/10.3367/UFNe.2016.09.037967>
34. A. V. Burdakov and V. V. Postupaev, *Phys.—Usp.* **61**, 582 (2018). <https://doi.org/10.3367/UFNe.2018.03.038342>
35. A. D. Beklemishev, *Fusion Sci. Technol.* **63**, 355 (2013). <https://doi.org/10.13182/FST13-A16953>
36. A. D. Beklemishev, P. A. Bagryansky, M. S. Chaschin, and E. I. Soldatkina, *Fusion Sci. Technol.* **57**, 351 (2010). <https://doi.org/10.13182/FST10-A9497>
37. D. V. Yakovlev, A. G. Shalashov, E. D. Gospodchikov, V. V. Maximov, V. V. Prikhodko, V. Ya. Savkin, E. I. Soldatkina, A. L. Solomakhin, and P. A. Bagryansky, *Nucl. Fusion* **58**, 094001 (2018). <https://doi.org/10.1088/1741-4326/aacb88>
38. P. P. Khvostenko, I. O. Anashkin, E. N. Bondarchuk, N. V. Inyutin, V. A. Krylov, I. V. Levin, A. B. Mineev, and M. M. Sokolov, *Vopr. At. Nauki Tekh., Ser.: Termoyad. Sint.* **42** (1), 15 (2019). <https://doi.org/10.21517/0202-3822-2019-42-1-15-38>
39. J. Anderson, M. Clark, C. Forest, B. Geiger, V. Mirnov, S. Oliva, J. Pizzo, O. Schmitz, J. Wallace, G. Kristofek, R. Mumgaard, E. Peterson, A. Ram, D. Whyte, J. Wright, et al., in *Proceedings of the 62nd Annual Meeting of the APS Division of Plasma Physics, Remote, 2020*, Vol. 65 (11), Paper CP20.00003. <https://meetings.aps.org/Meeting/DPP20/Session/CP20.3>
40. M. Gryaznevich, TE. Ltd Physics Team, and TE. Ltd HTS Team for Tokamak Energy Ltd., *Nucl. Fusion* **62**, 042008 (2022). <https://doi.org/10.1088/1741-4326/ac26ee>
41. A. Molodyk, S. Samoilenkov, A. Markelov, P. Degtyarenko, S. Lee, V. Petrykin, M. Gaifullin, A. Mankevich, A. Vavilov, B. Sorbom, J. Cheng, S. Garberg, L. Kesler, Z. Hartwig, S. Gavrilkin, et al., *Sci. Rep.* **11**, 2084 (2021). <https://doi.org/10.1038/s41598-021-81559-z>
42. R. Gupta, M. Anerella, P. Joshi, J. Higgins, S. Lalitha, W. Sampson, J. Schmalzle, and P. Wanderer, *IEEE Trans. Appl. Supercond.* **26**, 5700208 (2016). <https://doi.org/10.1109/TASC.2016.2517404>
43. A. Vorobieva, A. Shikov, A. Silaev, E. Dergunova, V. Lomaev, M. Nasibulin, K. Mareev, and S. Kuznetsov, *IEEE Trans. Appl. Supercond.* **11**, 3588 (2001). <https://doi.org/10.1109/77.919840>
44. J.-H. Feist, A. Stabler, W. Ert, B. Heinemann, and E. Speth, in *Fusion Technology 1992: Proceedings of the 17th Symposium On Fusion Technology, Rome, Italy, 1992*, Ed. by C. Ferro, M. Gasparotto, and H. Knoepfel (North-Holland, Amsterdam, 1993), Vol. 1, p. 262. <https://doi.org/10.1016/B978-0-444-89995-8.50044-8>
45. E. D. Bender, *Vopr. At. Nauki Tekh., Ser.: Termoyad. Sint.* **10** (4), 41 (1987).
46. P. A. Bagryansky, E. D. Bender, A. A. Ivanov, A. N. Karpushov, S. V. Murachtin, K. Noack, St. Krahl, and S. Collatz, *J. Nucl. Mater.* **265**, 124 (1999). [https://doi.org/10.1016/S0022-3115\(98\)00510-8](https://doi.org/10.1016/S0022-3115(98)00510-8)
47. H. Gota, M. W. Binderbauer, T. Tajima, A. Smirnov, S. Putvinski, M. Tuszewski, S. A. Dettrick, D. K. Gupta, S. Korepanov, R. M. Magee, J. Park, T. Roche, J. A. Romero, E. Trask, X. Yang, et al., *Nucl. Fusion* **61**, 106039 (2021). <https://doi.org/10.1088/1741-4326/ac2521>
48. P. Deichuli, V. Davydenko, A. Ivanov, S. Korepanov, V. Mishagin, A. Smirnov, A. Sorokin, and N. Stupishin, *Rev. Sci. Instrum.* **86**, 113509 (2015). <https://doi.org/10.1063/1.4936292>
49. D. D. Ryutov, *Fusion Sci. Technol.* **47**, 148 (2005). <https://doi.org/10.13182/FST05-A627>
50. E. I. Soldatkina, E. I. Pinzhenin, O. A. Korobeynikova, V. V. Maximov, D. V. Yakovlev, A. L. Solomakhin, V. Ya. Savkin, K. S. Kolesnichenko, A. A. Ivanov, Yu. A. Trunev, R. V. Voskoboynikov, G. I. Shulzhenko, V. V. Annenkov, E. P. Volchok, I. V. Timofeev, et al., *Nucl. Fusion* **62**, 066034 (2022). <https://doi.org/10.1088/1741-4326/ac3be3>
51. I. V. Timofeev, V. V. Annenkov, E. P. Volchok, and V. V. Glinnskiy, *Nucl. Fusion* **62**, 066033 (2022). <https://doi.org/10.1088/1741-4326/ac3cdc>

52. V. A. Zhil'tsov, A. Yu. Kuyanov, A. A. Skovoroda, and A. V. Timofeev, *Plasma Phys. Rep.* **20**, 242 (1994).
53. K. Ichimura, K. Ichimura, Y. Nakashima, H. Takeda, K. Hosoi, S. Kigure, S. Takahashi, M. Iwamoto, Y. Hosoda, M. Hirata, R. Ikezoe, K. Oki, M. Yoshikawa, M. Sakamoto, T. Imai, et al., *Plasma Fusion Res.* **9**, 3406098 (2014).
<https://doi.org/10.1585/pfr.9.3406098>
54. D. V. Yakovlev, A. G. Shalashov, E. D. Gospodchikov, A. L. Solomakhin, V. Ya. Savkin, and P. A. Bagryansky, *Nucl. Fusion* **57**, 016033 (2017).
<https://doi.org/10.1088/0029-5515/57/1/016033>
55. S. Kojima, K. Hanada, H. Idei, T. Onchi, R. Ikezoe, Y. Nagashima, M. Hasegawa, K. Kuroda, K. Nakamura, A. Higashijima, T. Nagata, S. Kawasaki, S. Shimabukuro, H. Elserafy, M. Fukuyama, et al., *Plasma Phys. Control. Fusion* **63**, 105002 (2021).
<https://doi.org/10.1088/1361-6587/ac1838>
56. S. N. Rodionov, *J. Nucl. Energy, Part C* **1**, 247 (1960).
57. D. V. Sivukhin, in *Reviews of Plasma Physics*, Ed. by M. A. Leontovich (Consultants Bureau, New York, 1968), Vol. 4, p. 93.
58. V. V. Mirnov and D. D. Ryutov, *Sov. Tech. Phys. Lett.* **5**, 279 (1979).
59. *Fusion Basics*, Ed. by M. Kikuchi, K. Lackner, and M. Q. Tran (IAEA, Vienna, 2012).
60. I. K. Konkashbaev, I. S. Landman, and F. R. Ulinich, *Sov. Phys. JETP* **47**, 501 (1978).
61. E. E. Yushmanov, *Sov. Phys. JETP* **22**, 409 (1965).
62. D. I. Skovorodin, *Phys. Plasmas* **26**, 012503 (2019).
<https://doi.org/10.1063/1.5043072>
63. I. S. Abramov, E. D. Gospodchikov, R. A. Shaposhnikov, and A. G. Shalashov, *Nucl. Fusion* **59**, 106004 (2019).
<https://doi.org/10.1088/1741-4326/ab2ef8>
64. S. A. Dettrick, D. C. Barnes, F. Ceccherini, L. Galeotti, S. A. Galkin, S. Gupta, K. Hubbard, O. Koshkarov, C. K. Lau, Y. Mok, A. Necas, B. S. Nicks, M. Onofri, J. Park, S. V. Putvinski, et al., *Nucl. Fusion* **61**, 106038 (2021).
<https://doi.org/10.1088/1741-4326/ac1e5f>
65. I. S. Abramov, E. D. Gospodchikov, R. A. Shaposhnikov, and A. G. Shalashov, *Rev. Sci. Instrum.* **91**, 013514 (2020).
<https://doi.org/10.1063/1.5127574>
66. I. A. Kotelnikov, D. D. Ryutov, Yu. A. Tsidulko, V. V. Katyshev, A. V. Komin, and V. M. Krivosheev, Preprint No. 90-105 (Inst. Nucl. Phys., Sib. Branch, USSR Acad. Sci., Novosibirsk, 1990).
67. W. Yang, Q. Zeng, C. Chen, Z. Chen, J. Song, Z. Wang, J. Yu, D. Yakovlev, and V. Prikhodko, *Fusion Eng. Des.* **164**, 112221 (2021).
<https://doi.org/10.1016/j.fusengdes.2020.112221>
68. D. V. Yurov, V. V. Prikhodko, and Yu. A. Tsidulko, *Plasma Phys. Rep.* **42**, 210 (2016).
69. V. P. Pastukhov, in *Reviews of Plasma Physics*, Ed. by B. B. Kadomtsev (Consultants Bureau, New York, 1987), Vol. 13, p. 203.
70. A. Loarte, B. Lipschultz, A. S. Kukushkin, G. F. Matthews, P. C. Stangeby, N. Asakura, G. F. Counsell, G. Federici, A. Kallenbach, K. Krieger, A. Mahdavi, V. Philipps, D. Reiter, J. Roth, J. Strachan, et al., *Nucl. Fusion* **47**, S203 (2007).
<https://doi.org/10.1088/0029-5515/47/6/S04>
71. A. Berman, *Vacuum* **47**, 327 (1996).
[https://doi.org/10.1016/0042-207X\(95\)00246-4](https://doi.org/10.1016/0042-207X(95)00246-4)
72. S. Yamanaka and M. Miyake, *Solid State Phenom.* **73–75**, 1 (2000).
<https://doi.org/10.4028/www.scientific.net/ssp.73-75.1>
73. W. T. Chandler and R. J. Walter, in *Refractory Metal Alloys Metallurgy and Technology*, Ed. by I. Machlin, R. T. Begley, and E. D. Weisert (Springer, New York, 2012), p. 197.
https://doi.org/10.1007/978-1-4684-9120-3_6
74. *Hydrogen Recycling at Plasma Facing Materials*, Ed. by C. H. Wu (Springer, Dordrecht, 2000).
<https://doi.org/10.1007/978-94-011-4331-8>
75. D. D. Ryutov, P. N. Yushmanov, D. C. Barnes, and S. V. Putvinski, *AIP Conf. Proc.* **1721**, 060003 (2016).
<https://doi.org/10.1063/1.4944029>
76. R. K. Janev, W. D. Langer, K. J. Evans, and D. E. J. Post, *Elementary Processes in Hydrogen–Helium Plasmas* (Springer, Berlin, 1987).
<https://doi.org/10.1007/978-3-642-71935-6>
77. S. K. Combs and L. R. Baylor, *Fusion Sci. Technol.* **73**, 493 (2018).
<https://doi.org/10.1080/15361055.2017.1421367>
78. A. D. Sladkomedova, A. N. Voronin, A. G. Alekseev, V. K. Gusev, G. S. Kurskiev, Yu. V. Petrov, N. V. Sakharov, S. Yu. Tolstyakov, and V. V. Zabrodsky, *Phys. Scr.* **93**, 105601 (2018).
<https://doi.org/10.1088/1402-4896/aadb85>
79. D. D. Ryutov, H. L. Berk, B. I. Cohen, A. W. Molvik, and T. C. Simonen, *Phys. Plasmas* **18**, 092301 (2011).
<https://doi.org/10.1063/1.3624763>
80. A. D. Beklemishev, *AIP Conf. Proc.* **1069**, 3 (2008).
<https://doi.org/10.1063/1.3033729>
81. V. V. Prikhodko, P. A. Bagryansky, A. D. Beklemishev, E. Yu. Kolesnikov, I. A. Kotelnikov, V. V. Maximov, A. N. Pushkareva, E. I. Soldatkina, Yu. A. Tsidulko, and K. V. Zaytsev, *Fusion Sci. Technol.* **59**, 94 (2011).
<https://doi.org/10.13182/FST11-A11582>
82. I. Kotelnikov, Q. Zeng, V. Prikhodko, D. Yakovlev, K. Zhang, Z. Chen, and J. Yu, *Nucl. Fusion* **62**, 096025 (2022).
<https://doi.org/10.1088/1741-4326/ac81da>
83. F. Waelbroeck and L. Chen, *Phys. Fluids B* **3**, 601 (1991).
<https://doi.org/10.1063/1.859858>
84. T. Cho, J. Kohagura, T. Numakura, M. Hirata, H. Higaki, H. Hojo, M. Ichimura, K. Ishii, K. Md. Islam, A. Itakura, I. Katanuma, R. Minami, Y. Nakashima, T. Saito, Y. Tatematsu, et al., *Phys. Rev. Lett.* **97**, 055001 (2006).
<https://doi.org/10.1103/PhysRevLett.97.055001>
85. T. Cho, V. P. Pastukhov, W. Horton, T. Numakura, M. Hirata, J. Kohagura, N. V. Chudin, and J. Pratt, *Phys. Plasmas* **15**, 056120 (2008).
<https://doi.org/10.1063/1.2906262>
86. V. P. Pastukhov and V. N. Chudin, *Fusion Sci. Technol.* **59**, 84 (2011).
<https://doi.org/10.13182/FST11-A11580>
87. R. Z. Sagdeev and V. D. Shafranov, *Sov. Phys. JETP* **12**, 130 (1961).

88. D. C. Watson, *Phys. Fluids* **23**, 2485 (1980).
<https://doi.org/10.1063/1.862949>
89. G. R. Smith, *Phys. Fluids* **27**, 1499 (1984).
<https://doi.org/10.1063/1.864773>
90. G. R. Smith, W. M. Nevins, and W. M. Sharp, *Phys. Fluids* **27**, 2120 (1984).
<https://doi.org/10.1063/1.864837>
91. Yu. A. Tsidulko and I. S. Chernoshtanov, *Plasma Phys. Rep.* **40**, 955 (2014).
<https://doi.org/10.1134/S1063780X1412006X>
92. T. A. Casper and G. R. Smith, *Phys. Rev. Lett.* **48**, 1015 (1982).
<https://doi.org/10.1103/PhysRevLett.48.1015>
93. T. C. Simonen, *Nucl. Fusion* **25**, 036 (1985).
<https://doi.org/10.1088/0029-5515/25/9/036>
94. R. Katsumata, M. Ichimura, M. Inutake, H. Hojo, A. Mase, and T. Tamano, *Phys. Plasmas* **3**, 4489 (1996).
<https://doi.org/10.1063/1.872067>
95. K. V. Zaitsev, A. V. Anikeev, P. A. Bagryansky, A. S. Donin, O. A. Korobeinikova, M. S. Korzhavina, Yu. V. Kovalenko, A. A. Lizunov, V. V. Maximov, E. I. Pinzhenin, V. V. Prikhodko, E. I. Soldatkina, A. L. Solomakhin, V. Ya. Savkin, and D. V. Yakovlev, *Phys. Scr.* **2014**, 014004 (2014).
<https://doi.org/10.1088/0031-8949/2014/T161/014004>
96. A. V. Anikeev, P. A. Bagryanskii, K. V. Zaitsev, O. A. Korobeinikova, S. V. Murakhtin, D. I. Skovorodin, and D. V. Yurov, *Plasma Phys. Rep.* **41**, 773 (2015).
<https://doi.org/10.1134/S1063780X15100025>
97. A. V. Anikeev, P. A. Bagryansky, I. S. Chernoshtanov, M. S. Korzhavina, V. V. Prikhodko, and Yu. A. Tsidulko, *Fusion Sci. Technol.* **59**, 104 (2011).
<https://doi.org/10.13182/FST11-A11584>
98. L. V. Berzins and T. A. Casper, *Phys. Rev. Lett.* **59**, 1428 (1987).
<https://doi.org/10.1103/PhysRevLett.59.1428>
99. I. S. Chernoshtanov, *J. Phys.: Conf. Ser.* **1125**, 012007 (2018).
<https://doi.org/10.1088/1742-6596/1125/1/012007>
100. W. C. Turner, J. F. Clauser, F. H. Coengen, D. L. Correll, W. F. Cummins, R. P. Freis, R. K. Goodman, A. L. Hunt, T. B. Kaiser, G. M. Melin, W. E. Nexsen, T. C. Simonen, and B. W. Stallard, *Nucl. Fusion* **19**, 1011 (1979).
<https://doi.org/10.1088/0029-5515/19/8/002>
101. A. B. Mikhailovskii, *Yad. Sint.* **5**, 125 (1965).
102. R. F. Post and M. N. Rosenbluth, *Phys. Fluids* **9**, 730 (1966).
<https://doi.org/10.1063/1.1761740>
103. M. J. Gerver, *Phys. Fluids* **19**, 1581 (1976).
<https://doi.org/10.1063/1.861363>
104. I. A. Kotelnikov, I. S. Chernoshtanov, and V. V. Prikhodko, *Phys. Plasmas* **24**, 122512 (2017).
<https://doi.org/10.1063/1.5013059>
105. W. M. Tang, L. D. Pearlstein, and H. L. Berk, *Phys. Fluids* **15**, 1153 (1972).
<https://doi.org/10.1063/1.1694044>
106. G. N. Chulkov and A. V. Timofeev, *Nucl. Fusion* **20**, 9 (1980).
<https://doi.org/10.1088/0029-5515/20/1/002>
107. B. I. Kanaev and E. E. Yushmanov, *Sov. Phys. JETP* **40**, 290 (1974).
108. B. I. Kanaev, V. P. Pastukhov, and E. E. Yushmanov, *JETP Lett.* **18**, 204 (1973).
109. D. E. Baldwin, H. L. Berk, and L. D. Pearlstein, *Phys. Rev. Lett.* **36**, 1051 (1976).
<https://doi.org/10.1103/PhysRevLett.36.1051>
110. I. A. Kotelnikov, I. S. Chernoshtanov, and V. V. Prikhodko, *Plasma Fusion Res.* **14**, 2403001 (2019).
<https://doi.org/10.1585/pfr.14.2403001>
111. M. G. Haines, *Nucl. Fusion* **17**, 811 (1977).
<https://doi.org/10.1088/0029-5515/17/4/015>
112. I. M. Lanskii, Preprint No. 93-96 (Inst. Nucl. Phys., Sib. Branch, USSR Acad. Sci., Novosibirsk, 1993).
113. H. Grad, in *Proceedings of Symposia in Applied Mathematics*, Ed. by H. Grad (Am. Math. Soc., Providence, 1967), Vol. 18, p. 162.
<https://doi.org/10.1090/psapm/018/0215567>
114. W. A. Newcomb, *J. Plasma Phys.* **26**, 529 (1981).
<https://doi.org/10.1017/S0022377800010904>
115. I. A. Kotelnikov, P. A. Bagryansky, and V. V. Prikhodko, *Phys. Rev. E: Stat., Nonlinear, Soft Matter Phys.* **81**, 067402 (2010).
<https://doi.org/10.1103/PhysRevE.81.067402>
116. I. A. Kotelnikov, *Fusion Sci. Technol.* **59**, 47 (2011).
<https://doi.org/10.13182/FST11-A11572>
117. K. V. Lotov, *Phys. Plasmas* **3**, 1472 (1996).
<https://doi.org/10.1063/1.871739>
118. A. M. Zhilukhin, V. M. Safronov, V. V. Sidnee, and Yu. V. Skvortsov, *JETP Lett.* **39**, 293 (1984).
119. J. M. Turner, L. F. Burlaga, N. F. Ness, and J. F. Le-maire, *J. Geophys. Res.* **82**, 1921 (1977).
<https://doi.org/10.1029/JA082i013p01921>
120. R. L. Kaufmann, J.-T. Horng, and A. Wolfe, *J. Geophys. Res.* **75**, 4666 (1970).
<https://doi.org/10.1029/JA075i025p04666>
121. B. T. Tsurutani, G. S. Lakhina, O. P. Verkhoglyadova, E. Echer, F. L. Guarnieri, Y. Narita, and D. O. Constantinescu, *J. Geophys. Res.: Space Phys.* **116**, A02103 (2011).
<https://doi.org/10.1029/2010JA015913>
122. E. A. Kuznetsov, T. Passot, V. P. Ruban, and P. L. Sulem, *Phys. Plasmas* **22**, 042114 (2015).
<https://doi.org/10.1063/1.4919027>
123. M. S. Ioffe, B. I. Kanaev, V. P. Pastukhov, V. V. Piter-skii, and E. E. Yushmanov, in *Advances in Science and Technology, Ser. Plasma Physics*, Ed. by V. D. Shafranov (VINITI, Moscow, 1989), Vol. 9 [in Russian].
124. A. I. Morozov and V. V. Savel'ev, *Phys.—Usp.* **41**, 1049 (1998).
<https://doi.org/10.1070/PU1998v041n11ABEH000501>
125. M. S. Khristo and A. D. Beklemishev, *Plasma Fusion Res.* **14**, 2403007 (2019).
<https://doi.org/10.1585/pfr.14.2403007>
126. M. S. Khristo and A. D. Beklemishev, *Plasma Phys. Control. Fusion* **64**, 095019 (2022).
<https://doi.org/10.1088/1361-6587/ac8616>
127. E. I. Soldatkina, P. A. Bagryanskii, and A. L. Solomakhin, *Plasma Phys. Rep.* **34**, 259 (2008).
128. T. B. Kaiser and L. D. Pearlstein, *Phys. Fluids* **28**, 1003 (1985).
<https://doi.org/10.1063/1.865092>

129. H. L. Berk, H. V. Wong, and K. T. Tsang, *Phys. Fluids* **30**, 2681 (1987).
<https://doi.org/10.1063/1.866033>
130. I. Kotelnikov, *Plasma Phys. Control. Fusion* **62**, 075002 (2020).
<https://doi.org/10.1088/1361-6587/ab8a63>
131. I. S. Chernoshtanov, arXiv:2002.03535v1, 2020.
<http://arxiv.org/abs/2002.03535>.
132. L. R. Morse, *Phys. Fluids* **10**, 1560 (1967).
<https://doi.org/10.1063/1.1762322>
133. I. A. Kotel'nikov and A. I. Shchetnikov, Preprint No. 87-10 (Inst. Nucl. Phys., Sib. Branch, USSR Acad. Sci., Novosibirsk, 1987).
134. I. A. Kotelnikov, in *Open Plasma Confinement Systems for Fusion: Proceedings of the International Conference*, Ed. by A. N. Skrinsky and A. A. Kabantsev (World Scientific, Singapore, 1993), p. 545.
135. V. P. Pastukhov, *Sov. J. Plasma Phys.* **6**, 549 (1980).
136. V. P. Pastukhov, *Plasma Phys. Rep.* **47**, 892 (2021).
137. R. M. Magee, T. Roche, M. C. Thompson, M. Tobin, M. Beall, B. H. Deng, and S. Korepanov, *Nucl. Fusion* **58**, 082011 (2018).
<https://doi.org/10.1088/1741-4326/aab6c6>
138. R. M. Magee, A. Necas, R. Clary, S. Korepanov, S. Nicks, T. Roche, M. C. Thompson, M. W. Binderbauer, and T. Tajima, *Nat. Phys.* **15**, 281 (2019).
<https://doi.org/10.1038/s41567-018-0389-0>
139. A. J. Lichtenberg and V. V. Mirnov, in *Reviews of Plasma Physics*, Ed. by B. B. Kadomtsev (Consultants Bureau, New York, 1996), Vol. 19, p. 53.
140. J. D. Huba, *NRL Plasma Formulary* (Naval Research Laboratory, Washington, DC, 2013).
141. B. A. Knyazev, V. V. Mirnov, and P. Z. Chebotaev, *Vopr. At. Nauki Tekh., Ser.: Termoyad. Sint.* **6** (3), 12 (1983).
142. V. T. Astrelin, A. V. Burdakov, and V. V. Postupaev, *Plasma Phys. Rep.* **24**, 414 (1998).
143. A. V. Arzhannikov, V. T. Astrelin, A. V. Burdakov, I. A. Ivanov, V. S. Koidan, K. I. Mekler, V. V. Postupaev, A. F. Rovenskikh, S. V. Polosatkin, and S. L. Sinitskii, *JETP Lett.* **77**, 358 (2003).
<https://doi.org/10.1134/1.1581960>
144. A. D. Beklemishev, *Fusion Sci. Technol.* **51**, 180 (2007).
<https://doi.org/10.13182/FST07-A1344>
145. M. N. Rosenbluth and C. L. Longmire, *Ann. Phys.* **1**, 120 (1957).
[https://doi.org/10.1016/0003-4916\(57\)90055-6](https://doi.org/10.1016/0003-4916(57)90055-6)
146. Yu. V. Vasil'ev and V. V. Mirnov, *Prikl. Mekh. Tekh. Fiz., No. 6*, 14 (1974).
147. F. Najmabadi, A. J. Lichtenberg, and M. A. Lieberman, *Phys. Fluids* **26**, 1018 (1983).
<https://doi.org/10.1063/1.864233>
148. A. D. Beklemishev, *Phys. Plasmas* **22**, 103506 (2015).
<https://doi.org/10.1063/1.4932075>
149. V. V. Postupaev, A. V. Sudnikov, A. D. Beklemishev, and I. A. Ivanov, *Fusion Eng. Des.* **106**, 29 (2016).
<https://doi.org/10.1016/j.fusengdes.2016.03.029>
150. A. V. Sudnikov, A. D. Beklemishev, V. V. Postupaev, A. V. Burdakov, I. A. Ivanov, N. G. Vasilyeva, K. N. Kuklin, and E. N. Sidorov, *Fusion Eng. Des.* **122**, 86 (2017).
<https://doi.org/10.1016/j.fusengdes.2017.09.005>
151. A. V. Sudnikov, A. D. Beklemishev, V. V. Postupaev, I. A. Ivanov, A. A. Inzhevatkina, V. F. Sklyarov, A. V. Burdakov, K. N. Kuklin, A. F. Rovenskikh, and N. A. Melnikov, *Plasma Fusion Res.* **14**, 2402023 (2019).
<https://doi.org/10.1585/pfr.14.2402023>
152. A. V. Sudnikov, I. A. Ivanov, A. A. Inzhevatkina, M. V. Larichkin, K. A. Lomov, V. V. Postupaev, M. S. Tolkachev, and V. O. Ustyuzhanin, *J. Plasma Phys.* **88**, 905880102 (2022).
<https://doi.org/10.1017/S0022377821001276>
153. I. S. Chernoshtanov and D. A. Ayupov, *Phys. Plasmas* **28**, 032502 (2021).
<https://doi.org/10.1063/5.0040715>
154. V. V. Postupaev, A. V. Burdakov, and A. A. Ivanov, *Fusion Sci. Technol.* **68**, 92 (2015).
<https://doi.org/10.13182/FST14-846>
155. V. V. Postupaev and D. V. Yurov, *Plasma Phys. Rep.* **42**, 1013 (2016).
<https://doi.org/10.1134/S1063780X16110076>
156. V. V. Postupaev, V. I. Batkin, A. D. Beklemishev, A. V. Burdakov, V. S. Burmasov, I. S. Chernoshtanov, A. I. Gorbovsky, I. A. Ivanov, K. N. Kuklin, K. I. Mekler, A. F. Rovenskikh, E. N. Sidorov, and D. V. Yurov, *Nucl. Fusion* **57**, 036012 (2017).
<https://doi.org/10.1088/1741-4326/57/3/036012>
157. I. A. Ivanov, V. I. Batkin, A. V. Burdakov, V. S. Burmasov, K. N. Kuklin, K. I. Mekler, S. V. Polosatkin, V. V. Postupaev, E. N. Sidorov, and A. F. Rovenskikh, *AIP Adv.* **7**, 125121 (2017).
<https://doi.org/10.1063/1.5009528>
158. V. V. Postupaev, V. I. Batkin, A. V. Burdakov, V. S. Burmasov, I. A. Ivanov, K. N. Kuklin, K. I. Mekler, A. F. Rovenskikh, and E. N. Sidorov, *Plasma Phys. Control. Fusion* **62**, 025008 (2020).
<https://doi.org/10.1088/1361-6587/ab53c2>
159. V. V. Mirnov and D. D. Ryutov, *Nucl. Fusion* **12**, 627 (1972). with corrigenda: V. V. Mirnov and D. D. Ryutov, *Nucl. Fusion* **13**, 314 (1973).
<https://doi.org/10.1088/0029-5515/13/2/029>
<https://doi.org/10.1088/0029-5515/12/6/001>
160. V. V. Postupaev, V. I. Batkin, A. V. Burdakov, V. S. Burmasov, I. A. Ivanov, K. N. Kuklin, Yu. A. Lykova, N. A. Melnikov, K. I. Mekler, A. V. Nikishin, S. V. Polosatkin, A. F. Rovenskikh, E. N. Sidorov, and D. I. Skovorodin, *Nucl. Fusion* **62**, 086003 (2022).
<https://doi.org/10.1088/1741-4326/ac69fa>
161. V. V. Postupaev, V. I. Batkin, A. V. Burdakov, V. S. Burmasov, I. A. Ivanov, K. N. Kuklin, Yu. A. Lykova, K. I. Mekler, N. A. Melnikov, A. V. Nikishin, S. V. Polosatkin, A. F. Rovenskikh, E. N. Sidorov, V. F. Sklyarov, and D. I. Skovorodin, *Plasma Phys. Rep.* **48**, 1137 (2022).
<https://doi.org/10.1134/S1063780X22600682>

Translated by L. Mosina